Photoinduced Electron Transfer in Supramolecular Thin Films Composed of *N*-Ethylcarbazole-Containing Compounds

Tomoyuki Morita

1999

Photoinduced Electron Transfer in Supramolecular Thin Films Composed of *N*-Ethylcarbazole-Containing Compounds

Tomoyuki Morita

1999

Contents

List of Abbreviations

16AP	16-(9-anthroyloxy)palmitic acid
^{1}H NMR	proton nuclear magnetic resonance spectroscopy
2AS	2-(9-anthroyloxy)stearic acid
5Cz18	*N',N',N'*-trimethylammoniohexanoyl-L-3-(3-*N*-ethylcarbazolyl)alanine dioctadecylamide bromide
5Cz18Z	*N',N'*-dimethyl-*N'*-carboxymethylammoniohexanoyl-L-3-(3-*N*-ethylcarbazolyl)alanine dioctadecylamide
9A18	*N',N',N'*-trimethylammoniohexanoyl-D-3-(9-anthryl)alanine dioctadecylamide bromide
Aib	α-aminoisobutyric acid
Ala	L-alanine
Ant	anthryl
Ant$^{+\bullet}$	radical cation of an anthryl group
Ant-A12-SS	Boc-AntAla-(Ala-Aib)$_6$-NH(CH$_2$)$_5$CHCH$_2$CH$_2$SS
AntAla	D-3-(9-anthryl)alanine
ATP	adenine triphosphate
BA4OBzl	Boc-(Ala-Aib)$_2$-OBzl
BA4OH	Boc-(Ala-Aib)$_2$-OH
BA4-ECzAla-OEt	Boc-(Ala-Aib)$_2$-ECzAla-OEt
BA4-SS	Boc-(Ala-Aib)$_2$-NH(CH$_2$)$_5$CHCH$_2$CH$_2$SS
BA8OH	Boc-(Ala-Aib)$_4$-OH
BA12OBzl	Boc-(Ala-Aib)$_6$-OBzl
BA12-ECzAla-OEt	Boc-(Ala-Aib)$_6$-ECzAla-OEt
BA12-SS	Boc-(Ala-Aib)$_6$-NH(CH$_2$)$_5$CHCH$_2$CH$_2$SS
BA20-SS	Boc-(Ala-Aib)$_{10}$-NH(CH$_2$)$_5$CHCH$_2$CH$_2$SS
Boc	*tert*-butyloxycarbonyl
Boc-ECzAla	*N'*-(*tert*-butyloxycarbonyl)-L-3-(3-*N*-ethylcarbazolyl)alanine
C12SH	*n*-dodecanethiol
CD	circular dichroism
CDI	1,1'-carbonyl-bis-1H-imidazole
cyt.c	cytochrome c
DDAB	dioctadecyldimethylammonium bromide
DIEA	*N,N*-diisopropylethylamine
DMAA	*N,N*-dimethylacetamide
DMTP	dimethyl terephthalate
EA	electron acceptor
ECz	*N*-ethylcarbazolyl
ECz$^{+\bullet}$	radical cation of an *N*-ethylcarbazolyl group

ECz-A12	Boc-ECzAla-(Ala-Aib)$_6$-OBzl
ECz-A12-SS	Boc-ECzAla-(Ala-Aib)$_6$-NH(CH$_2$)$_5$CHCH$_2$CH$_2$SS
ECz-A20-SS	Boc-ECzAla-(Ala-Aib)$_{10}$-NH(CH$_2$)$_5$CHCH$_2$CH$_2$SS
ECz-C11-SS	Boc-ECzAla-N((CH$_2$)$_{11}$S)$_2$
ECzAla	L-3-(3-*N*-ethylcarbazolyl)alanine
ECzAla-OEt	L-3-(3-*N*-ethylcarbazolyl)alanine ethyl ester
ED	electron donation
EDTA	ethylenediaminetetraacetic acid
EM	energy migration
EnT	energy transfer
ET	electron transfer
FAB	fast atom bomberdment
FTIR-RAS	Fourier transform infrared reflection-absorption spectroscopy
GC	gas chromatography
HATU	*O*-(7-azabenzotriazol-1-yl)-1,1,3,3-tetramethyluronium haxafluorophosphate
HT	hole transfer
LB	Langmuir-Blodgett
MS	mass spectroscopy
MV^{2+}	methyl viologen
NADP	nicotinamide adenine dinucleotide phosphate sodium salt
OBzl	benzyloxy
OEt	ethoxy
OMe	methoxy
QCM	quartz crystal microbalance
RAS	reflection-absorption spectroscopy
SAM	self-assembled monolayer
SS-A12	SSCH$_2$CH$_2$CH(CH$_2$)$_4$CO-(Ala-Aib)$_6$-OBzl
SS-A12-ECz	SSCH$_2$CH$_2$CH(CH$_2$)$_4$CO-(Ala-Aib)$_6$-ECzAla-OEt
Tc	phase-transition temperature
TEOA	triethanolamine
Ter18	methyl terephthaloyldioctadecylamide
TLC	thin-layer chromatography
$V^{+\bullet}$	monocation radical of a viologen group
Vio18	*N*-(6-(*N*'-(*N*''-ethyl-4',4''-bipyridinium))hexanoyl)-L-alanine dioctadecylamide dibromide
VioAnt18	*N*-(6-(*N*'-(*N*''-ethyl-4',4''-bipyridinium))hexanoyl)-D-3-(9-anthryl)alanine dioctadecylamide dibromide
VioECz18	*N*'-(6-(*N*''-(*N*'''-ethyl-4',4''-bipyridinium))hexanoyl)-L-3-(3-*N*-ethylcarbazolyl)alanine dioctadecylamide dibromide
π-*A*	surface pressure-surface area

Introduction

In the first stage of natural photosynthesis by green plants, photoenergy is efficiently harvested and transferred to the reaction center at the interior of the thylakoid membrane through the chromophoric array composed of chlorophylls.[1,2] Subsequently, the reaction center sensitizes the photoinduced electron transfer between an electron donor and an electron acceptor adjacent to the center, producing a charge-separated state. It is followed by transport of charges (electron and hole) to each limb of the membrane by an electron-transport system, which are composed of protein assemblies.[3] The separated charges are used for reduction of nicotinamide adenine dinucleotide phosphate and oxidation of water molecule.[4,5] A gradient of proton concentration across the membrane is formed during these processes and coupled with the synthesis of adenine triphosphate (ATP) by an ATP synthetase.[6] The efficient photoenergy harvest in the thylakoid membranes arises from a highly ordered arrangement of chromophores in the chromophore-protein complexes. The excellent electron transport is attributed to the effective pathway of electron transfer which is built by the protein assembly.[7,8] The distance between chromophores, the driving force for electron transfer, and the environmental electrostatic field are strictly controlled in the molecular assemblies, resulting in the suppression of the reverse electron transfer.[9-11] The present thesis describes the construction of the novel molecular assemblies which mimic the photoenergy-harvesting system and electron-transport system in the natural photosynthesis. The molecular assemblies containing chromophores shown here will contribute to the development of interesting photochemical and photoelectronic systems for the future molecular devices. The author starts with the introduction of historical background of molecular assembly and electron transfer.

Supramolecular chemistry provides us with various methods to assemble chemical components using electrostatic interaction, hydrophobic interaction, hydrogen bond formation, van der Waals force, etc.[12] In 1933, Langmuir reported the monolayer preparation by spreading amphiphilic

compounds carrying hydrophilic and hydrophobic parts at the air/water interface.[13] He also reported the preparation of multi-layer films, called Langmuir-Blodgett (LB) films by transferring monolayers at the air/water interface onto a solid substrate.[14] In 1964, Bangham prepared vesicular bilayer membranes from phospholipids (liposomes) in water.[15] It was in 1972 that the fluid mosaic model of biomembranes was proposed by Singer and Nicolsen.[16] Kunitake et al. prepared bilayer membranes from synthetic compounds in 1977,[17] which established the preparative method of bilayer membranes by sonication of amphiphilic compounds in water. The preparation of monolayers, LB films, or bilayer membranes from amphiphilic compounds carrying functional groups have enabled the arrangement of the functional groups in an ordered way to achieve a specific functionality. Polypeptides have been also used to construct molecular assemblies by controlling the amphiphilicity.[18,19] Peptides having α-helical conformation, which is one of the secondary structures of proteins, have been assembled in liposome[20] or at the air/water interface.[21] In addition, a water-soluble assembly from a ß-sheet peptide[22] and nanotubes composed of cyclic oligopeptides have been reported.[23] Another method of monolayer formation on a solid substrate, which is different from the LB method, has been developed using Au-S linkage to immobilize of the molecules on a gold substrate. This monolayer is named self-assembled monolayers (SAMs).[24,25] For the high stability and regularity of the monolayers, this method has been considered as a useful technique to prepare functional organic thin films.

Artificial photoenergy-harvesting systems have been constructed extensively by supramolecular thin films containing chromophores. Kuhn and Möbius studied the excitation energy transfer across layers in LB films, and indicated for the first time the occurrence of the Förster-type energy transfer.[26] Lateral energy transfer in a layer and sequential multi-step energy transfer traversing the layers in LB films have been investigated as well.[27,28] With regard to energy transfer, there have

been a number of studies using bilayer membranes, on which chlorophyll derivatives are absorbed.[29] In some studies, fluorescent molecules were introduced in the hydrophobic region of bilayer membrane or electrostatically concentrated on the surface of bilayer membrane,[30-32]. In other studies, bilayer membranes were composed of amphiphiles carrying chromophores.[33-35] Based on these investigations, monolayers or bilayer membranes composed of chromophoric amphiphiles have been proven to be suitable for photoenergy harvesting because of their ordered arrangement in a high density (Figure 1). Polypeptide chains,[36,37] polymeric LB films, [38,39] and dendritic polymer[40,41] carrying chromophores have been also successful to regulate chromophore arrangement.

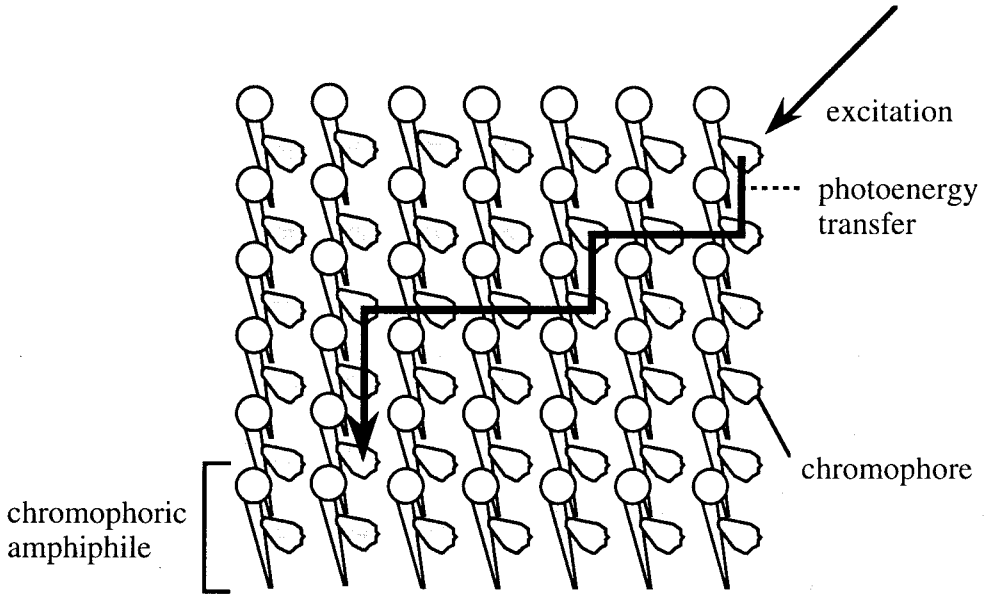

Figure 1. Schematic illustration of photoenergy transfer in a monolayer or a bilayer membrane composed of amphiphiles carrying a chromophore.

Since Marcus's classical thoery[42] and quantum mechanical treatment[43] for electron transfer were presented, simplified model systems have been investigated to clarify the mechanism of electron-transfer reactions in photosynthesis. Especially, the medium effect on the rate of electron transfer between an electron donor and an electron acceptor has been investigated vigorously. For example, the donor-spacer-acceptor systems have been designed using various kinds of spacer chains; flexible methylene chain,[44] rigid steroid[45] or norbornane frame[46], aromatic spacers,[47,48] unsaturated hydrocarbon chain,[49] and peptide chains.[50-52] The general conclusion reached is that a spacer chain connecting an electron donor to an electron acceptor having a low-energy LUMO is a good medium for electron transfer based on the superexchange mechanism.[53,54] Hence, peptide chains have been shown to mediate electron transfer effectively using the π and n (nonbonding) orbitals of amide bonds, which may be related to the efficient electron transport in natural protein assemblies.[55,56]

In order to mimic electron-transfer reactions in photosynthesis, photoinduced electron transfer in various supramolecular systems has been studied. In early period, electron transfer reactions were investigated with systems modeling for photosynthesis, which were composed of porphyrin or quinone molecules.[57-59] The hydrogen-bonded complex of a porphyrin derivative with a quinone derivative[60] or with other porphyrin derivative containing different kind of metal ion[61] was prepared, and the hydrogen bonds were shown to act as the effective pathway of electron transfer. The photoinduced electron transfer occurring at the interface of supramolecular assembly has been investigated in micelles,[62,63] LB films,[64,65] and bilayer membranes.[66-68] In particular, vesicular bilayer membranes are useful for utilizing inner and outer aqueous phases. Indeed, photoinduced electron transfer across the bilayer membrane and the generation of proton gradient have been achieved.[69-71] The mechanism of photoinduced electron transfer has been also studied in organic thin films formed on the surface of semiconductor and metal.[72-75] The SAMs with regular structure and

tightly bound to the surface of a gold substrate are suitable for the electron-transfer system.[76-79] On the other hand, electron transfer through polypeptides has been also actively investigated in terms of the electron-mediating ability of α-helix and ß-sheet structures.[80-85] Significantly, hydrogen bonds, which are involved in these secondary structures, strengthen electronic coupling between an electron donor and an electron acceptor, and the electrostatic field generated by the dipole moment of the peptide accelerates the electron transfer.[83,86] Therefore, an α-helix structure has been expected to be a good medium for electron transfer (Figure 2).

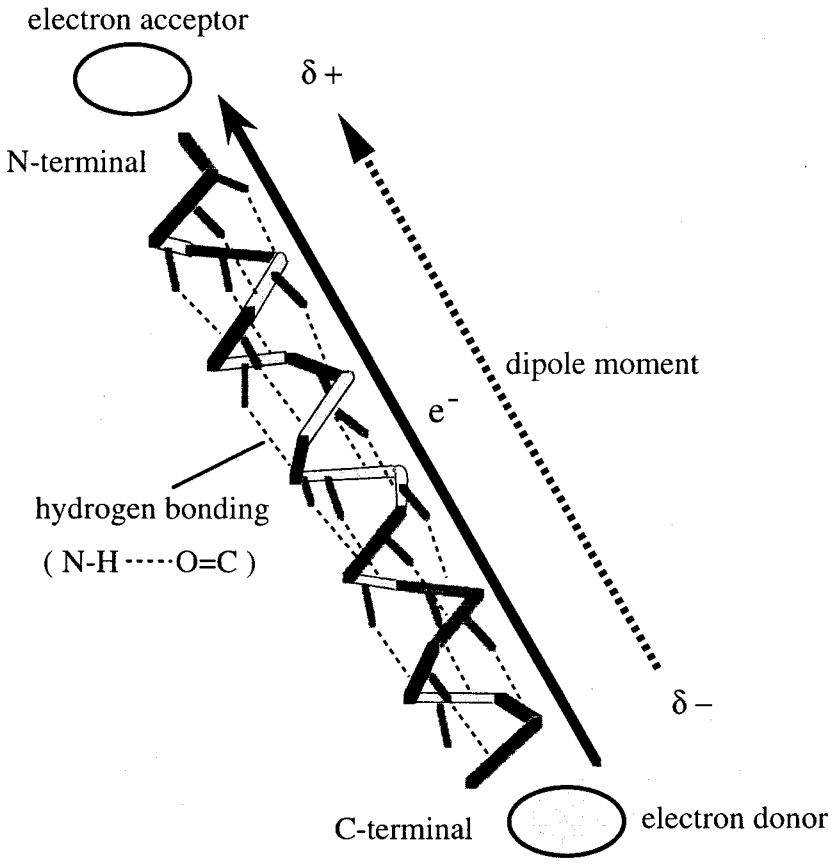

Figure 2. Schematic illustration of electron transfer through an α-helical structure.

Organic materials are commonly used for the photoelectronic materials such as display devices of liquid crystals[87] or electroluminescent materials,[88,89] xerographic materials from organic photoconductor,[90] and photochromic optical memory.[91] Given stalemate of semiconductor technology supporting the current electronics industry, the development of organic molecular devices is indispensable. Downsizing of semiconductor circuits below the sub-micrometer region is difficult due to the limit of optical lithography. On the other hand, organic molecules and their assemblies are within the size of the nanometer region. If the methodology of molecular assembling and nanofabrication technology progress to realize their use as computation and memory element, memory device of higher density, downsizing of circuits and processing with higher speed will become a reality. Because cheap and versatile organic materials are available, organic molecular devices are the most promising for the fundamental technology of the 21st century. Since the proposal of molecular electronics by Carter,[92] one molecule system such as molecular wires,[93,94] molecular transistors,[95] molecular optical switches and optical gates[96-98] has been reached for.

With the background described above, artificial photoenergy-harvesting system and electron-transport system were constructed by molecular-assembling techniques, and photoinduced energy transfer and electron transfer were investigated in the present thesis. Monolayers or vesicular bilayer membranes composed of chromophoric amphiphiles were designed for photoenergy-harvesting system, because they hold the chromophores in an ordered arrangement. The present author chose self-assembled monolayers composed of oriented α-helical peptides for electron-transport system for their stability and regularity, peptide-bond mediation of electron transfer and dipolar acceleration of electron transfer. The present investigation includes several characteristic points. First, the photophysical processes in molecular assemblies including energy migration, energy transfer, and electron transfer were fully explained on the basis of the elemental photophysical processes of isolated molecules or molecules in solution. Second, photoenergy-harvesting chromophores, photoenergy-

trapping sensitizers and electron acceptors were built for the first time in bilayer membranes to mimic the photosynthetic reaction center. Third, photocurrent generation was demonstrated in the helical peptide SAMs, showing the helical peptides to mediate electron transfer efficiently on the gold substrate. Fourth, the photoenergy-harvesting system and the photocurrent-generation system were combined together to construct a novel photon-electron conversion system.

A nonnatural amino acid carrying an *N*-ethylcarbazolyl (ECz) group[99] was used in all molecular systems in this thesis. Due to the long critical distance of an ECz group for energy migration,[100] efficient energy migration is expected to take place among ECz groups arranged in a high density in membrane. As photoexcited ECz group is a strong electron donor, it will become an excellent photosensitizer.[101] Furthermore, by using amphiphile compounds containing an ECz-carrying amino acid derivative, hydrogen bonds are formed among amphiphiles to stabilize their monolayers and bilayer membranes and to provide electron-transfer pathway in the membranes.

This thesis consists of seven chapters in two parts. In Part I of the thesis, efficient photoinduced energy transfer or electron transfer utilizing facile energy migration among ECz groups in monolayers or bilayer membranes composed of amphiphiles carrying an ECz group (5Cz18, 5Cz18Z; Figure 3) were investigated. The membrane composed of 5Cz18 has a cationic surface, while the surface of 5Cz18Z membrane is electrostatically neutral. Although excimer is easily formed to act as a photoenergy trap in films of polymers carrying a chromophoric group in the side chain[102-104], which interferes with energy migration among chromophores, excimer is hardly formed in the bilayer membranes of amphiphiles carrying an *N*-alkylcarbazolyl group despite of high density of chromophores.[99,105]

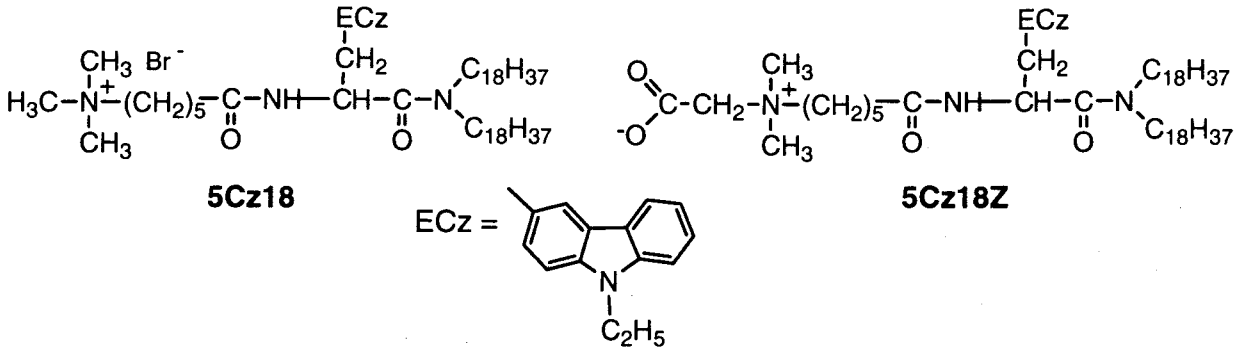

Figure 3. Molecular structures of 5Cz18 and 5Cz18Z.

In Chapter 1, an electron acceptor carrying a terephthaloyl group was introduced in the 5Cz18 bilayer membrane (Figure 4) and the fluorescence quenching by the terephthaloyl group was measured and analyzed by computer simulation to determine the number of energy migration steps among ECz groups within the fluorescent lifetime. The rate of hole transfer among ECz groups was also investigated on the basis of the lifetime of the ECz radical cation generated by laser photolysis of the bilayer membrane. The rate of hole transfer is one of the important factors determining the stability of charge-separated state.

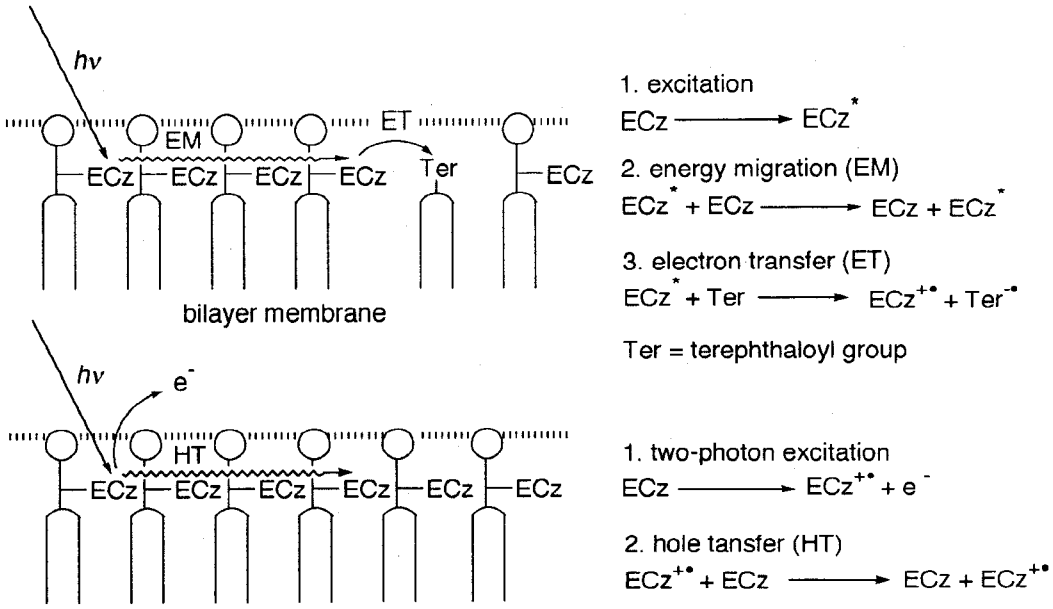

Figure 4. Schematic illustration for photoinduced electron transfer from the ECz group to the terephthaloyl group after energy migration among ECz groups (top), and hole transfer among ECz groups (bottom) in the bilayer membrane composed of 5Cz18.

In Chapter 2, monolayers composed of 5Cz18Z and amphiphiles carrying an energy-accepting anthryl (Ant) group were prepared at the air/water interface, and energy transfer in the monolayers at the various molecular areas was examined by *in situ* fluorescence spectroscopy (Figure 5). Furthermore, a natural redox protein, cytochrome c (cyt.c), was introduced in the subphase of monolayer, and the dependence of the cyt.c partitioning into the monolayer on the molecular area and electrostatic properties of the monolayers were investigated by monitoring the fluorescence quenching by electron or energy transfer from the ECz group to cyt.c.

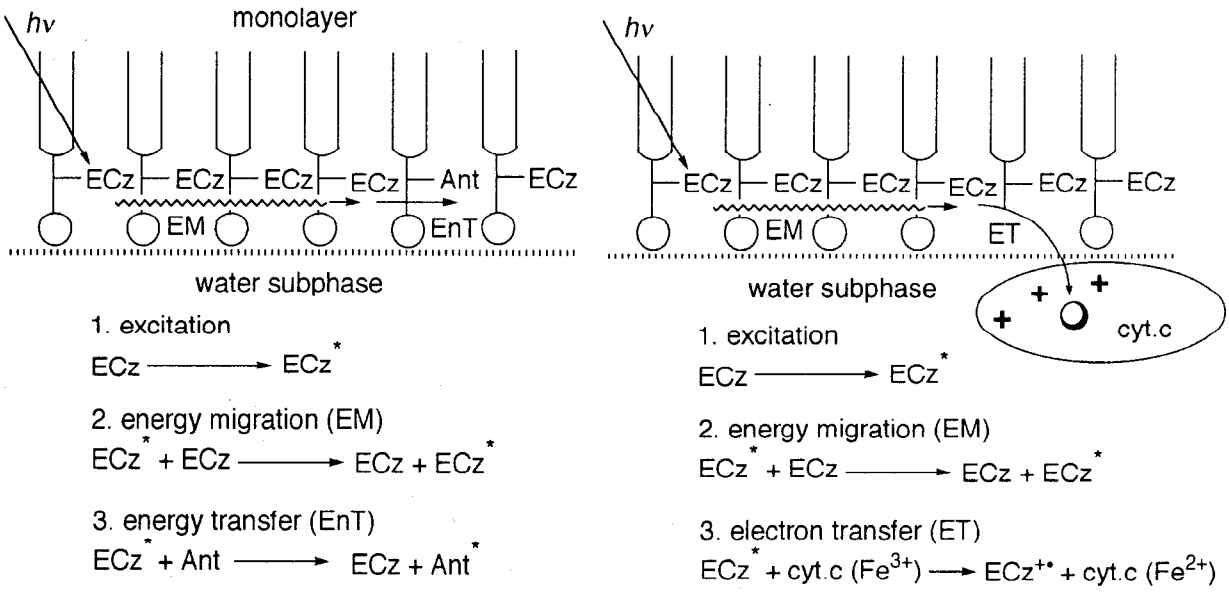

Figure 5. Schematic illustration for photoinduced energy transfer from the ECz group to the anthryl (Ant) group (left), and electron transfer to cytochrome c (cyt.c) (right) in the monolayer composed of 5Cz18Z at the air/water interface.

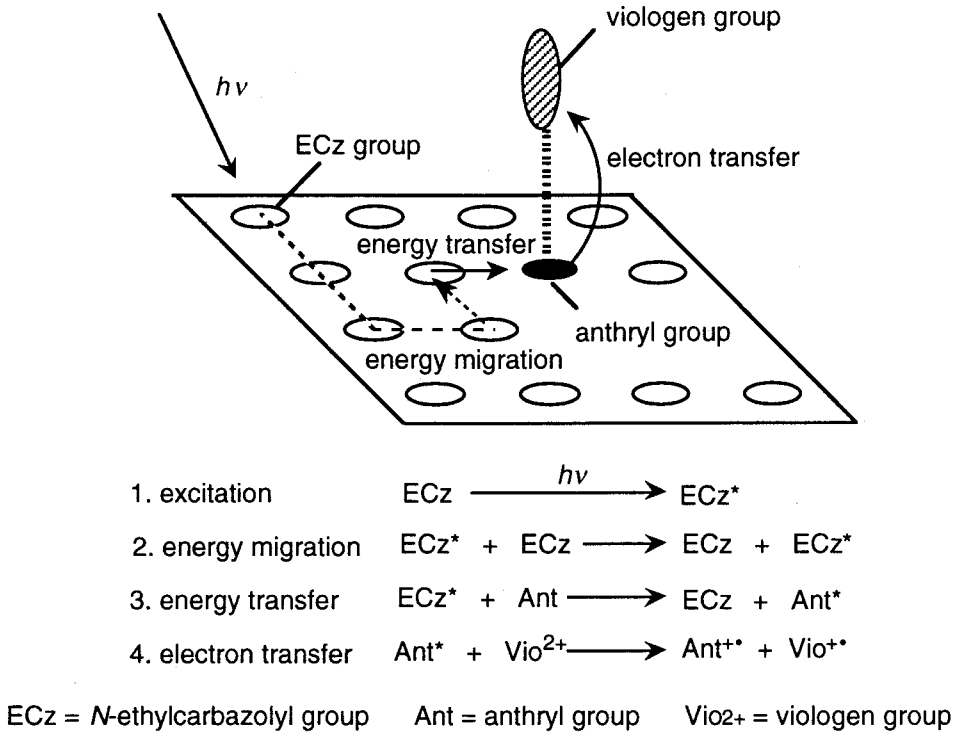

Figure 6. Schematic illustration for the novel photoinduced electron transfer system composed of 5Cz18Z and an amphiphilic acceptor carrying an anthryl group and a viologen group in a molecule.

In Chapter 3, a novel ternary system of photoinduced electron transfer was constructed by introducing amphiphilic acceptor carrying an energy-trapping Ant group and an electron-accepting viologen group into the 5Cz18Z bilayer membrane. In the membrane, the Ant group traps photoenergy migrating among ECz groups, and the excited Ant group transfers electron to the viologen group in a molecule (Figure 6). The electron transfer process including energy migration among ECz groups was analyzed by computer simulation to determine the number of energy migration steps. In Chapter 4, cyt.c was partitioned into the bilayer membranes of 5Cz18 or 5Cz18Z, and photoreduction of cyt.c utilizing energy migration among ECz groups in the presence of a sacrificial donor was investigated (Figure 7). The effects of electrostatic properties of the membrane surface and sacrificial donors on the reduction rate of cyt.c were investigated.

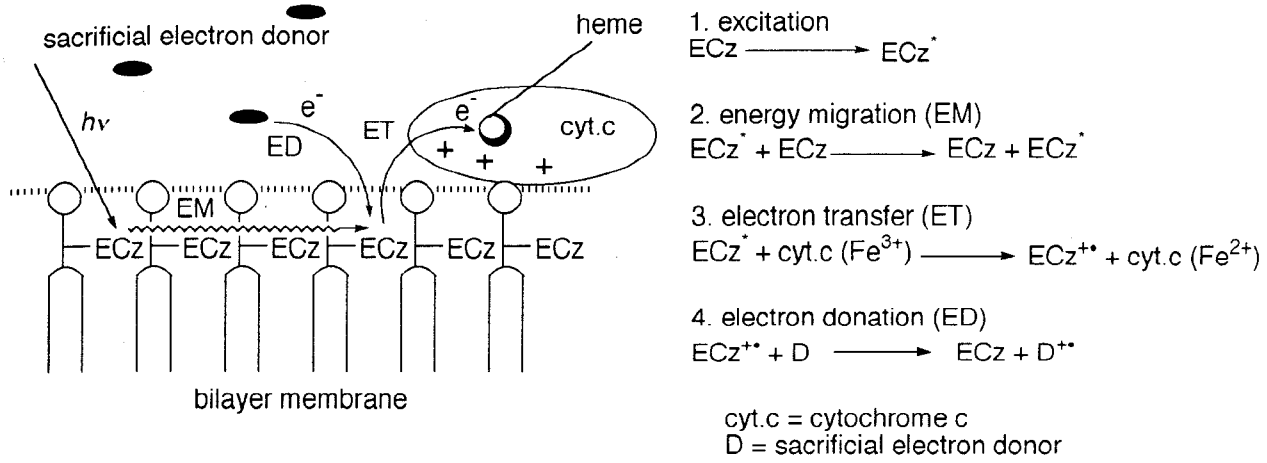

Figure 7. Schematic illustration for photoreduction of cytochrome c (cyt.c) by electron transfer from the ECz group after efficient energy migration among ECz groups in the bilayer membrane composed of ECz-containing amphiphiles.

In Part II of the thesis, α-helical peptide carrying an ECz group and a disulfide group at the respective terminals were synthesized, and self-assembled monolayers (SAMs) on the gold substrate were prepared from the helical peptide. Photoinduced electron transfer across the monolayer was investigated. These SAMs are expected to be an effective electron transport assembly due to the mediator property of the peptide linkage and acceleration effect of dipole moment. An alternating sequence of L-alanine (Ala) and α-aminoisobutyric acid (Aib) was chosen for the peptide backbone to take a helical structure either in monolayers at the air/water interface or in SAMs.[21,106,107] In Chapter 5, the arrangement and orientation of helical peptides carrying an ECz group in monolayers formed at the air/water interface and on a gold substrate were investigated by various spectroscopic methods. The arrangement and orientation of the helices at the air/water interface were investigated by *in situ* fluorescence spectroscopy, computer simulation, and circular dichroism (CD) spectroscopy, and those in SAMs were investigated by fluorescence spectroscopy, Fourier transform infrared reflection-absorption spectroscopy (FTIR-RAS), and quartz crystal microbalance (QCM) measurements (Figure 8).

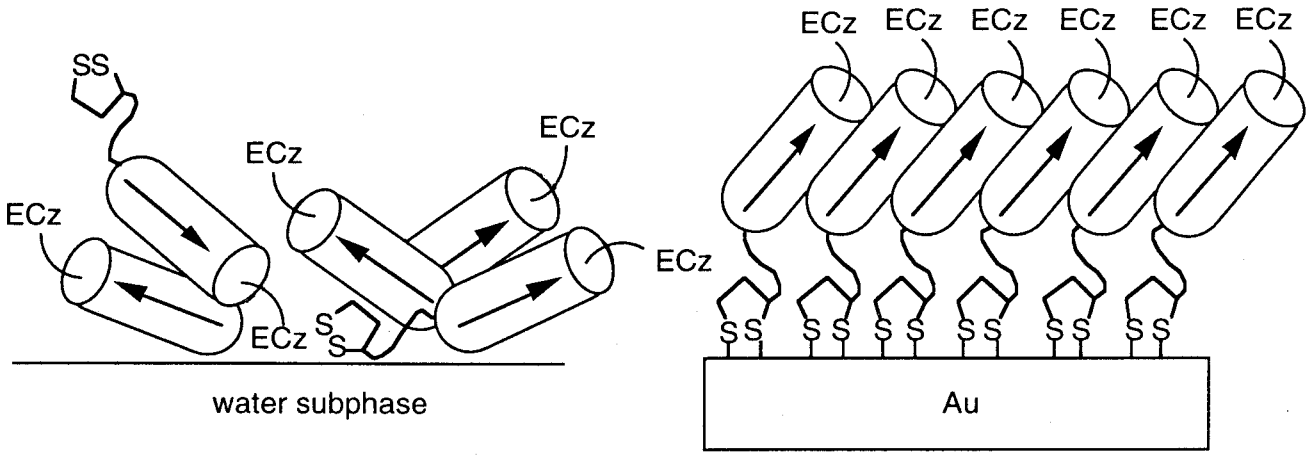

Figure 8. Schematic illustration of the arrangement and orientation of helical peptide carrying an ECz group and a disulfide group in the monolayer at the air/water interface (left) and in a self-assembled monolayer on a gold substrate (right).

In Chapter 6, photocurrent generation from these helical peptide SAMs by photoexcitation of the ECz groups in an aqueous solution containing an electron donor or acceptor was investigated (Figure 9). The dependence of the efficiency of photocurrent generation on the direction of dipole and the length of peptide chain were investigated. Furthermore, peptide chain and saturated hydrocarbon chain were compared in terms of mediation of electron transfer. In Chapter 7, a bicomponent SAM of dialkyl compounds carrying an ECz group and helical peptides carrying an Ant group were prepared for efficient generation of photocurrent as a result of photoenergy harvest by energy migration among ECz groups and electron transport through the helical peptide (Figure 10). This system is an integrated artificial photosynthetic system by the combination of a photoenergy-harvesting membrane system containing chromophores of high density and helical peptide mediator for electron transport. These molecular assemblies are useful for clarifying the fundamental chemistry of photosynthesis, and helpful for development of photoelectronic devices which are indispensable in the 21st century. The experimental results will be described in the following chapters.

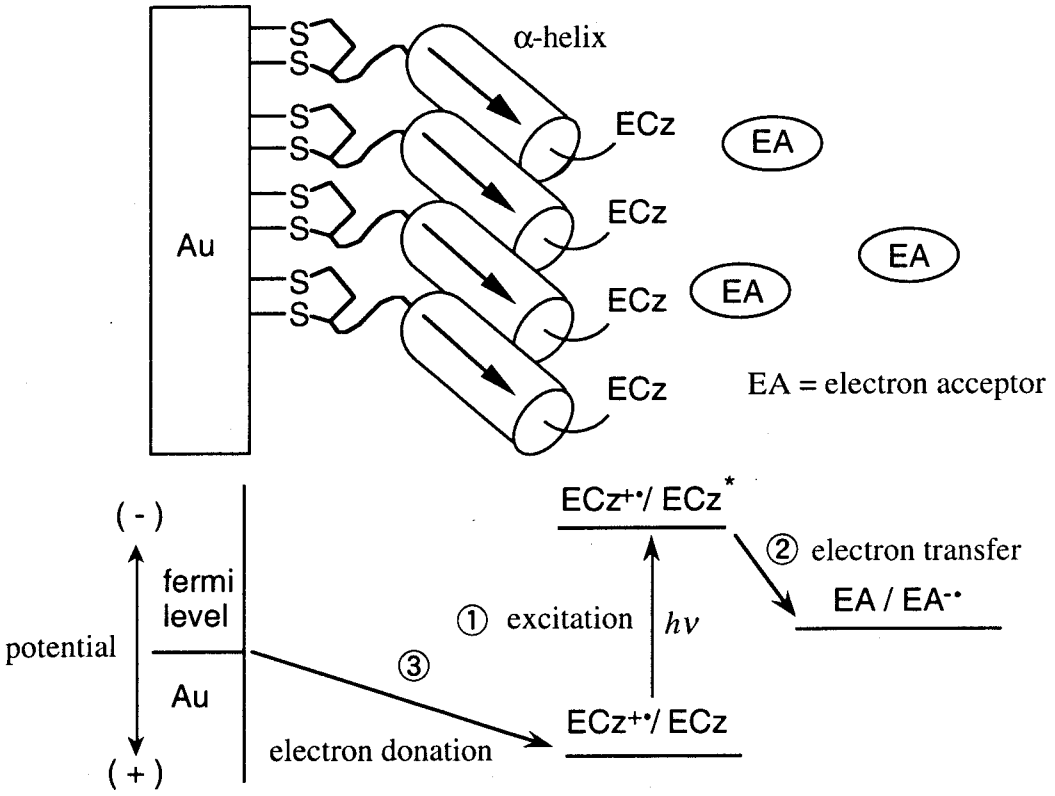

Figure 9. Schematic illustration for photocurrent generation by an α-helical peptide SAM where the electron donation is accelerated by the dipole moment of the helix.

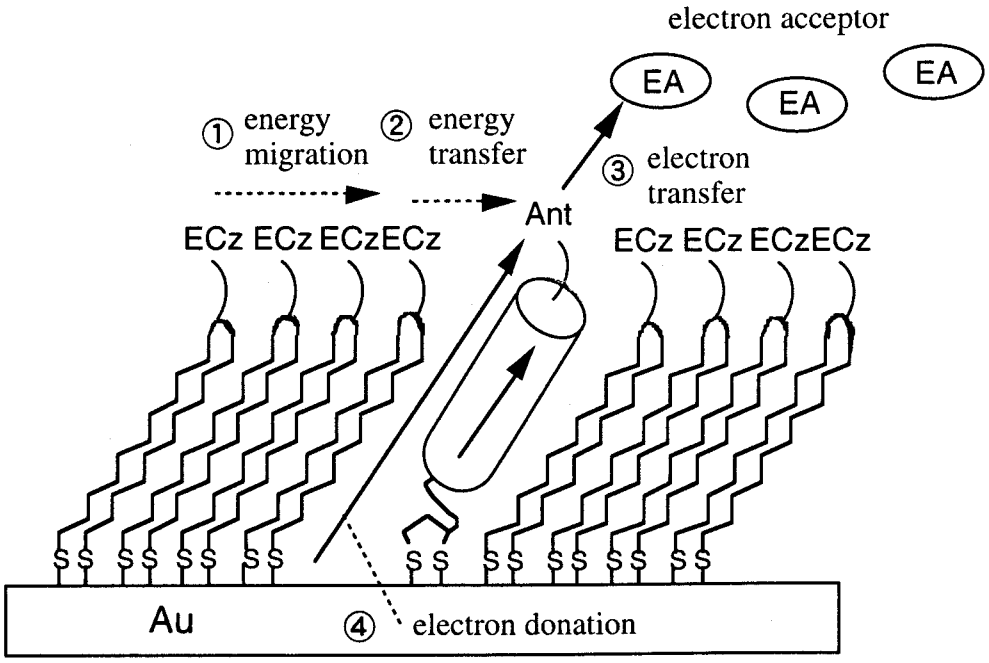

Figure 10. Schematic illustration of a photocurrent generation system by combination of photoenergy-harvesting and electron-transport systems. This system is the bicomponent self-assembled monolayer composed of dialkyl compounds carrying an ECz group and helical peptides carrying an anthryl group.

Reference

1) Förster, T. *Comprehensive Biochemistry*, vol 22; Elsevier: Amsterdam, 1967.

2) Duysens, L. N. M. *Transfer of Excitation Energy in Photosynthesis, PhD Thesis*: Utrecht, 1952.

3) Austin, R., Buhks, E., Chance, D., DeVault, D., Dutton, P. L., Frauenfelder, H., Gol'denskii, V. I., Eds. *Protein Structure: Molecular and Electronic Reactivity*; Springer-Verlag: New York, 1987.

4) Shin, M.; Tagawa, K.; Arnon, D. I. *Biochem. Z.* **1963**, *338*, 84.

5) Joliot, P. *Biochim. Biophys. Acta* **1965**, *102*, 116.

6) Kagawa, Y. *Methods in Enzymol.* **1986**, *126*, 1.

7) Beratan, D. N.; Onuchic, J. N.; Winkler, J. R.; Gray, H. B. *Science* **1992**, *258*, 1740.

8) Betts, J. N.; Beratan, D. N.; Onuchic, J. N. *J. Am. Chem. Soc.* **1992**, *114*, 4043.

9) Deisenhofer, J.; Michel, H. *Angew. Chem., Int. Ed. Engel.* **1989**, *28*, 829.

10) Warshel, A.; Chu, Z. T.; Parson, W. W. *Science* **1989**, *246*, 112.

11) Hol, W. G. J. *Prog. Biophys. Mol. Biol.* **1985**, *45*, 149.

12) Lehn, J. -M. *Science* **1985**, *227*, 849.

13) Langmuir, I. *J. Chem. Phys.* **1933**, *1*, 756.

14) Blodgett, K. B.; Langmuir, I. *Phys. Rev.* **1935**, *51*, 964.

15) Bangham, A. D.; Horne, R. W. *J. Mol. Biol.* **1964**, *8*, 660.

16) Singer, S. J.; Nicolson, G. L. *Science* **1972**, *175*, 720.

17) Kunitake, T.; Okahata, Y. *J. Am. Chem. Soc.* **1977**, *99*, 3860.

18) Bader, H.; Ringsdorf, H.; Schmidt, B. *Angew. Makromol. Chem.* **1984**, *123/124*, 457.

19) Yokoyama, M.; Inoue, S.; Kataoka, K.; Yui, N.; Okano, T.; Sakurai, Y. *Makromol. Chem.* **1989**, *190*, 2041.

20) Otoda, K.; Kimura, S.; Imanishi, Y. *Biochim. Biophys. Acta* **1993**, *1150*, 1.

21) Fujita, K.; Kimura, S.; Imanishi, Y.; Rump, E.; Ringsdorf, H. *J. Am. Chem. Soc.* **1994**, *116*, 2185.

22) LaBrenz, S. R.; Kelly, J. W. *J. Am. Chem. Soc.* **1995**, *117*, 1655.

23) Ghadiri, M. R.; Granja, J. R.; Milligan, R. A.; McRee, E. E.; Kazanovich, N. *Nature* **1993**, *366*, 324.

24) Laibinis, P. E.; Hickman, J. J.; Wrighton, M. S.; Whitesides, G. M. *Science* **1989**, *245*, 845.

25) Ulman, A. *An Introduction to Ultrathin Organic Films*; Academic Press: San Diego, CA, 1991.

26) Kuhn, H.; Möbius, D. *Angew. Chem.* **1971**, *83*, 672.

27) Tamai, N.; Yamazaki, T.; Yamazaki, I. *J. Phys. Chem.* **1987**, *91*, 841.

28) Yamazaki, I.; Tamai, N.; Yamazaki, T.; Murakami, A.; Mimuro, M.; Fujita, Y. *J. Phys. Chem.* **1988**, *92*, 5035.

29) Beddard, G. S.; Carlin, S. E.; Porter, G. *Chem. Phys. Lett.* **1976**, *43*, 27.

30) Fung, B. K. K.; Stryer, L. *Biochemistry* **1978**, *17*, 5241.

31) Takami, A.; Mataga, N. *J. Phys. Chem.* **1987**, *91*, 618.

32) Tamai, N.; Yamazaki, T.; Yamazaki, I.; Mizuma, A.; Mataga, N. *J. Phys. Chem.* **1987**, *91*, 3503.

33) Nakashima, N.; Kimizuka, N.; Kunitake, T. *Chem. Lett.* **1985**, 1817.

34) Kunitake, T.; Shimomura, M.; Hashiguchi, Y.; Kawanaka, T. *J. Chem. Soc., Chem. Commun.* **1985**, 833.

35) Sasaki, H.; Sisido, M.; Imanishi, Y. *Langmuir* **1990**, *6*, 1008.

36) Stryer, L.; Haugland, R. P. *Proc. Natl. Acad. Sci. U.S.A.* **1967**, *58*, 719.

37) Sisido, M.; Yagyo, K.; Kawakubo, H.; Imanishi, Y. *Int. J. Biol. Macromol.* **1982**, *4*, 313.

38) Miyashita, T.; Yoshida, H.; Murakata, M. *Polymer* **1987**, *28*, 311.

39) Ito, S.; Okubo, H.; Ohmori, S.; Yamamoto, M. *Thin Solid Films* **1989**, *179*, 445.

40) Stewart, G. M.; Fox, M. A.; *J. Am. Chem. Soc.* **1996**, *118*, 4354.

41) Jiang, D.-L.; Aida, T. *Nature* **1997**, *388*, 454.

42) Marcus, R. A. *J. Chem. Phys.* **1956**, *24*, 966.

43) Freed, K. F. *Acc. Chem. Res.* **1978**, *11*, 74.

44) DeSchryver, F. C.; Boens, N.; Put, J. *Adv. Photochem.* **1977**, *10*, 359.

45) Calcaterra, L. T.; Closs, G. L.; Miller, J. R. *J. Am. Chem. Soc.* **1983**, *105*, 670.

46) Paddon-Row, M. N.; Oliver, A. M.; Warman, J. M.; Smit, K. J.; DeHaas, M. P.; Oevering, H.; Verhoeven, J. W. *J. Phys. Chem.* **1988**, *92*, 6958.

47) Sessler, J. M.; Johnson, M. R. *Angew. Chem., Int. Ed. Engl.* **1987**, *26*, 678.

48) Wasielewski, M. R.; Niemczyk, M. P.; Johnson, D. G.; Svec, W. A.; Minsek, D. W. *Tetrahedron* **1989**, *45*, 4785.

49) Osuka, A.; Yamada, H.; Maruyama, K.; Mataga, N.; Asahi, T.; Yamazaki, I.; Nishimura, Y. *Chem. Phys. Lett.* **1991**, *181*, 419.

50) Beratan, D. N.; Onuchic, J. N.; Hopfield, J. J. *J. Chem. Phys.* **1987**, *86*, 4488.

51) Cadana, L. A.; Schanze, K. S. In *Electron Transfer in Biology and the Solid State, Inorganic Compounds with Unusual Properties*; Johnson, M. K., King, R. W., Kurtz, D. M., Jr., Kutal, G., Norton, M. L., Scott, R. A., Eds.; Advances in Chemistry 226, ACS: Washington, DC, 1990.

52) Isied, S. S.; Ogawa, M. Y.; Wishart, J. F. *Chem. Rev.* **1992**, *92*, 381.

53) Larsson, S. *J. Am. Chem. Soc.* **1981**, *103*, 4034.

54) Beratan, D. N.; Hopfield, J. J. *J. Am. Chem. Soc.* **1984**, *106*, 1584.

55) Larsson, S. *J. Chem. Soc., Faraday Trans. 2* **1983**, *79*, 1375.

56) Isied, S. S.; Ogawa, M. Y.; Wishart, J. F. *J. Phys. Chem.* **1993**, *97*, 11456.

57) Migita, M.; Okada, T.; Mataga, N.; Nishitani, S.; Kurata, N.; Sakata, Y.; Misumi, S. *Chem. Phys. Lett.* **1981**, *84*, 263.

58) Wasielewski, M. R.; Niemczyk, M. P. *J. Am. Chem. Soc.* **1984**, *106*, 5043.

59) Gust, D.; Moore, T. A. *Science* **1989**, *244*, 35.

60) Harriman, A.; Kubo, Y.; Sessler, J. *J. Am. Chem. Soc.* **1992**, *114*, 388.

61) Rege, P. J. F.; Williams, S. A.; Therien, M. J. *Science* **1995**, *269*, 1409.

62) Brugger, P. -A.; Grätzel, M. *J. Am. Chem. Soc.* **1980**, *102*, 2461.

63) Kalyanasundaram, K. *Photochemistry in Microheterogeneous System*; Academic Press: New York, 1987; Chapter 1.

64) Möbius, D. *Ber. Bunsenges. Phys. Chem.* **1978**, *82*, 848.

65) Richardson, T. *Chem. Br.* **1989**, 1218.

66) Ford, W. E.; Otvos, J. W.; Calvin, M. *Nature (London)* **1978**, *274*, 507.

67) Fendler, J. H. *Science* **1984**, *223*, 888.

68) Nakamura, H.; Motonaga, A.; Ogata, T.; Nakao, S.; Nagamura, T.; Matsuo, T. *Chem. Lett.* **1986**, 1615.

69) Ford, W. E.; Otvos, J. W.; Calvin, M. *Proc. Natl. Acad. Sci. U.S.A.* **1979**, *76*, 3590.

70) Rafaeloff, R.; Maliyackel, A. C.; Grant, J. L.; Otvos, J. W.; Calvin, M. *Nouv. J. Chim.* **1986**, *10*, 613.

71) Steinberg-Yfrach, G.; Liddell, P. A.; Hung, S.-C.; Moore, A. L.; Gust, D.; Moore, T. A. *Nature* **1997**, *385*, 239.

72) Wrighton, M. S. *J. Chem. Ed.* **1983**, *60*, 335.

73) Fox, M. A. *Pure. Appl. Chem.* **1988**, *60*, 1013.

74) Osa, T.; Fujihira, M. *Nature (London)* **1976**, *264*, 349.

75) Fujihira, M. In *The Photophysical Processes in Organic Molecular Systems*; Honda, K., Eds.; Elsevier: New York, 1991.

76) Hickman, J. J.; Ofer, D.; Zou, C.; Wrighton, M. S.; Laibinis, P. E.; Whitesides, G. M. *J. Am. Chem. Soc.* **1991**, *113*, 1128.

77) Black, A. J.; Wooster, T. T.; Geigen, W. E.; Paddon-Row, M. W.; *J. Am. Chem. Soc.* **1993**, *115*, 7924.

78) Kondo, T.; Ito, T.; Nomura, S.; Uosaki, K. *Thin Solid Film* **1996**, *284/285*, 652.

79) Akiyama, T.; Imahori, H.; Ajawakom, A.; Sakata, Y. *Chem. Lett.* **1996**, 907.

80) Sisido, M. In *Photophysics of Polymer*; Hoyle, C. E., Torkelson, J. M., Eds.; ACS Symposium Ser. 358, ACS: Washington, DC,1987; Chapter 26.

81) Sisido, M.; Tanaka, R.; Inai, Y.; Imanishi, Y. *J. Am. Chem. Soc.* **1989**, *111*, 6790.

82) Basu, G.; Kubasik, M.; Anglos, D.; Secor, B.; Kuki, A. *J. Am. Chem. Soc.* **1990**, *112*, 9410.

83) Galoppini, E.; Fox, M. A. *J. Am. Chem. Soc.* **1996**, *118*, 2299.

84) Langen, R.; Chang, I.-J.; Germanas, J. P.; Richards, J. H.; Winkler, J. R.; Gray, H. B. *Science* **1995**, *268*, 1733.

85) Gretchikhine, A. B.; Ogawa, M. Y. *J. Am. Chem. Soc.* **1996**, *118*, 1543.

86) Gray, H. B.; Winkler, J. R. *J. Electroanal Chem.* **1997**, *438*, 43.

87) Clark, N. A.; Kagerwall, S. T. *Appl. Phys. Lett.* **1980**, *36*, 9.

88) Tang, C. W.; Vanslyke, S. A. *Appl. Phys. Lett.* **1987**, *51*, 913.

89) Burroughes, J. H.; Bradley, D. D. C.; Brown, A. R.; Marks, R. N.; Mackay, K.; Friend, R. H.; Burn, P. L.; Holmes, A. B. *Nature* **1990**, *347*, 539.

90) Eaton, D. F. *Top. Curr. Chem.* **1990**, *156*, 199.

91) Darcy, P. J.; Heller, H. G.; Strydom, P. J.; Whittal, J. *J. Chem. Soc. Perkin Trans.* **1981**, *1*, 202.

92) Carter, F. L., Siatkowsky, R. E., Woltjien, H., Eds. *Molecular Electronic Devices*; Elsevier: Amsterdam, 1988.

93) Arrhenius, T. S.; Blanchard-Deshe, M.; Dvolaitzky, M.; Lehn, J. -M.; Malthete, J. *Proc. Natl. Acad. Sci. USA* **1986**, *83*, 5355.

94) Goldhaber-Gordon, D.; Montemerlo, M. S.; Love, J. C.; Opitek, G. J.; Ellenbogen, J. C. *Proc. IEEE* **1997**, *85*, 521.

95) Jones, E. T. T.; Chyan, O. M.; Wrighton, M. S. *J. Am. Chem. Soc.* **1987**, *109*, 5526.

96) Hopfield, J. J.; Onuchic, J. N.; Beratan, D. *Science* **1988**, *241*, 817.

97) Debreczney, M. P.; Svec, W. A.; Wasielewski, M. R. *Science* **1996**, *274*, 584.

98) de Silvia, A. P.; Rademacher, J. T.; Rice, T. E. *Chem. Rev.* **1997**, *97*, 1515.

99) Taku, K.; Sasaki, H.; Kimura, S.; Imanishi, Y. *Amino Acids* **1994**, *7*, 311.

100) Förster, T. *Discuss. Faraday Soc.* **1959**, *27*, 7.

101) Tsuchida, A.; Yamamoto, M.; Nishijima, Y. *J. Phys. Chem.* **1984**, *88*, 5062.

102) Johnson, G. E. *J. Chem. Phys.* **1975**, *62*,4697.

103) Yokoyama, M.; Takayama, T.; Atsumi, M.; Yoshimura, M.; Shirota, Y.; Mikawa, H. *Macromolecules* **1975**, *8*, 101.

104) Yatsue, T.; Miyashita, T. *J. Phys. Chem.* **1995**, *99*, 16047.

105) Nakamura, H.; Fujii, H.; Sakaguchi, H.; Matsuo, T.; Nakashima, N.; Yoshihata, K.; Ikeda, T.; Tazuke, S. *J. Phys. Chem.* **1988**, *92*, 6151.

106) Otoda, K.; Kitagawa, Y.; Kimura, S.; Imanishi, Y. *Biopolymers* **1993**, *33*, 1337.

107) Miura, Y.; Kimura, S.; Imanishi, Y.; Umemura, J. *Langmuir* **1998**, *14*, 6935.

Part I Photoinduced Electron Transfer in a Monolayer or Bilayer Membrane Composed of *N*-Ethylcarbazole-Containing Amphiphiles

Chapter 1

Photoenergy Migration and Hole Transfer in a Bilayer Membrane of *N*-Ethylcarbazole-Containing Amphiphiles

Introduction

The photosynthetic process begins with photoenergy harvest and charge separation.[1] A bilayer membrane composed of chromophoric amphiphiles is expected to be an excellent model for a photoenergy-harvesting system because of the high density of chromophores in the two-dimensional membrane. In the membrane, the probability of photoinduced electron transfer to an acceptor molecule should be high due to efficient photoenergy migration among the chromophores. The molecular assembly of chromophoric amphiphiles may also stabilize chemical species produced in the process of charge separation. For example, in anionic micelles, the radical cation is stabilized by suppression of recombination with ejected electron by the negative charges on the micelle surface.[2]

A dialkylammonium-type amphiphile carrying an *N*-ethylcarbazolyl (ECz) group (5Cz18, Figure 1) has been synthesized, and the formation of vesicular assemblies in aqueous dispersion has been reported.[3] The bilayer membranes containing ECz groups have an advantage over polymer systems [4,5] in preventing excimer formation, which disturbs photoenergy migration, despite of high density of chromophores.[3,6] The 5Cz18 bilayer membrane showed facile energy migration among ECz groups as evidenced by fluorescence quenching with acrylamide. In order to estimate the efficiency of photoenergy migration in the 5Cz18 bilayer membrane, methyl terephthaloyldioctadecylamide (Ter18, Figure 1) was mixed in the membrane, and the fluorescence

quenching was investigated. The quenching experiment was simulated on the basis of electron transfer from the excited ECz group to the terephthaloyl group to determine the efficiency of photoenergy migration in the membrane.

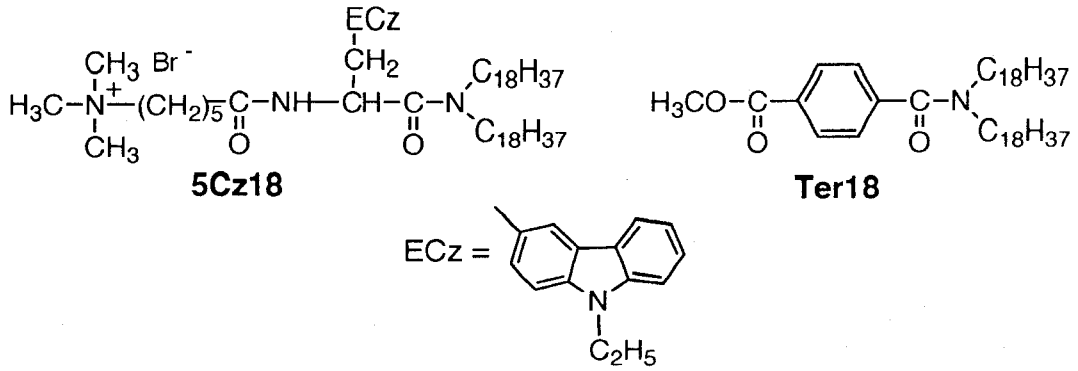

Figure 1. Molecular structures of 5Cz18 and Ter18.

An ECz group ejects an electron by two-photon excitation to produce a radical cation. The stability of the radical cation was investigated by transient absorption spectroscopy. The ejected electrons would be trapped by amide groups in the membrane. The radical cation might be quenched after reaching the anionic site by diffusion. The rate of hole transfer was estimated from the lifetime of the radical cation. The suitability of chromophoric bilayer membranes for charge separation is discussed in terms of the stability of the radical cation.

Experimental Section

Materials. 5Cz18 was synthesized by the method in the literature.[3] Dioctadecyldimethylammonium bromide (DDAB) was purchased from Tokyo Kasei Co., Ltd. (Japan), and was recrystallized from ethyl acetate before use. Ter18 was synthesized by the procedure described below. The purity was checked by thin-layer chromatography (TLC). Solvent systems for TLC were (A) chloroform/methanol/acetic acid (95/5/3 v/v/v), (B) chloroform/methanol/ammonia water (13/5/1 v/v/v). The reaction product was identified by ^{1}H NMR (90 MHz) and elementary analysis. Terephthaloylchloride monomethyl ester (38.1 mg) was reacted with dioctadecylamine (100 mg) in chloroform (10 ml) in the presence of triethylamine (26.5 μl) at 50 °C for 1 h. After removal of the solvent, the remaining solid was dissolved in tetrahydrofuran and insoluble triethylamine hydrochloride was removed by centrifuge. The solvent was removed, the remaining oil was purified by a Sephadex LH-20 column using tetrahydrofuran as eluant, and the purified product was recrystallized successively from methanol and ethanol (20.1 mg, 15.2 % yield). TLC: R_f(A)=0.83, R_f(B)=0.90. ^{1}H NMR (90 MHz, $CDCl_3$): δ (ppm) 0.86 (6H, t, $CH_2CH_2(CH_2)_{15}CH_3$), 1.23 (60H, brs, $CH_2CH_2(CH_2)_{15}CH_3$), 1.51 (4H, s, $CH_2CH_2(CH_2)_{15}CH_3$), 3.07-3.41 (4H, brm, $CH_2CH_2(CH_2)_{15}CH_3$), 3.91 (3H, s, OCH_3), 7.33, 7.44, 8.00, 8.08 (4H, s, C_6H_4). Anal. Calcd for $C_{45}H_{81}NO_3$: C, 79.00; H, 11.93; N, 2.05. Found: C, 78.84; H, 11.99; N, 1.83.

Membrane preparation. A chloroform solution of 5Cz18 (0.2 mg) and Ter18 (0-5 mol%) was evaporated to form a thin film. The film was dried under vacuum, and was dispersed in water (6 ml) by using a bath-type sonicator at 40 °C for 1 min and a probe-type sonicator at 45 °C for 2 min under N_2 atmosphere. The mixed membrane of 5Cz18 and DDAB was prepared in a similar way, too.

Measurement. UV and fluorescence spectra were recorded on a Ubest-50 spectrometer (Jasco Co., Ltd., Japan) and an MPF-4 fluorometer (Hitachi Co., Ltd., Japan), respectively. Transient absorption spectra were recorded on an IMUC-7000 spectrometer (Otsuka Electronics Co., Ltd., Japan). The excimer-laser photolysis experiment was carried out after passing argon gas through the sample solution for 30 min. The sample was photoexcited by focused light pulse (351 nm, 54 mJ) from a XeF excimer laser (LPX-105, Lambda Physik Co., Ltd., Germany). The time response of the apparatus is 1.0 μs, which is the gate width of the multichannel photo-diode array with the image-intensifier tube. A single-photon-counting method was used for the measurement of fluorescence decay curves. Details of the apparatus for the measurements have been described before except a Ti:S laser (Model 3950, Tsunami Co., Ltd., Japan).[7] The full-width at half-maximum of the overall excitation pulse was 600 ps.

The molecular area of 5Cz18 in the monolayer was determined as follows. 5Cz18 was dissolved in chloroform at the concentration of 7.2×10^{-4} M. The 5Cz18 solution was spread on the aqueous phase by using a microsyringe, and equilibrated for 10 min before compression. The π-A isotherm was recorded at a constant rate of reducing area of 5 cm^2/min with a Langmuir trough (USI Co., Ltd., Japan). The inflection point in the isotherm was determined from the differential of the curve.

Results and Discussion

Photoenergy Migration in a Bilayer Membrane. 5Cz18 has been shown to take a vesicular structure with a diameter of 20-80 nm in water.[3] The vesicles have a skin of bilayer membrane, where the ground-state interaction of ECz groups is prohibited.[8] A mixed membrane of 5Cz18 and Ter18 (95/5 mol/mol) showed an UV spectrum similar to the 5Cz18 membrane, suggesting that the Ter18 mixing does not influence the bilayer structure.

Fluorescence spectra of 5Cz18 in water were measured with varying concentrations of Ter18 and at two different temperatures. The fluorescence quenching of 5Cz18 with Ter18 is shown in the form of the Perrin plot in Figure 2.

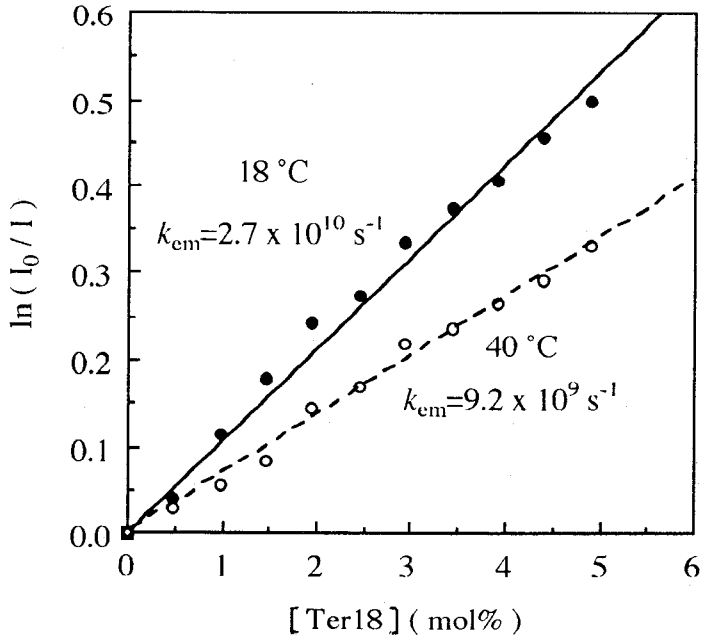

Figure 2. Perrin plot of the fluorescence quenching of the 5Cz18 bilayer membrane with Ter18. The experimental data at 18 °C (●) and 40 °C (○) are shown together with the result of computer simulation by taking k_{em} to be 2.7 x 10^{10} s^{-1} (—) and 9.2 x 10^{9} s^{-1} (---).

The quenching data were nearly on the straight line in the Perrin plot, which is reasonable because the diffusion of the amphiphiles in the membrane is severely restricted even at the higher temperature (less than 0.1 Å during the lifetime of the ECz group). Notably, the quenching rate at a temperature (18 °C) below the phase-transition temperature (Tc) of 25.4 °C [3] is higher than that above the Tc (40 °C). The quenching rate in the bilayer membrane is high because of facile energy migration. Therefore, the high quenching rate in a gel-state membrane may be due to easy migration of excitation energy among chromophores suitably fixed in the membrane.

Computer Simulation of the Fluorescence Quenching. Computer simulation of the fluorescence quenching process in the mixed membrane of 5Cz18 and Ter18 was carried out under an assumption that ECz groups and terephthaloyl groups are placed on a square lattice with a spacing of 8.8 Å (Figure 3), which is taken from the molecular area at the inflection point in the π-A isotherm of 5Cz18 spread on the water subphase. The surface pressure at the inflection point was 43 mN/m.

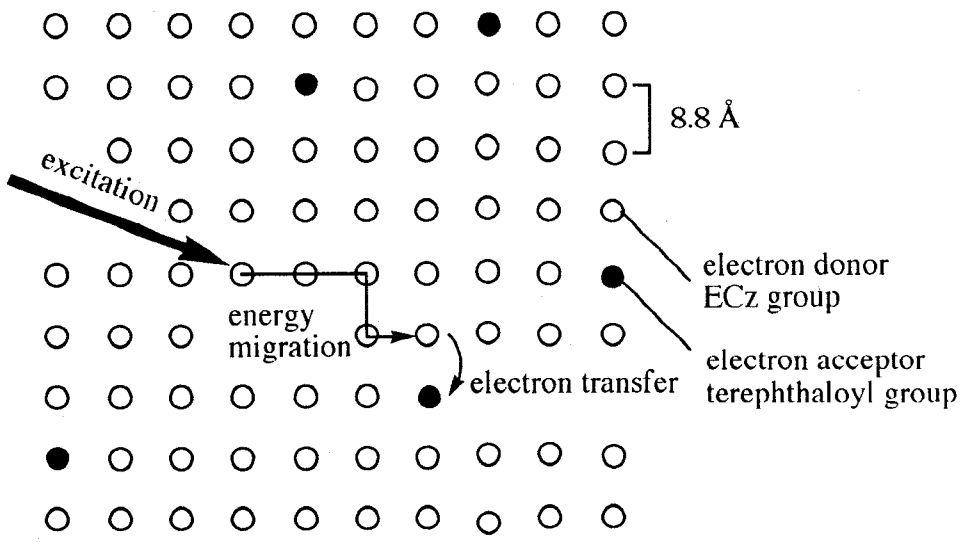

Figure 3. Schematic representation for the computer simulation of energy migration and electron transfer in the 5Cz18/Ter18 bicomponent bilayer membrane.

The ECz groups and the terephthaloyl groups were distributed randomly on 900 lattice points. The decay curve of the monomer fluorescence of the 5Cz18 membrane was measured and fitted to a two-exponential function. The decay times (their weights) are 1.25 ns (0.82) and 10.8 ns (0.18) (average = 2.98 ns) at 18 °C and 1.23 ns (0.84) and 10.5 ns (0.16) (average = 2.71 ns) at 40 °C. Since the quantum yield was 0.22 at 18 °C, k_f (the radiative transition rate) and k_{nr} (the nonradiative transition rate) are calculated to be 7.4 x 10^7 s^{-1} and 2.6 x 10^8 s^{-1}, respectively.[3] Similarly, the quantum yield of 0.19 at 40 °C gives 6.9 x 10^7 s^{-1} of k_f and 3.0 x 10^8 s^{-1} of k_{nr}. The electron transfer rate from the ECz group to the terephthaloyl group (k_{et}) was estimated from the quenching of *N*-ethylcarbazole by dimethyl terephthalate in the poly(methyl methacrylate) matrix.[9] The Perrin plot of the quenching were replotted by k_{et} vs. r (the average distance between *N*-ethylcarbazole and the quencher), which was well fitted by $k_{et} = 4.5 \times 10^{14} \times \exp(-1.55r)$. The excited ECz group may loose the excitation energy either by fluorescence emission (radiative deactivation), by internal quenching (nonradiative deactivation), or by quenching with the terephthaloyl group. The frequency of emission was calculated for 10^5 different distributions of 5Cz18 and Ter18 on the square lattice. The simulation was done by setting the value of k_{em} (the rate of energy migration between the ECz groups) with using k_f, k_{nr}, and k_{et} described above. The result of simulation is shown in Figure 2. The experimental points fall exactly on the simulation curves by taking values of k_{em} being 2.7 x 10^{10} s^{-1} at 18 °C and 9.2 x 10^9 s^{-1} at 40 °C. Thus, the number of energy migration during the lifetime of the excited ECz group is 360 at 18 °C and 113 at 40 °C.

Comparison of the k_{em} with the Expected Value. The rate of the energy migration between ECz groups in the membrane (k_{em}') was calculated by using the Förster 's equation (1).[10]

$$k_{em}' = \frac{9000\kappa^2(\ln 10)k_f J}{128\pi^5 n^4 N r^6} \qquad (1)$$

where κ^2, J, n, N, and r represent the orientation factor, the overlap integral of the fluorescence spectrum and the absorption spectrum of 5Cz18, the refractive index, the Avogadro number, and the distance between ECz groups in the membrane, respectively. The orientation factor and the quantum yield at 18 °C are taken to be 2/3 [11] and 0.22, respectively. The k_{em}' value at 18 °C was 1.9 x 10^{10} s^{-1}, which is agreeable to the experimental value of k_{em} (2.7 x 10^{10} s^{-1}). The slight difference between k_{em}' and k_{em} may be due to the orientation factor of random orientation for the calculation. The ECz groups should be packed tightly in the membrane below the phase transition temperature where the rotational mobility as well as the translational diffusion is hindered. Therefore, κ^2 may be larger than 2/3 in the membrane.[12,13] In the present case, κ^2 of 0.95 yields the coincidence of k_{em}' and k_{em}. It is considered that the simulation was carried out under consistent conditions, the square lattice with the spacing of 8.8 Å and the expression of k_{et}, etc. In addition, the bilayer membrane of 5Cz18 should have the regular structure even in the presence of Ter18, probably because 5Cz18 and Ter18 are the same dialkyl-type compounds. The number of the energy migration of 360 at 18 °C should mean the efficient photoenergy-harvesting system of the 5Cz18 membrane.

Hole Transfer among ECz Groups. When the bilayer membrane is irradiated by an excimer-laser beam, a radical cation ($ECz^{+\bullet}$) is yielded by a biphotonic ejection of an electron. The hole produced hops among ECz groups under Coulombic force of an radical anion which is produced by trapping the electron ejected from the ECz group. The position of the geminate electron has been reported to be about 20 Å apart from the parent radical cation.[14]

Figure 4 shows transient absorption spectra of the 5Cz18 bilayer membrane at 18 °C.

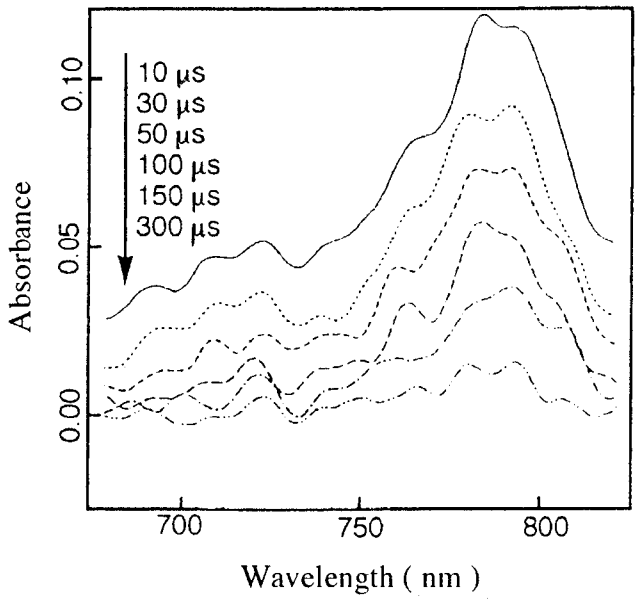

Figure 4. Transient absorption spectra of the 5Cz18 bilayer membrane at 18 °C at different time lapses after laser irradiation.

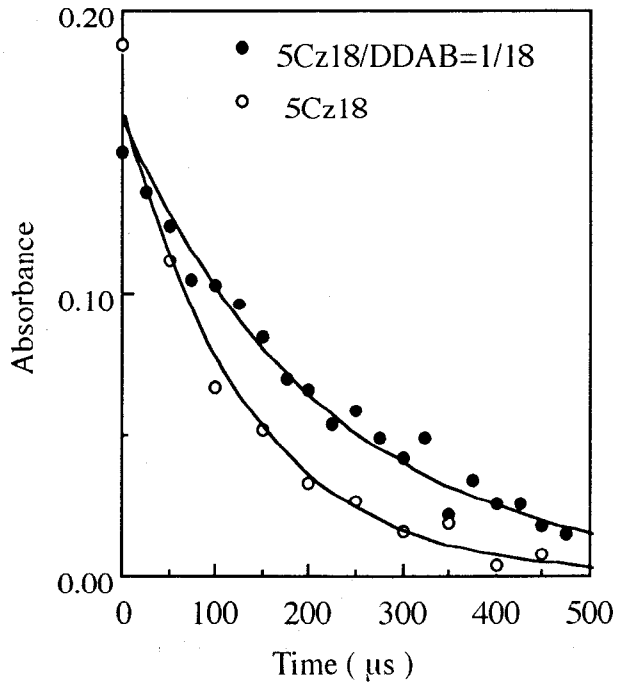

Figure 5. Decay profiles of transient absorption at 790 nm of the 5Cz18 bilayer membrane or the 5Cz18/DDAB (1/18 mol/mol) bicomponent bilayer membrane on laser photolysis at 18 °C.

The time-dependent change of the 790-nm absorbance (Figure 5) was fitted by a single exponential curve to obtain the lifetime of 130 μs for $ECz^{+\bullet}$ (Table 1).

Table 1. Lifetimes of $ECz^{+\bullet}$ generated on laser photolysis of the 5Cz18 bilayer membrane or the 5Cz18/DDAB (1/18 mol/mol) bicomponent bilayer membrane at two kinds of temperatures.

	5Cz18	5Cz18/DDAB
18 °C	130 μs	200 μs
50 °C	40 μs	60 μs

The lifetimes are longer than a few μs of the ECz group in a bilayer membrane reported by Nakamura et al.[6] A possible reason may be the existence of carbonyl groups in the present system. The electron ejected from the ECz group may first become a solvated electron and then be stabilized by trapping by the carbonyl group. On the other hand, the lifetime of $ECz^{+\bullet}$ was 40 μs at 50 °C (Table 1). The decreasing lifetime above Tc may be due to lateral diffusion of amphiphiles in the bilayer membrane, which facilitates encounter of $ECz^{+\bullet}$ with a radical anion.

The hole transfer among ECz groups was examined with a mixed membrane of 5Cz18 and DDAB. 5Cz18 and DDAB are the same type of cationic amphiphiles having a dioctadecyl group in the molecule. Therefore, a discrete phase separation of the mixed membrane should not occur. The decay of transient absorption at 790 nm of the mixed membrane with time was followed, and the results are shown in Figure 5. The lifetime of $ECz^{+\bullet}$ in the mixed membrane is significantly longer than that in the bilayer membrane of 5Cz18 (Table 1). The hole transfer in the mixed membrane must be hindered by separation of ECz groups by DDAB amphiphiles, resulting in suppression of recombination of $ECz^{+\bullet}$ and the radical anion. The different lifetimes for the 5Cz18 membrane and the mixed membrane below the Tc should be due to the faster hole transfer in the former membrane. The different lifetimes at the different temperatures should be due to the facilitated lateral diffusion of

the amphiphiles in the liquid-crystalline membrane. The difference of lifetimes of the radical cation in 5Cz18 membrane at different temperatures is nearly the same as the difference of lifetimes of the radical cation in the 5Cz18 membrane and in the 5Cz18/DDAB mixed membrane at 18 °C (Table 1), suggesting that the rate of hole transfer in the bilayer membrane of 5Cz18 is comparable to the rate of lateral diffusion of the amphiphile in the membrane (10^{-8} cm^2/s).[15]

The rate of the hole transfer in the poly(*N*-vinylcarbazole) film has been reported to be 10^{-5} cm^2/s.[16] Thus, the rate of the hole transfer in the bilayer membrane is considered to be remarkably slow. The radical cation in the bilayer membrane is not likely to interact with the neighboring ECz groups, because the broadening of the absorption of the radical cation seen in the poly(*N*-vinylcarbazole) film was not observed. Therefore, the slow rate should be due to the longer distance between the neighboring ECz groups (about 9 Å) than that in poly(*N*-vinylcarbazole) (3-4 Å). The longer distance should weaken the electronic coupling for the hole transfer. The hole transfer is slow in the membrane, leading to the suppression of charge recombination to generate the long-lived radical cation.

References and Notes

1) Deisenhofer, J.; Michel, H. *Angew. Chem. Int. Ed. Engl.* **1989**, *28*, 829.

2) Takeyama, N.; Sakaguchi, H.; Hashiguchi, Y.; Shimomura, M.; Nakamura, H.; Kunitake, T.; Matsuo, T. *Chem. Lett.* **1985**, 1735.

3) Taku, K.; Sasaki, H.; Kimura, S.; Imanishi, Y. *Amino Acids* **1994**, *7*, 311.

4) Johnson, G. E. *J. Chem. Phys.* **1975**, *62*,4697.

5) Yatsue, T.; Miyashita, T. *J. Phys. Chem.* **1995**, *99*, 16047.

6) Nakamura, H.; Fujii, H.; Sakaguchi, H.; Matsuo, T.; Nakashima, N.; Yoshihata, K.; Ikeda, T.; Tazuke, S. *J. Phys. Chem.* **1988**, *92*, 6151.

7) Ohmori, S.; Ito, S.; Yamamoto, M. *Macromolecules* **1991**, *24*, 2377.

8) Taku, K.; Sasaki, H.; Kimura, S.; Imanishi, Y. *Biophys. Chem.* **1992**, *44*, 187.

9) Private communication with Tsuchida, A. *N*-Ethylcarbazole at a low concentration and dimethyl terephthalate with varying concentrations were fixed in poly(methyl methacrylate) matrix. The fluorescence quenching data were analyzed by Perrin equation. Related papers: Tsuchida, A.; Sakai, W.; Nakano, M.; Yamamoto, M. *J. Phys. Chem.* **1992**, *96*, 8855, and Mataga, N.; Kubota, T. *Molecular Interaction and Electronic Spectra*; Marcel Deeker, Inc.: New York, 1970; pp 179-199.

10) Förster, T. *Discuss. Faraday Soc.* **1959**, *27*, 7.

11) Estep, T. N.; Thompson, T. E. *Biophys. J.* **1979**, *26*, 195.

12) Haas, E.; Katzir, E. K.; Steinberg, I. Z. *Biochemistry* **1978**, *17*, 5064.

13) Uemura, A.; Kimura, S.; Imanishi, Y. *Biochim. Biophys. Acta* **1983**, *729*, 28.

14) Tsuchida, A.; Sakai, W.; Nakano, M.; Yoshida, M.; Yamamoto, M. *Chem. Phys. Lett.* **1992**, *188*, 254.

15) Devaux, P.; McConnell, H. M. *J. Am. Chem. Soc.* **1972**, *94*, 4475.

16) Itaya, A.; Yamada, T.; Masuhara, H. *Chem. Phys. Let.* **1990**, *145*, 174.

Chapter 2

In situ Fluorescence Spectroscopic Studies of Energy Migration and Energy Transfer in a Monolayer of *N*-Ethylcarbazole-Containing Amphiphiles

Introduction

A monolayer composed of chromophoric amphiphiles is expected to be a suitable model for a photoenergy-harvesting system because of the highly ordered arrangement of chromophores in the two-dimensional membrane as well as a bilayer membrane as described in Chapter 1. The investigation on energy migration among chromophores, photoenergy transfer, or electron transfer from a donor to an acceptor in the monolayer is important, for example, for the development of molecular photoelectronic devices. In this chapter, the photophysical processes in the monolayer were investigated by *in situ* fluorescence spectroscopy to obtain informations on interaction of a donor amphiphile with an acceptor amphiphile within the same monolayer or with an acceptor protein in the water subphase at various surface pressures.

The bicomponent chromophoric monolayer is useful to investigate fundamental photophysical processes by a continuous measurement of fluorescence from chromophores in the monolayer which are placed at various interchromophoric distances by choosing suitable molecular areas.[1,2] For example, the efficiencies of photoenergy transfer or electron transfer in the monolayer at various average distances between chromophores (i.e. molecular area) can be compared between experimentally observed and theoretically calculated values to obtain information on interactions between a donor amphiphile and an acceptor amphiphile in the monolayer. In addition, interaction of

the monolayer with a specific compound in the subphase can be directly observed by *in situ* fluorescence spectroscopy at ambient surface pressures and molecular areas. Consequently, the partitioning of a compound added in the subphase into the monolayer can be investigated at various surface pressures. [3,4]

Two kinds of dialkylammonium-type amphiphiles carrying an ECz group (5Cz18, 5Cz18Z; Figure 1) were used to prepare monolayers. The monolayer of 5Cz18 possesses a cationic membrane surface, on the other hand, the monolayer of a zwitter ionic amphiphile 5Cz18Z will tolerate electrostatic interaction with a charged compound.

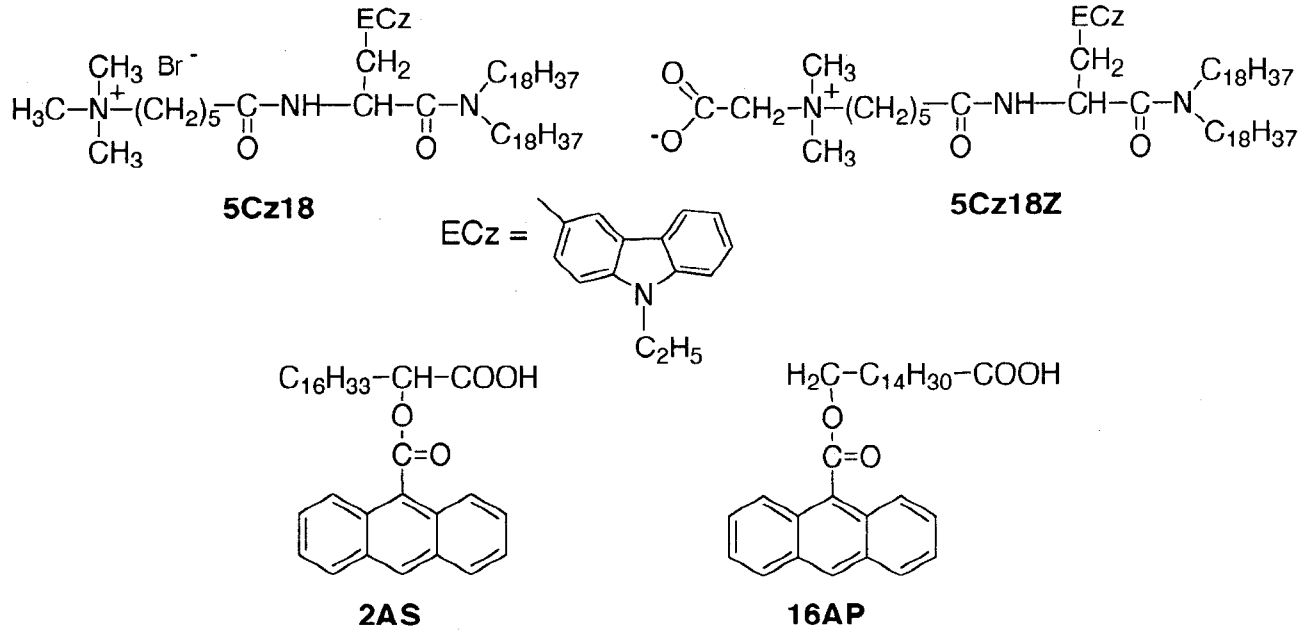

Figure 1. Molecular structures of 5Cz18, 5Cz18Z, 2AS, and 16AP.

Fluorescence from monolayers of 5Cz18 and 5Cz18Z was investigated at various surface pressures in the presence of two different acceptor molecules. One is anthracene-containing fatty acid, 2AS or 16AP (Figure 1), which is incorporated in the monolayer as an energy acceptor. The other is a familiar natural redox protein, cytochrome c (cyt.c) from horse heart, which is partitioned into the monolayer in equilibrium with that in the subphase. According to the Förster's mechanism, the energy migration by dipole-dipole interaction is affected by the distance and the orientation of the

chromophores.[5] The intensity change of the anthryl fluorescence upon compression of the monolayer was measured by *in situ* fluorescence spectroscopy and discussed in terms of the distance and orientation of chromophores. As electron transfer from the excited ECz group to cyt.c is thermodynamically favorable, the ECz group can be quenched by electron transfer.[6] However, cyt.c can be also an acceptor of photoenergy migrated via ECz groups because of the presence of heme group. Namely, the quenching of the ECz group arises from the both processes. In order to investigate the interaction between the monolayer and cyt.c, the quenching of the ECz group was investigated by *in situ* fluorescence spectroscopy on changing molecular area. Upon compression of the monolayer, energy migration among ECz groups will be accelerated to result in an efficient quenching by cyt.c, but desorption of cyt.c from the monolayer may result in suppression of the quenching.

Experimental Section

Materials. 5Cz18Z was synthesized from L-3-(3-*N*-ethylcarbazolyl)alanine (ECzAla) by the procedure described below. All intermediates were identified by ^{1}H NMR (270 MHz), and the final product was identified by ^{1}H NMR, elemental analysis, and mass spectroscopy. The purity was checked by TLC. Solvent systems for TLC were (A) chloroform/methanol/acetic acid (95/5/3 v/v/v), (B) chloroform/methanol/ammonia water (13/5/1 v/v/v), (C) *n*-butanol/acetic acid/water (10/1/3 v/v/v), and (D) *n*-butanol/acetic acid/water/pyridine (5/4/3/1 v/v/v/v).

***N'*-(*tert*-Butyloxycarbonyl)-L-3-(3-*N*-ethylcarbazolyl)alanine dioctadecylamide [1].** ECzAla (173 mg) was reacted with di-*tert*-butylcarbonate (240 mg) with $NaHCO_3$ (100 mg) in water (10 ml) / dioxane (20 ml) at 0 °C for 2 h and at 25 °C for 4 h. The solvent was evaporated, and *n*-hexane was added to precipitate the reaction product. The product was coupled with dioctadecylamine (180 mg) using *O*-(7-azabenzotriazol-1-yl)-1,1,3,3-tetramethyluronium haxafluoro-phosphate (HATU) (164 mg) with *N,N*-diisopropylethylamine (DIEA) (113 µl) in chloroform (10 ml) at 0 °C for 10 min and at 25 °C for 12 h. The solvent was evaporated, and methanol was added to precipitate the reaction product (197 mg, 36.3 % yield). TLC: R_f(A)=0.88, R_f(C)=0.94. ^{1}H NMR (270 MHz, $CDCl_3$): δ (ppm) 1.08 (6H, t, $CH_2(CH_2)_{16}CH_3$), 1.26 (64H, brs, $CH_2(CH_2)_{16}CH_3$), 1.43 (12H, brs, NCH_2CH_3,$(CH_3)_3CO$), 2.80 (4H, brm, $CH_2(CH_2)_{16}CH_3$), 3.14 (2H, d, $NHCHCH_2$), 4.33 (2H, q, NCH_2CH_3), 4.81 (1H, q, $NHCHCH_2$), 5.43 (1H, d, $NHCHCH_2$), 7.20-8.14 (7H, carbazolyl-*H*).

6-*N,N*-Dimethyl-*N*-methoxycarbonylmethylammoniohexanoic acid bromide [2]. *N,N*-Dimethylglycine methyl ester (1.90 ml) was dissolved in ethyl acetate (20 ml) containing 6-bromohexanoic acid (3.00 g) and the solution was refluxed at 70 °C for 4 h. The oil produced was separated and dried in vacuo. The product was washed with diethyl ether (1.45 g, 30.2 % yield). TLC: R_f(B)=0.20, R_f(D)=0.61. ^{1}H NMR (270 MHz, $CDCl_3$): δ (ppm) 1.37 (6H, brm, $N^+CH_2(CH_2)_3$), 2.24 (2H, t, CH_2COOH), 3.20 (8H, brs, N^+CH_3,$N^+CH_2(CH_2)_3$), 3.73 (3H, s, $COOCH_3$), 4.34 (2H, s, $N^+CH_2COOCH_3$).

***N'*,*N'*-Dimethyl-*N'*-carboxymethylammoniohexanoyl-L-3-(3-*N*-ethylcarbazolyl) alanine dioctadecylamide [5Cz18Z].** The Boc group of **1** (116 mg) was removed by treatment with 4 N HCl in dioxane, and the product dissolved in chloroform was reacted with **2** (81 mg) in the presence of HATU (105 mg) and DIEA (93 μl) at 0 °C for 30 min and at 25 °C for 18 h. After condensing the solution, the residual oil was dissolved in chloroform and precipitated with methanol. The solid product was hydrolyzed in a mixed solution of dioxane (1.9 ml) and 1 N aqueous NaOH solution (430 μl). The hydrolysis product was extracted with chloroform (50 ml) and washed with Tris-buffered solution (100 mM, pH 7.7). The solvent was removed and the remaining oil was purified by a Sephadex LH-20 column using methanol as eluant (121 mg, 46.9 % yield). TLC: R_f(B)=0.43, R_f(C)=0.20. ^{1}H NMR (270 MHz, $CDCl_3$): δ (ppm) 0.86 (6H, t , $CH_2(CH_2)_{16}CH_3$), 1.24 (64H, brs, $CH_2(CH_2)_{16}CH_3$), 1.38 (3H, t, NCH_2CH_3), 1.57 (6H, brm, $CH_2(CH_2)_3CH_2CO$), 2.18 (2H, t, $CH_2(CH_2)_3CH_2CO$), 2.92 (2H, d, $NHCHCH_2$), 3.16 (8H, brs, N^+CH_3,$CH_2(CH_2)_3CH_2CO$), 3.30 (4H, brm, $CH_2(CH_2)_{16}CH_3$), 3.97 (1H, q, $NHCHCH_2$), 4.33 (2H, q, NCH_2CH_3), 5.11 (2H, m, $N^+CH_2COO^-$), 6.83 (1H, d, $NHCHCH_2$), 7.18-8.04 (7H, carbazolyl-*H*). Anal. Calcd for $C_{63}H_{108}N_4O_4$+2.5H_2O: C,73.42; H,11.05; N,5.44. Found: C,73.39; H,10.89; N,5.45. MS (FAB): m/z 986 (calcd for $C_{63}H_{108}N_4O_4$ [(M+H)$^+$] m/z 985.84).

Cyt.c was purchased from Sigma Co., Ltd. (MO), and used without further purification. 2AS and 16AP were purchased from Molecular Probes Inc.(OR), and used after conversion to carboxylate form by washing with a 4 wt% aqueous $NaHCO_3$ solution. Experimental procedure for monolayer preparation was described in Chapter 1.

Measurement. *In situ* fluorescence spectroscopy was performed by a home-made apparatus schematically shown in Figure 2.

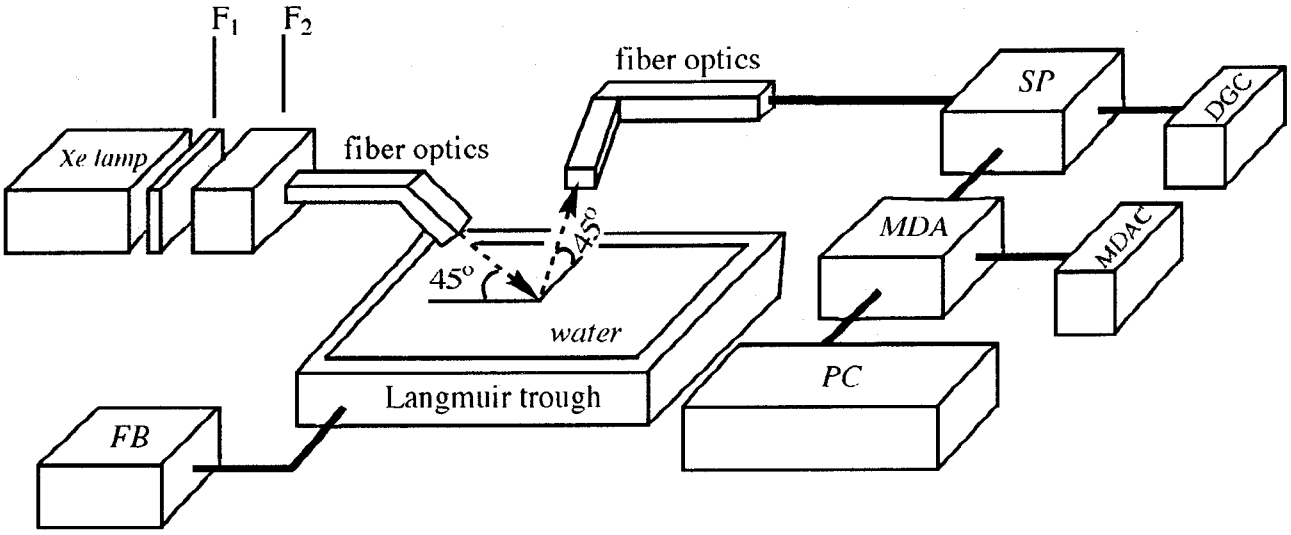

Figure 2. Experimental set-up for *in situ* fluorescence spectroscopy. F_1, a colored optical glass; F_2, a solution filter (methanol solution of anthracene-9-carboxylic acid); SP, spectrometer; DGC, diffraction-grating controller; MDA, multichannel diode array; MDAC, multichannel diode array controller; PC, personal computer; FB, film balance controller.

The light is sourced from a Xe lamp (500W, JASCO Co., Ltd., Japan), and filtered by a colored optical glass (U-340, HOYA Co., Ltd., Japan) and a solution filter (a methanol solution of anthracene-9-carboxylic acid). The light intensity was attenuated by setting a metal mesh on the optical path. The incident light occupied the area of 0.2 cm^2 on the surface. Fluorescence from the surface was guided by a fiber optics to a spectrometer (Unisoku Co., Ltd., Japan) with a multichannel photodiode array (C3966 PC-IMD, Hamamatsu Photonics Co., Ltd., Japan). The monolayer compression was operated by a Langmuir trough using a film balance controller (FSD-110, USI Co., Ltd., Japan). All measurements were performed at 20 °C.

Results and Discussion

***In Situ* Fluorescence Spectroscopy of Monolayers.** π-*A* Isotherms of the 5Cz18 and 5Cz18Z monolayers are shown in Figure 3. Both isotherms look similarly and show a collapse point at high surface pressures (41 mN/m for 5Cz18 and 43 mN/m for 5Cz18Z), indicating formation of stable monolayers.

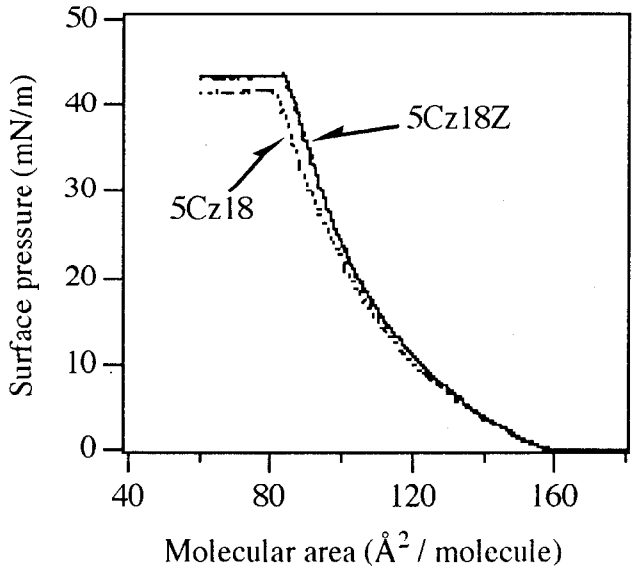

Figure 3. π-*A* Isotherms of the 5Cz18 and 5Cz18Z monolayers.

In situ fluorescence spectra of 5Cz18Z monolayer at various molecular areas are shown in Figure 4. Since the monolayer might have island structure of a sub-mm scale especially in the gaseous state,[4] the incident light was controlled to occupy a circular area of around 5-mm diameter on the surface to obtain embracing information of the monolayer. The intensity of the excitation light was attenuated so as not to cause any photobleaching during the measurement. Only the monomer emission of an ECz group (358 nm, 375 nm) without accompanying excimer emission (420 nm) was observed even at high surface pressures. This observation is consistent with that of 5Cz18 vesicles in water, which is attributed to the intrinsic property of an ECz group. Fluorescence intensity increased with initial

compression of the monolayer, but reached to a plateau level by further compression before collapse point (Figure 5). It is considered that concentration quenching occurs at higher densities of ECz groups in the monolayer, which overcomes increasing fluorescence intensity due to increasing density of chromophore.

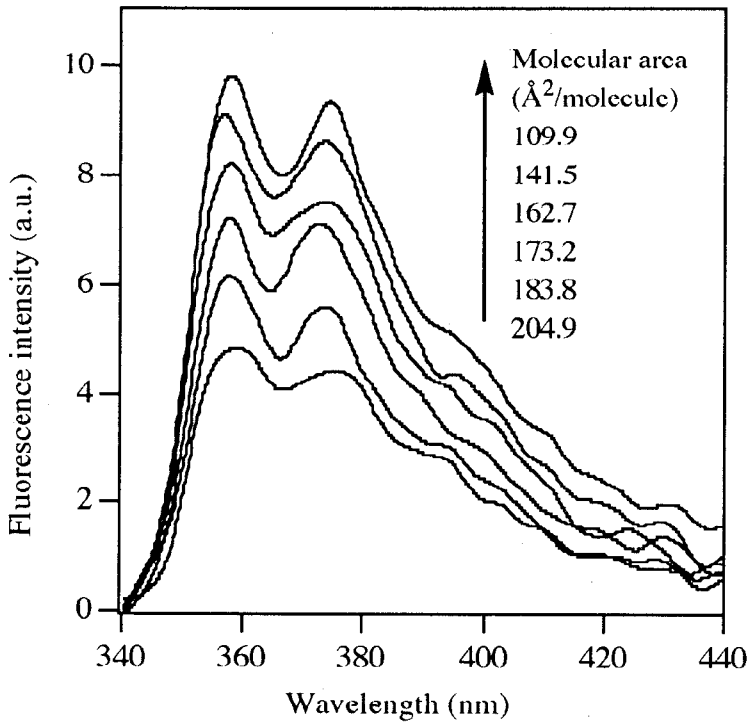

Figure 4. *In situ* fluorescence spectra of the 5Cz18Z monolayer at various molecular areas.

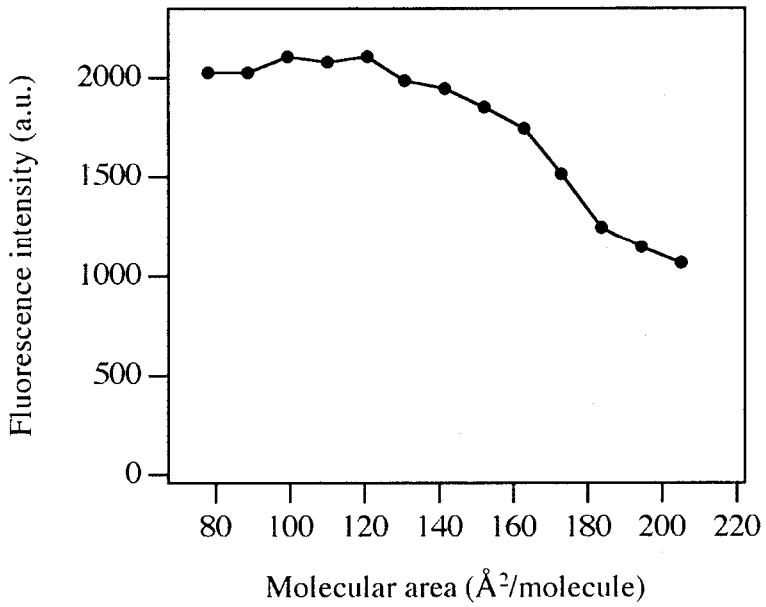

Figure 5. The dependence of the fluorescence intensity on the molecular area of the 5Cz18Z monolayer.

Energy Migration and Energy Transfer in a Monolayer. A bicomponent monolayer of 5Cz18Z and 2AS or 16AP was prepared, and energy migration among ECz groups and energy transfer from the ECz group to the anthryl group were investigated by *in situ* fluorescence spectroscopy. The critical distances for the energy migration between ECz groups and for the energy transfer from an ECz group to an anthryl group were calculated by using the Förster's equation to be 17.1 Å and 24.3 Å, respectively.[5,7] Therefore, photoenergy absorbed by the ECz groups in the monolayer is transferred to the anthryl group after migration via neighboring ECz groups.

Figure 6 shows *in situ* fluorescence spectra of 5Cz18Z/2AS and 5Cz18Z/16AP bicomponent monolayers at various molecular areas. The fluorescence from the anthryl group at 440 nm was observed, and the intensity increased with compression of the monolayer. These results together with the absence of fluorescence in the 2AS monolayer indicate the energy transfer from the ECz group to the anthryl group occurred in the bicomponent monolayers.

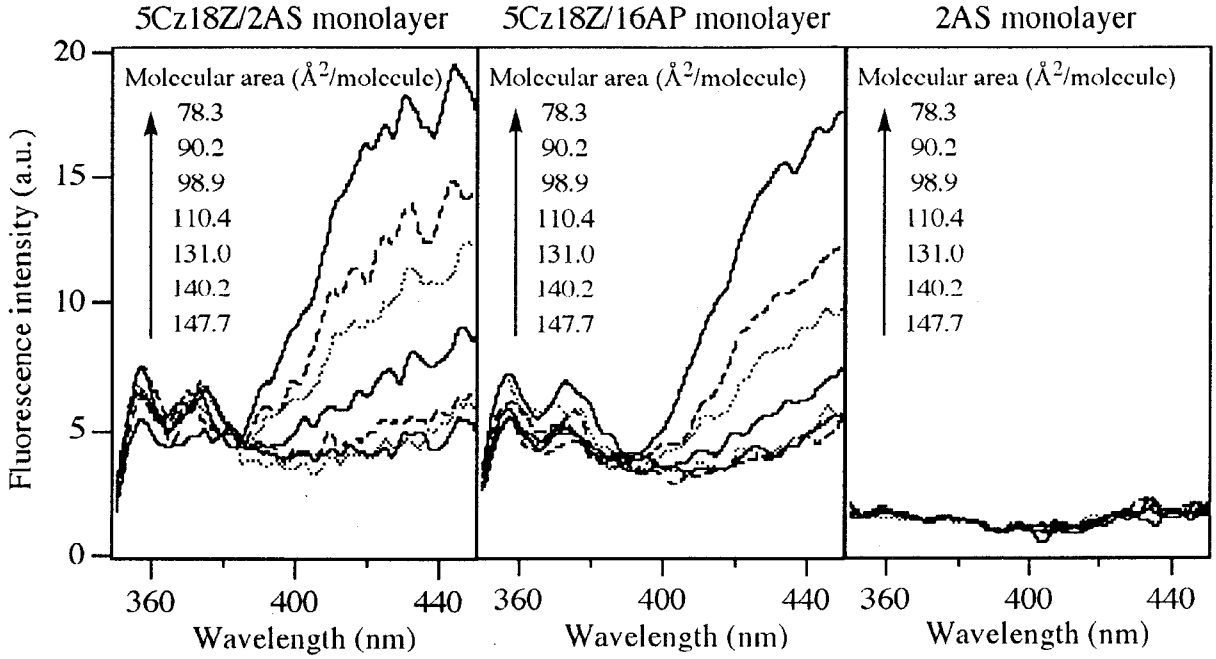

Figure 6. *In situ* fluorescence spectra of the 5Cz18Z/2AS, 5Cz18Z/16AP, and 2AS monolayers at various molecular areas. [5Cz18Z]/[2AS] = [5Cz18Z]/[16AP] = 25/1.

The fluorescence intensities of the anthryl group are plotted against the average distance between ECz groups in the monolayer (Figure 7a). It is evident that 2AS is a better acceptor for 5Cz18Z than 16AP at any surface pressures. The anthryl group of 2AS is located close to the surface of the subphase, whilst that of 16AP is located at the end region of the hydrophobic chains in the monolayer. The ECz group of 5Cz18Z is also located close to the surface of the subphase. Therefore, the energy transfer from 5Cz18Z occurs more easily to 2AS than to 16AP for geometrical proximity of 2AS at the same acceptor density in the monolayer. To say in other words, chromophores can be fixed at a defined depth of monolayers.

The energy-transfer rate increases by compression, suggesting the acceleration of energy migration among ECz groups due to shorter distances between the ECz groups at higher surface pressures. A double logarithmic plot of the emission intensity of the anthryl group vs. the average distance between ECz groups (Figure 7b) shows a linear relationship with a slope of -6, which

supports the consideration of the efficient energy migration among ECz groups by Förster's dipole-dipole interaction mechanism.[8] In addition, it is considered that the orientation of chromophores in the monolayer may not be affected severely upon compression in the range investigated.[9] Phase separation, which is often observed in bicomponent membranes, should not occur significantly in the present case.

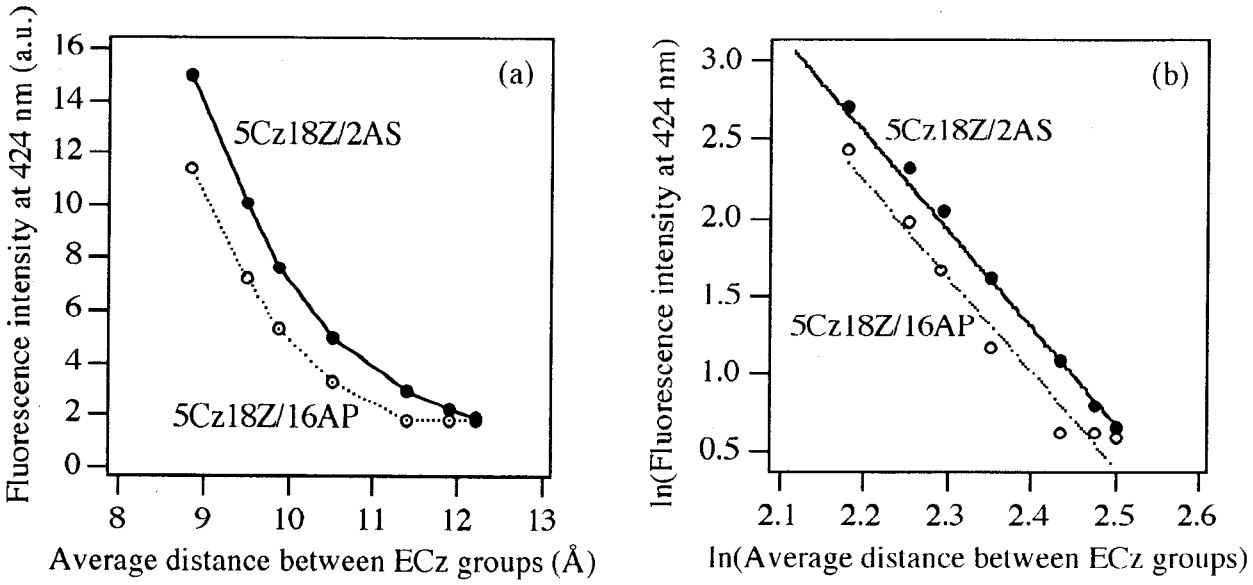

Figure 7. The relationship of (a) the emission intensity of the anthryl group with the average distance between the ECz groups in the 5Cz18Z/2AS or 5Cz18Z/16AP bicomponent monolayer and (b) its double logarithmic plot.

Interaction of Cytochrome c with Monolayers. The excited ECz group can reduce cyt.c by photoinduced electron transfer. On the other hand, as the critical distance for the energy transfer from an ECz group to cyt.c was calculated by using the Förster's equation[5] to be 38.8 Å (the orientation factor and the quantum yield are taken to be 2/3 [9] and 0.22 [10], respectively), photoenergy absorbed by the ECz groups will be transferred to cyt.c. Therefore, both processes will take part in the quenching of the ECz group competely. Cyt.c was injected into the subphase of the 5Cz18 or 5Cz18Z monolayer, and the quenching of the ECz group by cyt.c was investigated.

In situ fluorescence spectra of the monolayers were measured in the absence and the presence of cyt.c in the subphase at various molecular areas. The fluorescence intensity of the ECz group was plotted against the molecular area (Figure 8). Fluorescence of the 5Cz18 monolayer was hardly quenched by cyt.c in the subphase, indicating a scarce partitioning into the monolayer. The low affinity of cyt.c to the 5Cz18 monolayer should be due to electrostatic repulsion between the cationic cyt.c and the cationic monolayer.

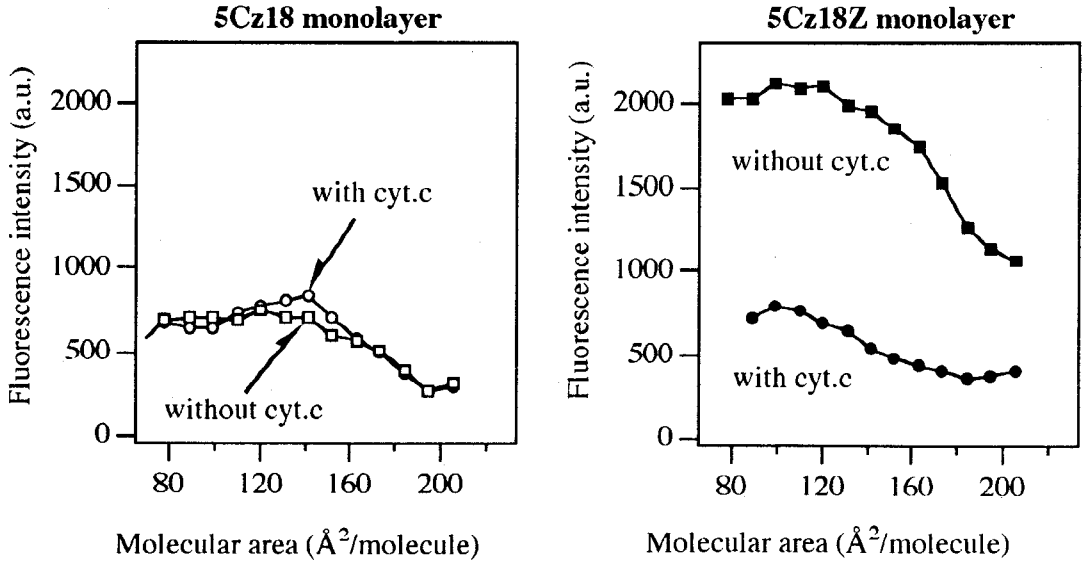

Figure 8. The fluorescence intensity of the monolayers at various molecular areas. The 5Cz18 monolayer in the presence of cyt.c (○), in the absence of cyt.c (□); 5Cz18Z monolayer in the presence of cyt.c (●), and in the absence of cyt.c (■), respectively.
[cyt.c] = 4.6 μM.

On the other hand, fluorescence intensity of 5Cz18Z monolayer was reduced remarkably by cyt.c in the subphase especially at larger molecular areas. However, the quenching behavior of 5Cz18Z was complex as shown in the plot of the quenching rate (I_0/I) vs. the molecular area (Figure 9). Upon initial compression of the monolayer, cyt.c effectively quenched the fluorescence of the ECz group probably because energy migration among ECz groups occurs effectively with decreasing interchromophore distance in the monolayer. However, further compression decreased the quenching rate, leaving a maximum quenching rate at a molecular area of 160 Å^2/molecule. At higher surface pressures, the effect of increasing energy migration should be overcome by the effect of increasing desorption of cyt.c from the monolayer due to increasing lateral pressure.[11] The amount of cyt.c partitioned to the monolayer was found, by the calculation taking energy migration into account, to decrease about 1/10 upon compression from 160 Å^2/molecule to 100 Å^2/molecule.

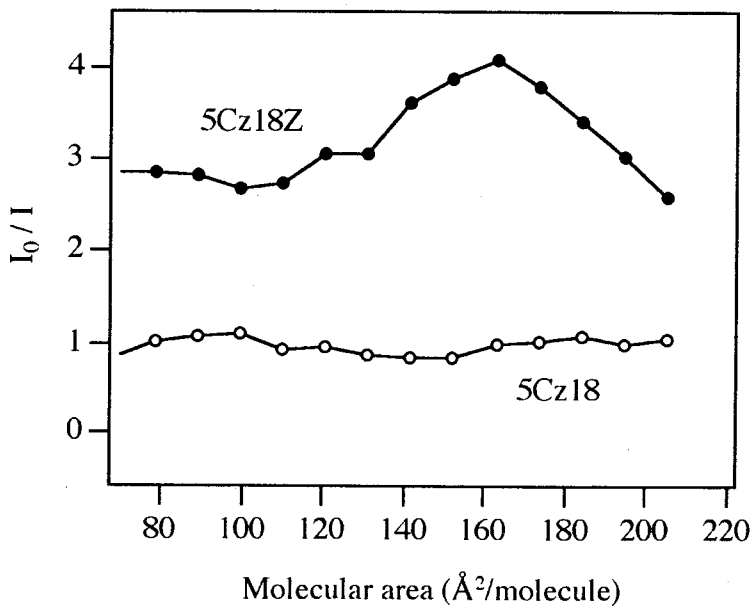

Figure 9. The dependence of the quenching rate (I_0/I) on the molecular area of the 5Cz18 (○) or 5Cz18Z (●) monolayer. I_0 and I represent the fluorescence intensity in the absence and presence of cyt.c ([cyt.c] = 4.6 μM), respectively.

References and Notes

1) Kimizuka, N.; Kunikake, T. *J. Am. Chem. Soc.* **1989**, *111*, 3758.

2) Kozarac, Z.; Ahuja, R. C.; Möbuis, D.; *Langmuir* **1995**, *11*, 568

3) Shimomura, M.; Fujii, K.; Karg, P.; Frey, W.; Sackmann, E.; Meller, P.; Ringsdolf, H. *Jpn. J. Appl. Phys.* **1988**, *27*, L1761.

4) Tanaka, H.; Hayashi, K.; Akatsuka, T.; Toyama, J.; Noda, K.; Kida, T.; Ogoma, Y.; Fujii, T.; Kondo, Y. *J. Biochem.* **1995**, *117*, 1151.

5) Förster, T. *Discuss. Faraday Soc.* **1959**, *27*, 7.

6) Kalyanasundaram, K.; Kiwi, J.; Grätzel, M. *Helv. Chim. Acta* **1978**, *61*, 2720.

7) Berlman, I. B. *Energy Transfer Parameters of Aromatic Compounds*; Academic Press: New York, 1973; Chapter 11.

8) The fluorescence intensity of the anthryl group is related with the distance between chromophores as follow: (the fluorescence intensity of the anthryl group) $\propto$ (the number of the excited ECz groups neighboring the anthryl group) $\propto$ (the average number of energy migration among ECz groups during the lifetime of the excited state) $\propto$ (the rate constant of energy migration among ECz groups) $= 1/\tau \times (r_0/r)^6$, where τ, r_0 and r represent the lifetime of the excited state, the critical distance for energy migration, and the distance between ECz groups, respectively.

9) Estep, T. N.; Thompson, T. E. *Biophys. J.* **1979**, *26*, 195.

10) The quantum yield was obtained with the vesicular assembly of 5Cz18 in water.

11) Marsh, D. *Biochim. Biophys. Acta* **1996**, 1286, 183.

Chapter 3

Donor-Sensitizer-Acceptor Triad System for Photoenergy Migration, Photoenergy Transfer, and Electron Transfer in a Bilayer Membrane

Introduction

As described in Chapter 1, in a bilayer membrane composed of chromophoric amphiphile molecules, the chromophores are two-dimensionally arranged in a high density. When an electron acceptor is added to the membrane, photoinduced electron transfer to the electron acceptor will also occur efficiently via efficient photoenergy migration among chromophores. In Chapter 1, the author described about bilayer membranes composed of ECz-containing amphiphiles and observed photoinduced electron transfer to a terephthalate group. It was shown that effective energy migration with some hundreds of steps occurs in the bilayer membrane. However, the efficiency of the electron transfer to the terephthalate group in the membrane was not so high, although the photoexcitation of chromophores adjacent to the electron-accepting group was frequent as a result of the effective photoenergy migration. The reason for the low extent of electron transfer should be due to quick dissipation of photoenergy to neighboring chromophores.

In order to overcome this difficulty, the author designed and synthesized a novel amphiphile having an anthryl group (photoenergy-accepting group) and a viologen group (electron-accepting group) in one molecule (VioAnt18; Figure 1). In the bicomponent bilayer membrane of 5Cz18Z (Figure 1) and VioAnt18, both ECz and anthryl (Ant) groups are expected to reside in the same plane (Figure 2). The excitation of the ECz group initiates energy migration among ECz groups, and energy transfer occurs to the Ant group from the excited ECz group near the Ant group. The excited

Ant group, then, reduces the viologen group in the same molecule. Since the photoenergy transferred to the Ant group is not transferred back to neighboring ECz groups, efficient photoinduced electron transfer might be realized in the membrane.

In this chapter, photoinduced electron transfer in the bilayer membranes composed of 5Cz18Z and one of the viologen-containing amphiphiles (VioAnt18, VioECz18, and Vio18; Figure 1) was investigated by fluorescence quenching measurements and transient absorption spectroscopy. Furthermore, the photoinduced electron transfer process was analyzed by computer simulation.

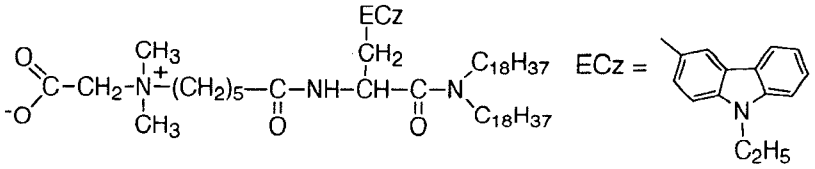

5Cz18Z

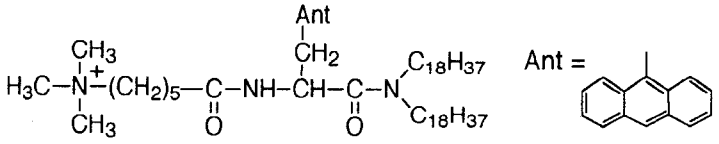

9A18

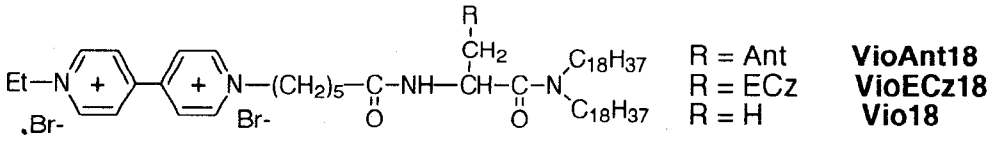

VioAnt18
VioECz18
Vio18

Figure 1. Molecular structures of 5Cz18Z, novel electron acceptors (VioAnt18, VioECz18 and Vio18) and energy acceptor 9A18.

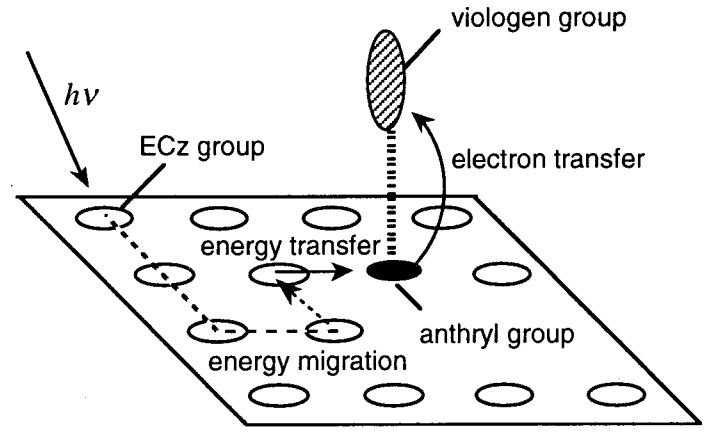

excitation $ECz \xrightarrow{h\nu} ECz^*$

energy migration $ECz^* + ECz \longrightarrow ECz + ECz^*$

energy transfer $ECz^* + Ant \longrightarrow ECz + Ant^*$

electron transfer $Ant^* + Vio^{2+} \longrightarrow Ant^{+\bullet} + Vio^{+\bullet}$

ECz = *N*-ethylcarbazolyl group Ant = anthryl group Vio^{2+} = viologen group

Figure 2. Schematic representation for the photoenergy harvest and photoinduced electron transfer in the 5Cz18Z/VioAnt18 bilayer membrane.

Experimental Section

Materials. The synthesis of 5Cz18Z was described in Chapter 2. *N'*,*N'*,*N'*-trimethyl-ammoniohexanoyl-D-3-(9-anthryl)alanine dioctadecylamide bromide (9A18, Figure 1) were synthesized by the method in the literature.[1] Ethylcarbazole and dimethyl terephthalate were purchased from Tokyo Kasei Co., Ltd.(Japan), and were recrystallized from ethyl acetate before use. *N*,*N*-Dimethylacetamide was purchased from Nacalai Tesque Co., Ltd. (Japan), and used without further purification. Novel amphiphilic acceptors, VioAnt18, VioECz18, and Vio18 were synthesized according to Scheme 1.

The synthesis of **1a** has been reported,[1] and that of **1b** was described in Chapter 2. **1c** was synthesized by a similar procedure. All intermediates were identified by ^{1}H NMR (270 MHz) and the final products were also identified by mass spectroscopy. The purity was checked by TLC. Solvent systems for TLC were (A) methanol/ammonia water (2/1 v/v), (B) chloroform/methanol /ammonia water (4/4/1 v/v/v), (C) chloroform/methanol (9/2 v/v), and (D) *n*-butanol/acetic acid /water/pyridine (5/3/4/1 v/v/v/v).

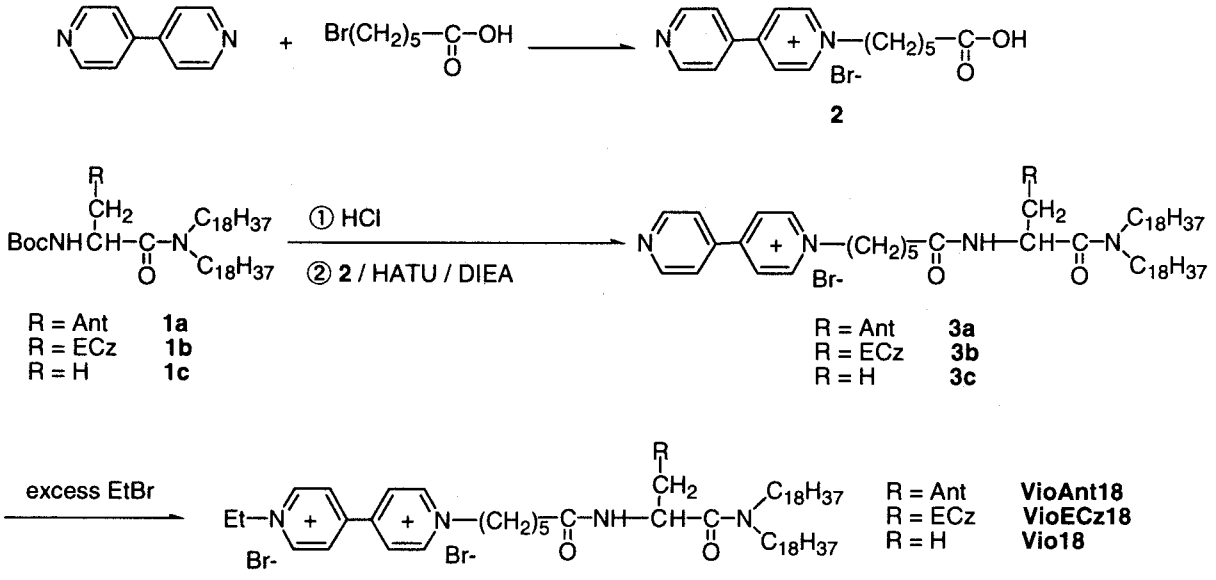

Scheme 1. Synthetic schemes of the electron acceptors, VioAnt18, VioECz18 and Vio18.

6-(*N*-(4'-(4''-Pyridyl)pyridinium))hexanoic acid [2]. Bromohexanoic acid (3.00 g) and 4,4'-dipyridyl (10.4 g) were dissolved in acetonitrile (30 ml) and the solution was refluxed at 110 °C for 2 h. After condensing the solution, diethyl ether was added to precipitate the reaction product (3.75 g, 30.2 % yield). TLC: R_f(A)=0.47, R_f(B)=0.21. ^{1}H NMR (270 MHz, $CDCl_3$): δ (ppm) 1.84-1.91 (4H, brm, $N^+CH_2CH_2CH_2CH_2CH_2$), 2.41 (2H, m, $N^+CH_2CH_2CH_2CH_2CH_2$), 2.66 (2H, t, $N^+CH_2CH_2CH_2CH_2CH_2$), 5.10 (2H, t, $N^+CH_2CH_2CH_2CH_2CH_2$), 8.37, 8.91 (4H, d, pyridyl-*H*), 9.23, 9.54 (4H, d, pyridinium-*H*).

***N*-(6-(*N'*-(4'-(4''-Pyridyl)pyridinium))hexanoyl)-D-3-(9-anthryl)alanine dioctadecylamide bromide [3a].** The Boc group of **1a** (88 mg) was removed by treatment with 4 N HCl in dioxane, and the product dissolved in chloroform (5 ml) was reacted with **2** (36 mg) in the presence of HATU (58 mg) with DIEA (40 μl) at 0 °C for 10 min and at 25 °C for 12 h. The solvent was removed and the remaining solid was purified by a Sephadex LH-20 column using methanol as eluant (57 mg, 53.8 % yield). TLC: R_f(B)=0.89, R_f(C)=0.54. ^{1}H NMR (270 MHz, $CDCl_3$): δ (ppm) 0.88 (6H, t, $CH_2(CH_2)_{16}CH_3$), 1.24 (64H, brs, $CH_2(CH_2)_{16}CH_3$), 1.65 (4H, brm, $N^+CH_2CH_2CH_2CH_2CH_2$), 2.18 (2H, m, $N^+CH_2CH_2CH_2CH_2CH_2$), 2.31 (2H, t, $^+CH_2CH_2CH_2CH_2CH_2$), 3.06 (2H, m, $NHCHCH_2$), 3.21 (4H, brm, $CH_2(CH_2)_{16}CH_3$), 3.90 (2H, t, $N^+CH_2CH_2CH_2CH_2CH_2$), 5.31 (1H, q, $NHCHCH_2$), 7.09 (1H, d, $NHCHCH_2$), 7.27, 7.45, 7.54, 7.96, 8.32, 8.47 (9H, anthryl-*H*), 7.63, 8.16, 8.24 (4H, d, pyridyl-*H*), 8.62, 8.85, 9.63, 9.74 (4H, d, pyridinium-*H*).

***N*-(6-(*N'*-(*N''*-Ethyl-4',4''-bipyridinium))hexanoyl)-D-3-(9-anthryl)alanine dioctadecylamide dibromide [VioAnt18].** **3a** (57 mg) was dissolved in ethylbromide (10 ml) and the solution was refluxed at 60 °C for 24 h. After removal of solvent, the remaining oil was purified by a Sephadex LH-20 column using methanol as eluant (6.4 mg, 10.2 % yield). TLC: R_f(B)=0.10, R_f(C)=0.21. ^{1}H NMR (270 MHz, $CDCl_3$): δ (ppm) 0.91 (6H, t, $CH_2(CH_2)_{16}CH_3$), 1.23 (64H, brs, $CH_2(CH_2)_{16}CH_3$), 1.46 (2H, brm, $N^+CH_2CH_2CH_2CH_2CH_2$), 1.69 (5H, m, $N^+CH_2CH_2CH_2CH_2CH_2$, $CH_3CH_2N^+$), 2.14 (2H, m, $N^+CH_2CH_2CH_2CH_2CH_2$), 2.30 (2H, t, $N^+CH_2CH_2CH_2CH_2CH_2$), 2.99 (2H, m, $NHCHCH_2$), 3.14 (4H, brm, $CH_2(CH_2)_{16}CH_3$), 4.95 (4H, brm, $N^+CH_2CH_2CH_2CH_2CH_2$, $CH_3CH_2N^+$), 5.27 (1H, q, $NHCHCH_2$), 7.29, 7.39, 7.48, 7.91, 8.32, 8.42 (9H, anthryl-*H*), 8.96, 9.47 (8H, bipyridinium-*H*). MS (FAB): m/z 1051 (calcd

for $C_{71}H_{110}N_4O_2$ [(M-Br_2)+] m/z 1051.69).

***N'*-(6-(*N''*-(4'-(4''-Pyridyl)pyridinium))hexanoyl)-L-3-(3-*N*-ethylcarbazolyl) alanine dioctadecylamide bromide [3b].** The Boc group of **1b** (58 mg) was removed by treatment with 4 N HCl in dioxane, and the product dissolved in chloroform (5 ml) was reacted with **2** (23 mg) in the presence of HATU (37 mg) and DIEA (25 μl) at 0 °C for 10 min and at 25 °C for 12 h. The solvent was removed and the remaining solid was purified by a Sephadex LH-20 column using methanol as eluant (53 mg, 76.1 % yield). TLC: R_f(B)=0.86, R_f(C)=0.70. ^{1}H NMR (270 MHz, $CDCl_3$): δ (ppm) 0.86 (6H, t, $CH_2(CH_2)_{16}CH_3$), 1.24 (64H, brs, $CH_2(CH_2)_{16}CH_3$), 1.38 (3H, t, carbazolyl-CH_2CH_3), 1.63 (4H, brm, $N^+CH_2CH_2CH_2CH_2CH_2$), 1.83 (2H, m, $^+CH_2CH_2CH_2CH_2CH_2$), 2.14 (2H, t, $N^+CH_2CH_2CH_2CH_2CH_2$), 3.07 (2H, m, $NHCHCH_2$), 3.13 (4H, brm, $CH_2(CH_2)_{16}CH_3$), 4.29 (4H, m, $N^+CH_2CH_2CH_2CH_2CH_2$, carbazolyl-CH_2CH_3), 5.11 (1H, q, $NHCHCH_2$), 6.52 (1H, d, $NHCHCH_2$), 7.16, 7.29, 7.36, 7.87, 8.01 (7H, carbazolyl-*H*), 7.48, 8.00 (4H, d, pyridyl-*H*), 8.57, 8.77 (4H, d, pyridinium-*H*).

***N'*-(6-(*N''*-(*N'''*-Ethyl-4',4''-bipyridinium))hexanoyl)-L-3-(3-*N*-ethylcarbazolyl) alanine dioctadecylamide dibromide [VioECz18].** **3b** (10 mg) was dissolved in ethylbromide (10 ml) and the solution was refluxed at 60 °C for 24 h. After removal of solvent, the remaining oil was purified by a Sephadex LH-20 column using methanol as eluant (3.0 mg, 27.3 % yield). TLC: R_f(C)=0.05, R_f(D)=0.19. ^{1}H NMR (270 MHz, $CDCl_3$): δ (ppm) 0.88 (6H, t, $CH_2(CH_2)_{16}CH_3$), 1.23 (66H, brs, $CH_2(CH_2)_{16}CH_3$, $N^+CH_2CH_2CH_2CH_2CH_2$), 1.32 (3H, t, carbazolyl-CH_2CH_3), 1.62 (5H, m, $N^+CH_2CH_2CH_2CH_2CH_2$, $CH_3CH_2N^+$), 1.90 (2H, m, $N^+CH_2CH_2CH_2CH_2CH_2$), 2.23 (2H, t, $N^+CH_2CH_2CH_2CH_2CH_2$), 2.96 (4H, brm, CH_2

$(CH_2)_{16}CH_3$), 3.17 (2H, brs, NHCHCH_2), 4.31 (2H, q, carbazolyl-CH_2CH$_3$), 4.60 (2H, t, N+CH_2CH$_2$CH$_2$CH$_2$CH$_2$), 4.83 (2H, q, CH$_3$CH_2N+), 5.07 (1H, q, NHCHCH$_2$), 7.11, 7.28, 7.39, 7.94, 7.97 (7H, carbazolyl-*H*), 8.99, 9.37 (8H, bipyridinium-*H*). MS (FAB): m/z 1068 (calcd for $C_{71}H_{113}N_5O_2$ [(M-Br$_2$)+] m/z 1068.72).

***N*-(6-(*N*'-(4'-(4''-Pyridyl)pyridinium))hexanoyl)-L-alanine dioctadecylamide bromide [3c].** The Boc group of **1c** (100 mg) was removed by treatment with 4 N HCl in dioxane, and the product dissolved in chloroform (5 ml) was reacted with **2** (51 mg) in the presence of HATU (82 mg) and DIEA (57 μl) at 0 °C for 10 min and at 25 °C for 12 h. The solvent was removed and the remaining solid was purified by a Sephadex LH-20 column using methanol as eluant (82 mg, 65.3 % yield). TLC: R_f(B)=0.85, R_f(C)=0.73. ^{1}H NMR (270 MHz, CDCl$_3$): δ (ppm) 0.85 (6H, t, CH$_2$(CH$_2$)$_{16}$CH_3), 1.26 (64H, brs, CH$_2$(CH_2)$_{16}$CH$_3$), 1.47 (3H, brs, NHCHCH_3), 1.63 (4H, brm, N+CH$_2$CH$_2$CH_2CH_2CH$_2$), 2.03 (2H, m, N+CH$_2$CH_2CH$_2$CH$_2$CH$_2$), 2.18 (2H, t, N+CH$_2$CH$_2$CH$_2$CH$_2$CH_2), 3.24 (4H, brm, CH_2(CH$_2$)$_{16}$CH$_3$), 4.63 (2H, t, N+CH_2CH$_2$CH$_2$CH$_2$CH$_2$), 4.74 (1H, q, NHCHCH$_3$), 6.65 (1H, d, NHCHCH$_3$), 7.63, 8.21 (4H, d, pyridyl-*H*), 8.82, 8.92 (4H, d, pyridinium-*H*).

***N*-(6-(*N*'-(*N*''-ethyl-4',4''-bipyridinium))hexanoyl)-L-alanine dioctadecylamide dibromide [Vio18].** **3c** (80 mg) was dissolved in ethylbromide (20 ml) and the solution was refluxed at 60 °C for 24 h. After removal of solvent, the remaining oil was purified by a Sephadex LH-20 column using methanol as eluant. The product was recrystallized successively from methanol and acetonitrile (4.8 mg, 5.4 % yield). TLC: R_f(B)=0.44, R_f(C)=0.13. ^{1}H NMR (270 MHz, CDCl$_3$): δ (ppm) 0.85 (6H, t, CH$_2$(CH$_2$)$_{16}$CH_3), 1.27 (64H, brs, CH$_2$(CH_2)$_{16}$CH$_3$), 1.43 (5H, m,

NHCHCH_3, N+$CH_2CH_2CH_2CH_2CH_2$), 1.63 (2H, m, N+$CH_2CH_2CH_2CH_2CH_2$), 1.69 (3H, t, CH_3CH_2N+), 2.02 (2H, m, N+$CH_2CH_2CH_2CH_2CH_2$), 2.18 (2H, t, N+$CH_2CH_2CH_2CH_2CH_2$), 3.24 (4H, brm, $CH_2(CH_2)_{16}CH_3$), 4.53 (2H, t, N+$CH_2CH_2CH_2CH_2CH_2$), 4.62 (2H, q, CH_3CH_2N+), 4.65 (1H, q, NHC*H*CH_3), 6.70 (1H, d, N*H*$CHCH_3$), 8.38, 8.84 (8H, bipyridinium-*H*). MS (FAB): m/z 875 (calcd for $C_{57}H_{102}N_4O_2$ [(M-Br_2)+] m/z 875.47).

Measurement. Experimental procedure for membrane preparation was described in Chapter 1. For the characterization of a bilayer membrane of 5Cz18Z in water, a transmission electron micrograph was obtained using a JEM-100SX microscope (JEOL Co., Ltd., Japan) and dynamic light scattering measurement was performed by DLS-700 (Otsuka Electronics Co., Ltd., Japan). Thermal transition of the bilayer was examined by differential scanning calorimetry using SSC-580S (Daini-Seikosha Co., Ltd., Japan). Fluorescence spectra were recorded on an F-4010 fluorometer (Hitachi Co., Ltd., Japan). Transient absorption spectra were recorded on the instruments described in Chapter 1 except for the time response of the apparatus. The gate widths of the multichannel photodiode array with the image-intensifier tube are 0.90 μs (for the aqueous dispersion), and 0.35 μs (for the acetonitrile solution). The molecular area of 5Cz18Z in the monolayer was determined in the procedure described in Chapter 1.

Results and Discussion

Fluorescence Quenching of the ECz Group in Bilayer Membranes. A transmission electron micrograph observation and dynamic light scattering measurement revealed that the 5Cz18Z formed a spherical molecular assembly in aqueous dispersion. Differential scanning calorimetry showed the presence of a bilayer membrane with Tc of 27.6 °C. Therefore, 5Cz18Z formed liposome in water similarly to the reports of the related amphiphiles.[2]

Fluorescence quenching of the ECz group in the 5Cz18Z membrane was investigated by using viologen-containing amphiphiles. Figure 3 shows the fluorescence spectra of the 5Cz18Z/VioAnt18 bilayer membrane with varying molar ratios at 17 °C, which is below the Tc of the membrane.

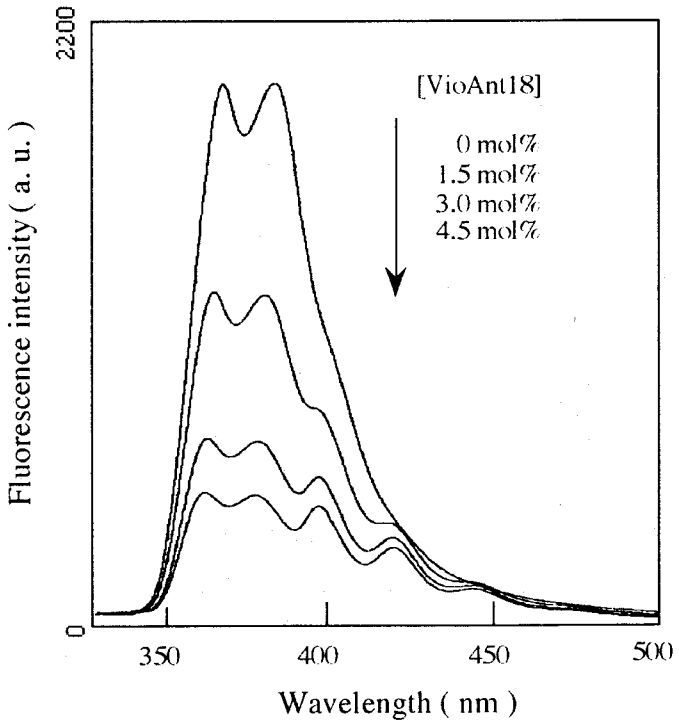

Figure 3. Fluorescence spectra of the 5Cz18Z/VioAnt18 bilayer membrane containing various amounts of VioAnt18 at 17 °C (excitation at 299 nm).

In the absence of the acceptor, only monomer emission of an ECz group (362, 378 nm) was observed. The fluorescence intensity decreased with increasing addition of the acceptor. Weak peaks at 397, 423, and 446 nm are assigned to emission of the Ant group. The fluorescence quenching of the ECz group by different electron acceptors is summarized in Figure 4 in the form of Perrin plot. The quenching rate increases in the order of Vio18 < VioECz18 < VioAnt18.

This order is consistent with the theoretical consideration, that the intramolecular quenching by VioECz18 in the membrane occurs more easily than the intermolecular quenching by Vio18 on the basis of the distance between the ECz group and the viologen group.

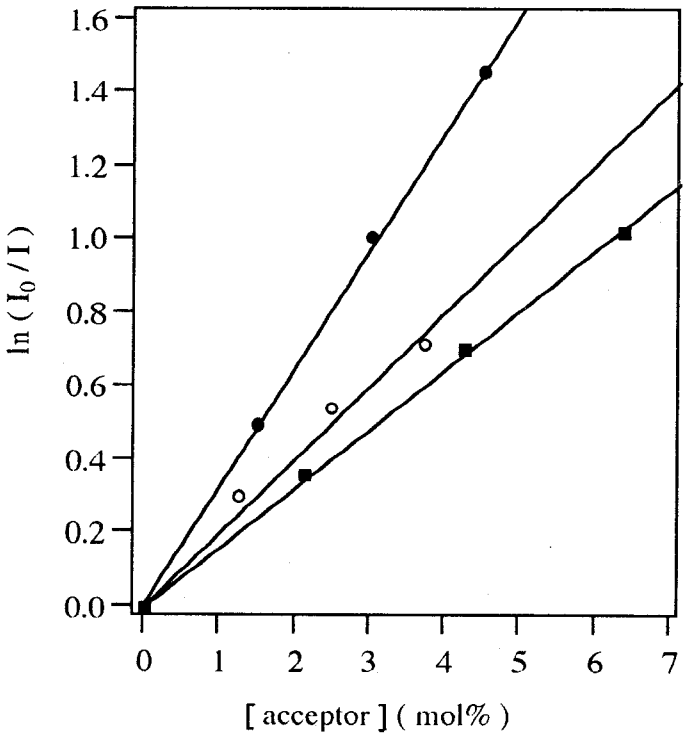

Figure 4. Perrin plot of the fluorescence quenching of the ECz group with the electron acceptors; VioAnt18 (●), VioECz18 (○) and Vio18 (■).

On the other hand, the high quenching rate of VioAnt18 (3 mol% VioAnt18 quenches about 70 % of the ECz emission) indicates that the Ant group efficiently accepts the excitation photoenergy which should migrate among ECz groups in the membrane. In the fluorescence spectra of the 5Cz18Z /VioAnt18 bilayer membrane, emission intensity of the Ant group was weak (Figure 3), that indicates the excited Ant group is quenched photooxidatively by the viologen group. Quantum yield of the electron transfer from the excited Ant group to the viologen group was determined by fluorescence quenching of the Ant group with the viologen group as follows. The fluorescence quenching of the ECz group in the 5Cz18Z membrane was measured by using two kinds of quencher, VioAnt18 and 9A18 (Figure 1). 9A18 in the 5Cz18Z/9A18 bilayer membrane quenched ECz emission to the same extent as VioAnt18 , indicating photoenergy transfer from the ECz group to the Ant group occurs to nearly the same extent in the two membrane systems (Figure 5).

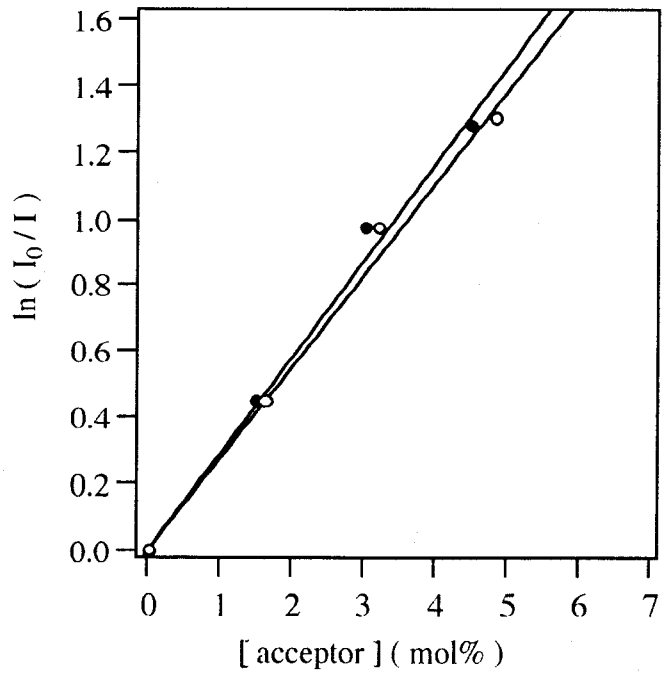

Figure 5. Perrin plot of the fluorescence quenching of the ECz group with VioAnt18 (●), 9A18 (○).

On the other hand, the Ant emission in the 5Cz18Z/VioAnt18 bilayer membrane is quenched more significantly than that in the 5Cz18Z/9A18 bilayer membrane (Figure 6). This significant quenching should be due to electron transfer from the excited Ant group to the viologen group. The quantum yield for the electron transfer is 0.95 in the VioAnt18 molecule, which is obtained by calculating $1-I/I_0$, where I_0 and I represents the emission intensity of the Ant group in the 5Cz18Z/9A18 membrane and that in the 5Cz18Z/VioAnt18 membrane, respectively. In the membrane containing 3 mol% VioAnt18, the Ant group accepts about 70 % of the excitation energy of the ECz group, thus the overall quantum yield for the photoinduced electron transfer is 0.67 in the membrane.

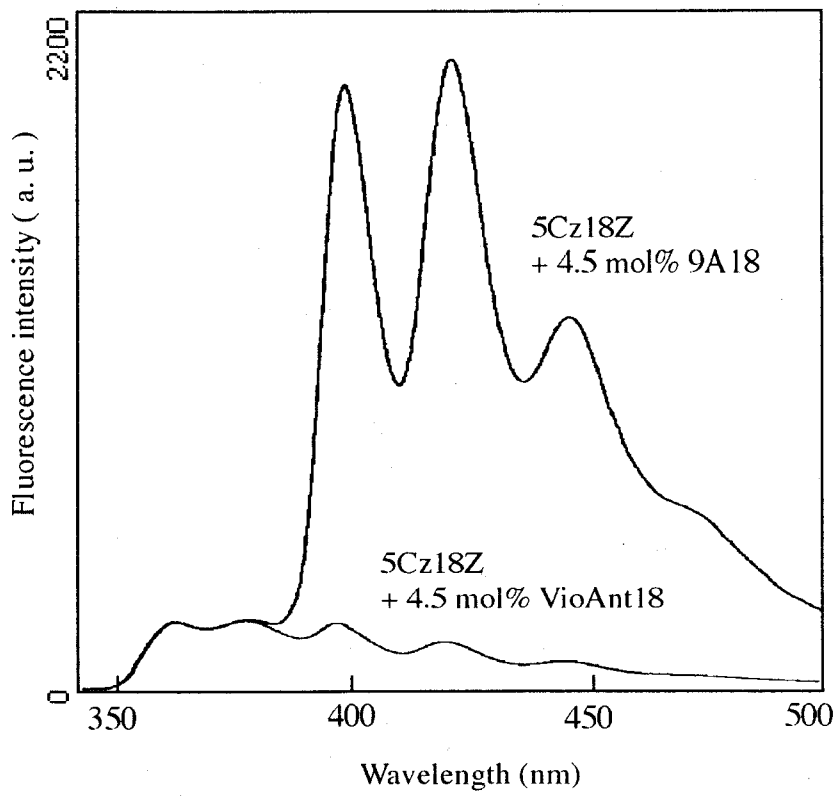

Figure 6. Fluorescence spectra of the 5Cz18Z/VioAnt18 bilayer membrane and the 5Cz18Z/9A18 bilayer membrane at 17 °C (excitation at 299 nm).

Photoinduced Electron Transfer to Viologen Group and Back Electron Transfer. The photoreduction of viologen group and the back electron transfer were investigated by transient absorption spectroscopy. Figure 7 shows the transient absorption spectra of the 5Cz18Z-containing unicomponent or bicomponent bilayer membranes at 500 ns after laser irradiation. In the case of 5Cz18Z bilayer membrane, ECz radical cation ($ECz^{+\bullet}$; 790 nm) was generated by two-photon absorption. When VioECz18 was added in the 5Cz18Z bilayer membrane, the reduced viologen ($V^{+\bullet}$; 610 nm) as well as $ECz^{+\bullet}$ was formed, indicating the photoinduced electron transfer from the ECz group to the viologen group.

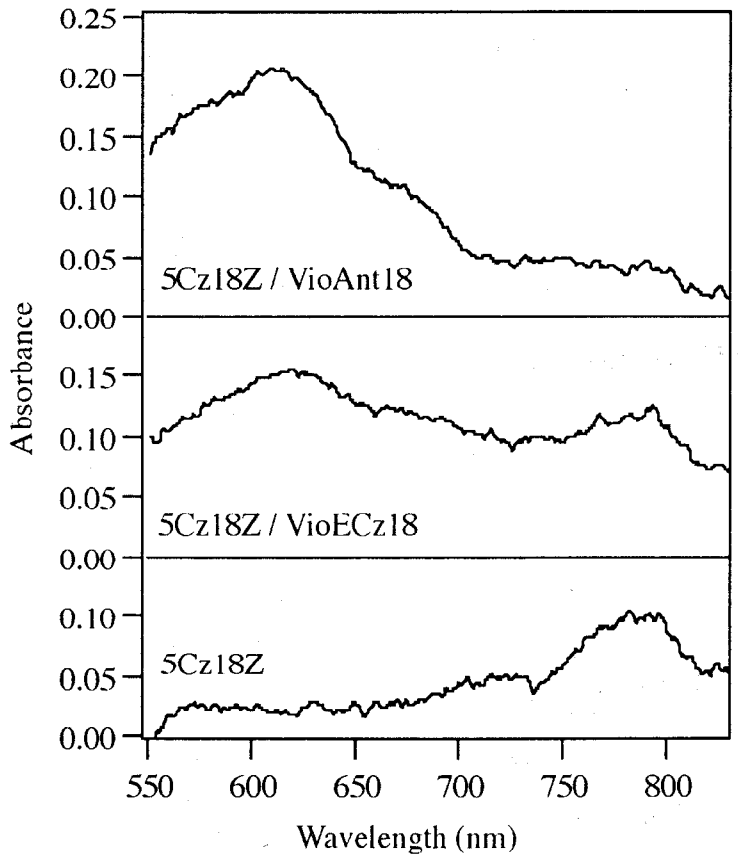

Figure 7. Transient absorption spectra of the 5Cz18Z bilayer membrane without electron acceptor and 10 mol% VioAnt18 or 10 mol% VioECz18 at 17 °C at 500 ns after laser irradiation.

In contrast to these bilayer membranes, only $V^{+\bullet}$ was formed in the 5Cz18Z/VioAnt18 bilayer membrane, suggesting the absence of $ECz^{+\bullet}$ production or rapid consumption of $ECz^{+\bullet}$. The difference between the two systems exists in the presence of an Ant group in the 5Cz18Z/VioAnt18 bilayer membrane. The absence of $ECz^{+\bullet}$ formation seems to be real, because the excitation energy of the ECz group (one-photon absorption) might be transferred quickly to the Ant group to suppress two-photon absorption of the ECz group.

It is notable that $V^{+\bullet}$ in the 5Cz18Z/VioECz18 bilayer membrane has a lifetime longer than a millisecond (Figure 8a). However, the lifetime does not agree with 150 μsec of $ECz^{+\bullet}$ (Figure 8b), indicating that the decay of $V^{+\bullet}$ and $ECz^{+\bullet}$ are not attributed to their recombination. $ECz^{+\bullet}$ should be reduced possibly by a certain electron donor in the system, not via the back electron transfer from $V^{+\bullet}$.

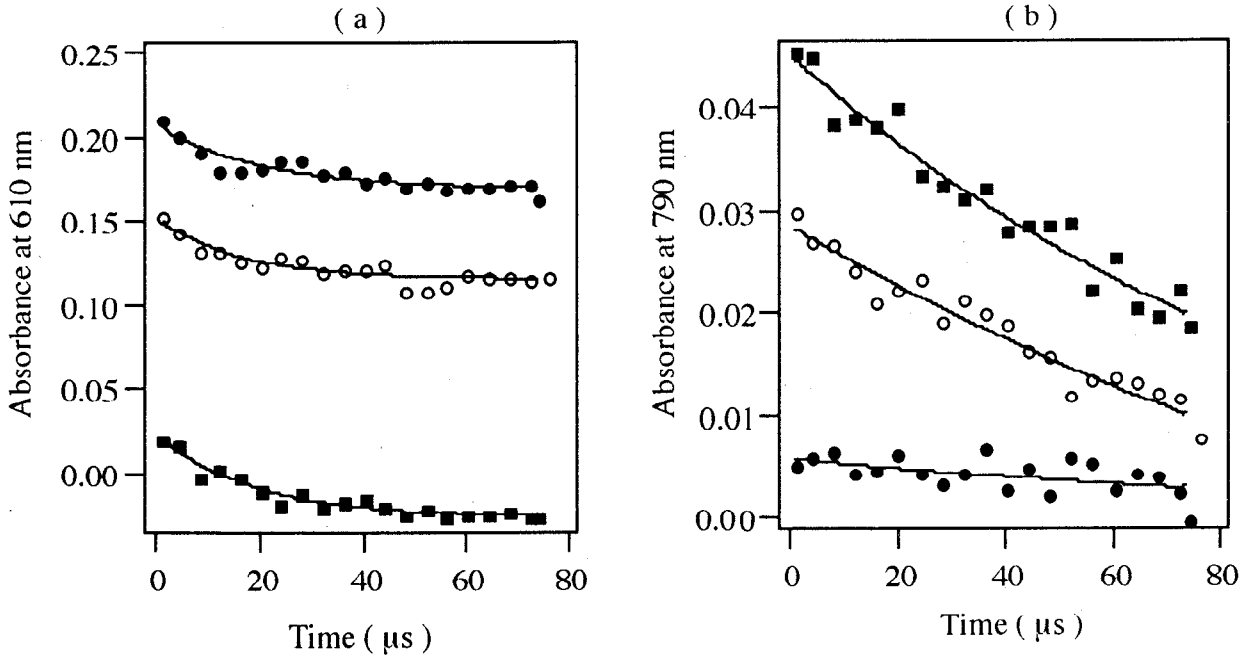

Figure 8. Decay profiles of the transient absorption at 610 nm (a) and 790 nm (b) of the 5Cz18Z (■), the 5Cz18Z/VioAnt18 (●) and the 5Cz18Z/VioECz18 (○) bilayer membranes on laser photolysis at 17 °C.

Similarly, the lifetime of $V^{+\bullet}$ in the 5Cz18Z/VioAnt18 bilayer membrane was longer than a millisecond although the oxidized Ant group ($Ant^{+\bullet}$) was not clearly observed. This point is referred in the following section.

Electron Transfer from Amide Group to the Photooxidized Chromophore. It is considered that the photooxidized chromophores, $ECz^{+\bullet}$ and $Ant^{+\bullet}$, should be reduced before the recombination reaction by a functional group in the membrane other than $V^{+\bullet}$. A possible candidate is an amide group involved in the amphiphile. This possibility was investigated by using *N*,*N*-dimethylacetamide (DMAA) as a model of electron donor.

Table 1. Lifetimes of the ethylcarbazole radical cation and DMTP radical anion generated on laser photolysis with various amount of DMAA in an acetonitrile solution.

	radical cation (μs)	radical anion (μs)
ECz + DMTP	4.14 ± 0.07	5.10 ± 0.03
ECz + DMTP + 0.1 M DMAA	3.50 ± 0.01	5.21 ± 0.05
ECz + DMTP + 1.0 M DMAA	3.00 ± 0.03	5.43 ± 0.02

Table 2. Lifetimes of the anthracene radical cation and DMTP radical anion generated on laser photolysis with various amount of DMAA in an acetonitrile solution.

	radical cation (μs)	radical anion (μs)
Ant + DMTP	2.12 ± 0.01	2.50 ± 0.03
Ant + DMTP + 0.1 M DMAA	1.73 ± 0.05	2.99 ± 0.08
Ant + DMTP + 1.0 M DMAA	1.18 ± 0.02	4.09 ± 0.06

ECz$^{+\bullet}$ was produced in an acetonitrile solution of *N*-ethylcarbazole and dimethyl terephthalate (DMTP) by laser irradiation. Lifetimes of ECz$^{+\bullet}$ under varying concentrations of DMAA were determined and are summarized in Table 1 together with those of terephthalate radical anion. The lifetime of the radical cation becomes shorter with the addition of acetamide, while that of the radical anion becomes longer, indicating that acetamide donates an electron to the cation radical. Similarly, Ant$^{+\bullet}$ was produced in an acetonitrile solution of anthracene and DMTP, and lifetimes under varying concentrations of DMAA were determined (Table 2). Acetamide is also shown to reduce anthracene radical cation. These results suggest that the amide group close to the chromophore in the molecule may become an electron donor to the oxidized chromophore. The oxidized Ant group might be instantly reduced by an amide group locating nearby in the membrane. This reduction may be the reason why the oxidized Ant group was not clearly observed in the 5Cz18Z/VioAnt18 membrane.

The electron donation by the amide group, however, can only account for the fast disappearance of the photooxidized chromophore, but can not explain entirely the reason for the long lifetime of V$^{+\bullet}$. The production of V$^{+\bullet}$ with a lifetime longer than a millisecond has been reported with micellar system.[3-5] The lifetime became longer in the micelles because the back electron transfer is suppressed due to low concentration of V$^{+\bullet}$ in micelles, which results from electrostatic repulsion between V$^{+\bullet}$ and the micellar surface. In the present case, however, the electron donor and the electron acceptor are immobilized in the membrane, bringing forth a situation different from the micellar system. Currently, this long lifetime is considered to be due to the hole migration among viologen groups in the membrane, which should suppress the back electron transfer because of large separation of the hole and electron.[6] However, this point is remained to be investigated further.

Computer Simulation of Photoenergy Harvest in Bilayer Membranes. In order to estimate the contribution of energy migration to the photoenergy harvest in the 5Cz18Z/VioECz18 or 5Cz18Z/Vio18 bilayer membranes, computer simulation was carried out under an assumption that ECz groups are placed on a square lattice with a spacing of 9.2 Å (Figure 9). The 9.2 Å space was taken from the molecular area at the inflection point in the π-A isotherm of 5Cz18Z spread on the water subphase. The surface pressure at the inflection point was 45 mN/m. The ECz groups were distributed randomly on 900 lattice points. Since the fluorescent lifetime of the ECz group is 7.93 ns and the quantum yield of the ECz emission is 0.091 at 17 °C, the rate constants of the radiative transition (k_f) and the nonradiative transition (k_{nr}) are 1.2 x 10^7 s^{-1} and 1.1 x 10^8 s^{-1}, respectively.

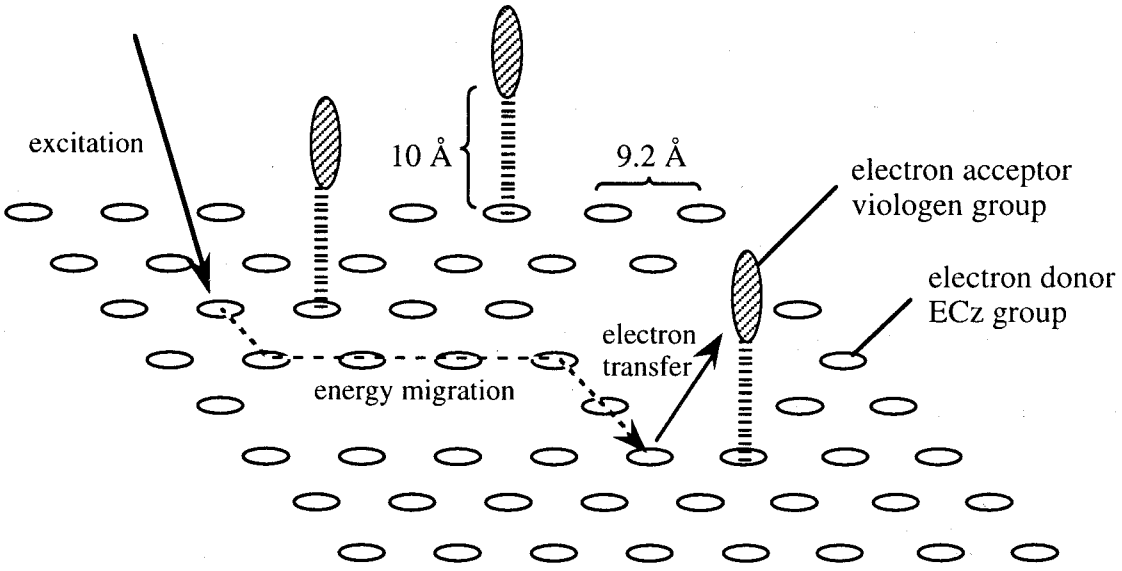

Figure 9. Schematic representation for the computer simulation of the energy migration and the electron transfer in the 5Cz18Z/VioECz18 bilayer membrane.

The rate constant of photoinduced electron transfer from the ECz group to the viologen group (k_{et}) is expressed by equation (1),

$$k_{et} = k_{et}' \exp \{ -\beta (r - r_0) \} \qquad (1)$$

where r represents the donor-acceptor distance and k_{et}' is k_{et} at $r = r_0$. β is the tunneling parameter which is determined by the electronic properties of the medium that lies between the donor and acceptor. r_0 and k_{et}' are evaluated by using molecular and fluorescent parameters of 5Cz18Z and VioECz18 in methanol as follows. r_0 is estimated to be 10 Å by assuming the extended chain conformation about the linker part between the ECz group and the viologen group of VioECz18. k_{et}' is obtained by comparing quantum yields of 5Cz18Z and VioECz18. Since fluorescent lifetime of the ECz group of 5Cz18Z is 8.92 ns, $k_f + k_{nr}$ is 1.12×10^8 s $^{-1}$ in methanol. The quantum yields of the ECz emission of 5Cz18Z and VioECz18 are 0.20 and 0.010, respectively, in methanol. The small quantum yield of the latter is due to photoinduced electron transfer from the ECz group to the viologen group. Taking these three values for calculation, the rate of electron transfer comes to be 2.1×10^9 s^{-1}. This value is taken as k_{et}' at $r_0 = 10$ Å.

The rate constant of energy migration among ECz groups (k_{em}) is expressed according to the Förster's equation (2),[7]

$$k_{em} = \frac{9000\kappa^2(\ln 10)k_f J}{128\pi^5 n^4 N r^6} \qquad (2)$$

where κ^2, J, n, N, and r represent the orientation factor, the overlap integral of the fluorescence spectrum and the absorption spectrum of the ECz group, the refractive index, the Avogadro number, and the distance between the ECz groups, respectively. The orientation factor and the quantum yield are taken to be 2/3 [8] and 0.091, respectively. The k_{em} values for the energy migration between the nearest ECz groups orthogonally and diagonally in the lattice are, then, 2.2×10^9 s^{-1} and 2.8×10^8

s^{-1}, respectively. The excited ECz group follows either process of donating the excitation energy to the neighboring ECz group, fluorescence emission, nonradiative deactivation, or quenching by the viologen group. Therefore, only the tunneling parameter, β, comes to be the variable parameter for the simulation of the present membrane system.

The quenching by VioECz18 or Vio18 was simulated by producing 10^5 different distributions of 5Cz18Z and VioECz18 or Vio18 on the square lattice with counting emission frequency. Varying values of the tunneling parameter, β, at the simulation, both experimental data of 5Cz18Z/VioECz18 and 5Cz18Z/Vio18 membranes meet exactly on the simulation curves when β is taken as 0.32 $Å^{-1}$ (Figure 10). β for typical donor-acceptor pairs separated by aliphatic spacers are reported to be greater than 1 $Å^{-1}$,[9,10] but the β value will become smaller in the presence of functional groups which have available electronic states for the electron transfer between the donor-acceptor pair due to the electronic coupling.[11] Since a few amide groups are locating in the space between ECz group and viologen group in the membrane, they might serve to reduce the β value.[12]

The number of energy migration steps within the fluorescent lifetime is calculated to be 78 from the simulation. A simulation curve without energy migration in the 5Cz18Z/VioECz18 membrane is shown in Figure 10, which is far below the experimental data, indicating that the high quenching rates of the present systems are due to the energy migration among ECz groups.

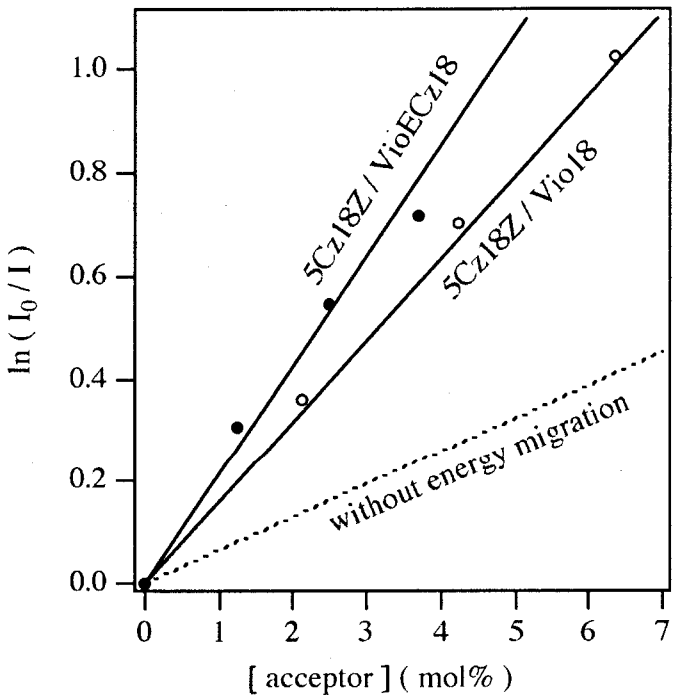

Figure 10. The result of the computer simulation of the fluorescence quenching in the 5Cz18Z/VioECz18 or 5Cz18Z/Vio18 membrane. The simulation curve with considering the theoretical energy migration (solid line) are shown together with the experimental data: 5Cz18Z/VioECz18 (●) and 5Cz18Z/Vio18 (○). The tunneling parameter β is assumed to be 0.32 $Å^{-1}$. Dotted line represents the simulation curve without energy migration in the 5Cz18Z/VioECz18 membrane.

References and Notes

1) Taku, K.; Sasaki, H.; Kimura, S.; Imanishi, Y. *Biophys. Chem.* **1992**, *44*, 187.

2) Kunitake, T.: Okahata, Y. *J. Am. Chem. Soc.* **1977**, *99*, 3860.

3) Brugger, P. A.; Grätzel, M. *J. Am. Chem. Soc.* **1980**, *102*, 2461.

4) Takeyama, N.; Sakaguchi, H.; Hashiguchi, Y.; Shimomura, M.; Nakamura, H.; Kunitake, T.; Matsuo, T. *Chem. Lett.* **1985**, 1735

5) Amao, Y.; Okura, I. *J. Mol. Catal. A-Chem.* **1996**, *105*, 125.

6) Fujihira, M.; Sakomura, M.; Aoki, D.; Koike, A. *Thin Solid Films* **1996**, *273*, 168.

7) Förster, T. *Discuss. Faraday Soc.* **1959**, *27*, 7.

8) Estep, T. N.; Thompson, T. E. *Biophys. J.* **1979**, *26*, 195.

9) Warman, J. M.; de Haas, M. P.; Paddon-Row, M. N.; Cotsaris, E.; Hush, N.S.; Oevering, H.; Verhoeven, J. W. *Nature*, **1986**, *320*, 615.

10) Miller, J. R.; Calceterra, L.T.; Closs, G. L. *J. Am. Chem. Soc.* **1984**, *106*, 3047.

11) Fox, M. A., Chanon, M., Eds. *Photoinduced electron transfer part A*; Elsevier: Amsterdam, 1988; pp 161-206.

12) Isied, S. S.; Vassilian, A. *J. Am. Chem. Soc.* **1984**, *106*, 1726.

Chapter 4

Photoreduction of Cytochrome c in the Presence of a Bilayer Membrane of *N*-Ethylcarbazole-Containing Amphiphiles

Introduction

As described in Chapter 1 and Chapter 3, in a bilayer membrane composed of amphiphile molecules covalently carrying a chromophore, the chromophores are regularly and densely packed in a plane, where effective photoenergy migration occurs. When an electron acceptor is embedded in the membrane system, efficient photoinduced electron transfer to an acceptor will be observed. In the present study, cytochrome c (cyt.c) was introduced into the chromophoric membrane composed of amphiphiles covalently carrying an ECz group, and photoreduction of cyt.c in the presence of a sacrificial electron donor was investigated.

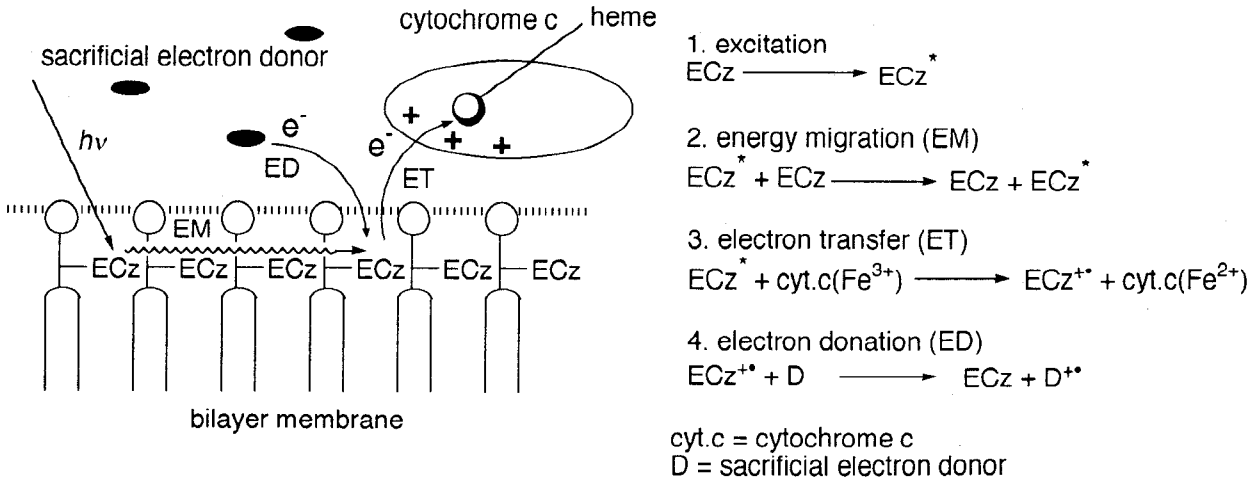

Figure 1. Schematic illustration for photoreduction of cytochrome c (cyt.c) in a bilayer membrane by electron transfer from the photoexcited ECz group to cyt.c.

Cyt.c belongs to a family of redox proteins that play an essential role in bioenergetics and drug metabolism.[1,2] Cyt.c has been most extensively studied in this class of proteins, and its interactions with lipid membranes[3], conformation[4,5] and morphology[6] on the surface of lipid membrane and electrochemical behaviors on an electrode[7,8] have been well investigated. Photoexcitation of the ECz group in the bilayer membrane composed of amphiphiles carrying an ECz group will initiate efficient energy migration among ECz groups and followed by electron transfer from the ECz group to the cyt.c partitioned into the bilayer membrane (Figure 1).

In Chapter 1, we showed that effective photoenergy migration with a few hundred steps occurs in this kind of bilayer membrane. Thus, the membrane is an efficient photoenergy-harvesting system, and is used for photoreduction of cyt.c in the present study. Such photoreduction system could be the basis for fabrication of biomimetic photoelectronic devices.[9]

Two kinds of dialkylammonium-type amphiphiles carrying an ECz group (5Cz18, 5Cz18Z; Figure 2) are used for the preparation of bilayer membranes. The zwitterionic membrane of 5Cz18Z is expected to show higher affinity for cyt.c than the cationic membrane of 5Cz18. In the latter system, unfavorable electrostatic repulsion might occur between cyt.c and the cationic membrane in the neutral pH region as described in Chapter 2.

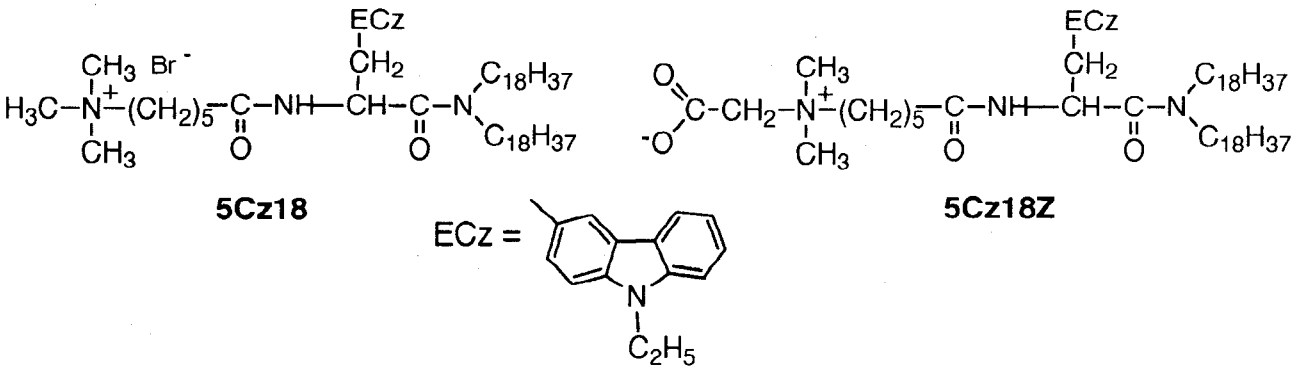

Figure 2. Molecular structures of 5Cz18 and 5Cz18Z.

Experimental Section

Materials. Sacrificial electron donors, triethanolamine (TEOA) and ethylenediaminetetra-acetic acid were purchased from Tokyo Kasei Co., Ltd. (Japan), and the latter was used as a water solution which was adjusted at pH 7.0 with a 4 wt% aqueous $NaHCO_3$ solution (EDTA).

Membrane Preparation. Bilayer membranes were prepared by the procedure described in Chapter 1. In addition, the dispersion was treated with extruder to obtain a uniform size of vesicles. A mixed membrane of 5Cz18 and DDAB was prepared in a similar way, too. Cyt.c and a sacrificial electron donor were added individually to the dispersion after the membrane preparation.

Measurement. UV and fluorescence spectra were recorded on the apparatus described in Chapter 1. Partitioning of cyt.c into the bilayer membrane was determined by measuring the amount of cyt.c in the supernatant after centrifugation of the mixture of cyt.c and the bilayer membrane using a Ultrafree-MC (100,000 NMWL, Millipore Co., Ltd., MA). Photoreduction experiment was carried out after replacement of air in the sample solution with argon. The excitation light was sourced from a Xe lamp (500W, JASCO Co., Ltd., Japan), and was filtered by a colored optical glass (U-340, HOYA Co., Ltd., Japan) and a solution filter (a methanol solution of anthracene-9-carboxylic acid) to obtain an excitation light of a narrow band centered at 300 nm. The quantum yields of photoreduction (the number of reduced cyt.c / the number of photon absorbed by an aqueous dispersion) were determined at light intensity of 4.80×10^{-11} einstein s^{-1} as measured by a potassium ferrioxalate actinometry.[10,11] The degree of photoreduction of cyt.c was determined by the change of absorbance at 550 nm. The concentrations of compounds used in the three experiments were as follows: centrifugal filtration; [5Cz18] = [5Cz18Z] = 21, 42, 84 μM, [cyt.c] =

40 μM, quenching experiment; [5Cz18] = [5Cz18Z] = 6.5 μM, [cyt.c] = 0 − 17 μM, in the case of the mixed membrane; [5Cz18] = 6.5 μM, [DDAB] = 650 μM, photoreduction of cyt.c; [5Cz18] = [5Cz18Z] = 56 μM, [cyt.c] = 16 μM, [sacrificial electron donor] = 160 μM. All measurements were performed at 20 °C, where the bilayer membrane of 5Cz18 or 5Cz18Z was in the gel-state.

Results and Discussion

Partitioning of Cytochrome c into Bilayer Membranes. Partitioning of cyt.c into the 5Cz18 or 5Cz18Z bilayer membrane was investigated with varying concentrations of the amphiphile (Figure 3). Cyt.c was found to be scarcely partitioned into the cationic 5Cz18 membrane but favorably partitioned into the zwitterionic 5Cz18Z membrane.

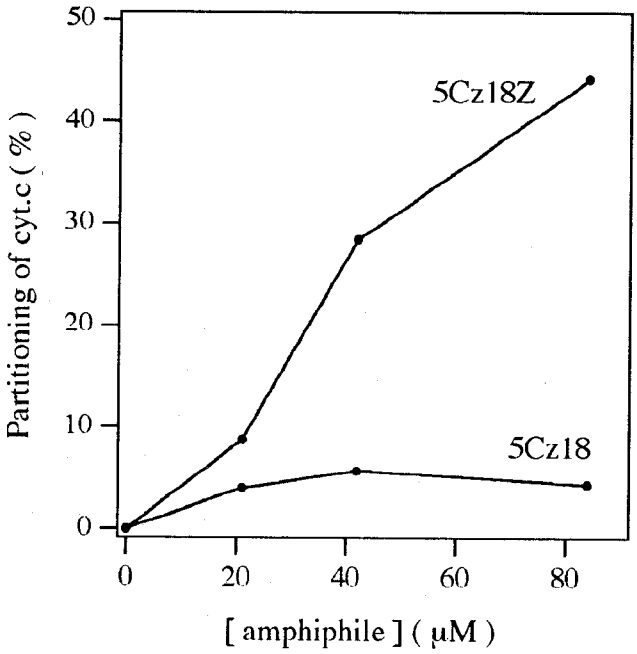

Figure 3. Partitioning of cyt.c into the 5Cz18 or 5Cz18Z membrane with varying the concentrations of amphiphiles.
Free and membrane-bound cyt.c were separated by centrifugal filtration. The amount of free cyt.c was determined by UV measurements.

This result can obviously be attributed to the cationic nature of cyt.c at the neutral pH. From the partitioning curve (Figure 3), About 30 molecules of 5Cz18 are calculated to be necessary for one molecule of cyt.c to be partitioned into the membrane.However, only 4.5 molecules are enough for cyt.c to bind to the 5Cz18Z membrane. Such extraordinary binding of cyt.c is also reported with the anionic membrane of dioleoyl phosphatidylglycerol, where the stoichiometry of the lipid and cyt.c at partitioning was 4.9.[12] However, cyt.c is generally reported to possess lower affinity for neutral membranes of zwitterionic amphiphiles such as phosphatidylcholine than that of anionic amphiphiles of phosphatidylglycerol or cardiolipin.[13] But cyt.c is partitioned into the 5Cz18Z membrane to the same extent as to the anionic dioleoyl phosphatidylglycerol membrane. The high partitioning of cyt.c into the 5Cz18Z membrane might be due to the molecular structure of 5Cz18Z where a carboxylate group is located at the terminal, thus, being exposed fully out of the membrane. This arrangement might be favorable for the electrostatic interaction of the cationic cyt.c molecule with the membrane.

Fluorescence Quenching of the ECz Group by Cytochrome c. Fluorescence quenching of 5Cz18, 5Cz18Z or 5Cz18/DDAB (mol/mol 1/100) membranes by electron transfer from the ECz group to cyt.c is shown in Figure 4 according to the Perrin plot. The quenching rate in the 5Cz18 or 5Cz18Z membrane was higher than that in the bicomponent membrane of 5Cz18 and DDAB. This difference is explained by efficient energy migration among ECz groups in the 5Cz18 or 5Cz18Z membrane, because the energy migration in the 5Cz18/DDAB membrane should be suppressed by DDAB molecules intervening in the lattice points of the ECz groups in the membrane. Although cyt.c is hardly partitioned into the 5Cz18 membrane as described above, the quenching rate was relatively high. This fact suggests that energy migration occurs efficiently to activate the ECz group near a small amount of cyt.c bound to the cationic 5Cz18 membrane by electrostatic interaction of anionic regions of cyt.c to the cationic surface of the membrane. This fact is in contradiction to the

result associated with the monolayer system described in Chapter 2. The relatively high quenching in the 5Cz18 bilayer membrane may arise from the favorable high curvature of bilayer membrane for cyt.c partitioning.

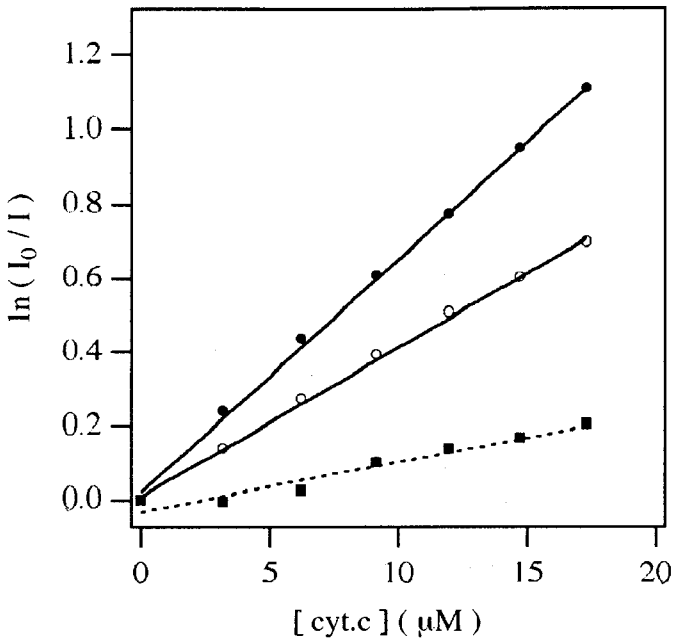

Figure 4. Perrin plots of fluorescence quenching of the ECz group in the 5Cz18 (○), 5Cz18Z (●) bilayer membrane or the 5Cz18Z/DDAB (■, 1/100 mol/mol) mixed bilayer membrane with varying concentrations of cyt.c. Excitation wavelength was 299 nm. Fluorescence intensity was calculated on the basis of the area in the fluorescence spectra.

Photoreduction of Cytochrome c in Bilayer Membranes. Photoreduction of cyt.c in the 5Cz18 or 5Cz18Z membrane was investigated in the presence of TEOA used as a sacrificial electron donor. The rate of cyt.c reduction is shown in Figure 5 together with the reference data in the absence of amphiphiles or without photoirradiation. Although cyt.c was hardly reduced in the control experiments, cyt.c reduction was promoted in the presence of membranes with photoexcitation of the ECz group. A slightly faster reduction in the presence of 5Cz18Z membrane

than 5Cz18 membrane qualitatively agrees with the results of the quenching experiment.

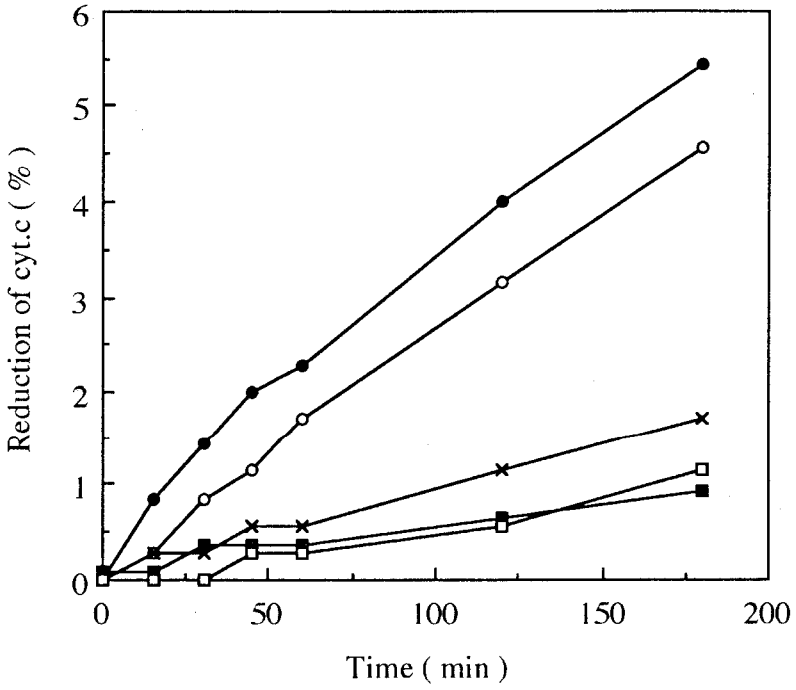

Figure 5. The effects of the 5Cz18 or 5Cz18Z membrane and photoirradiation on the photoreduction of cyt.c in the presence of TEOA: ●; 5Cz18Z/cyt.c/TEOA with irradiation, ○; 5Cz18/cyt.c/TEOA with irradiation, ×; cyt.c/TEOA with irradiation, ■; 5Cz18Z/cyt.c/TEOA without irradiation, □; 5Cz18/cyt.c/TEOA without irradiation.

Figure 6 shows the cyt.c reduction by EDTA used as a sacrificial donor. Cyt.c was reduced in the presence of the 5Cz18 membrane at a significantly higher rate than in the 5Cz18Z membrane and than in those systems shown in Figure 5. The quantum yields of these photoreduction systems are summarized in Table 1. The efficient cyt.c reduction should be attributed to the concentrated anionic EDTA molecules at the cationic membrane surface. It is notable that the cationic membrane surface does not seriously influence the rate of photoreduction of cyt.c with the electrically neutral sacrificial donor, but significantly promotes the photoreduction in the presence of the anionic donor. Therefore, the rate-determining step for this photoreduction system is the photoreduction of the oxidized ECz group by the sacrificial donor. In other words, the photoexcited ECz group should easily reduce

cyt.c due to the efficient photoenergy migration to the ECz group near to the cyt.c bound to the membrane.

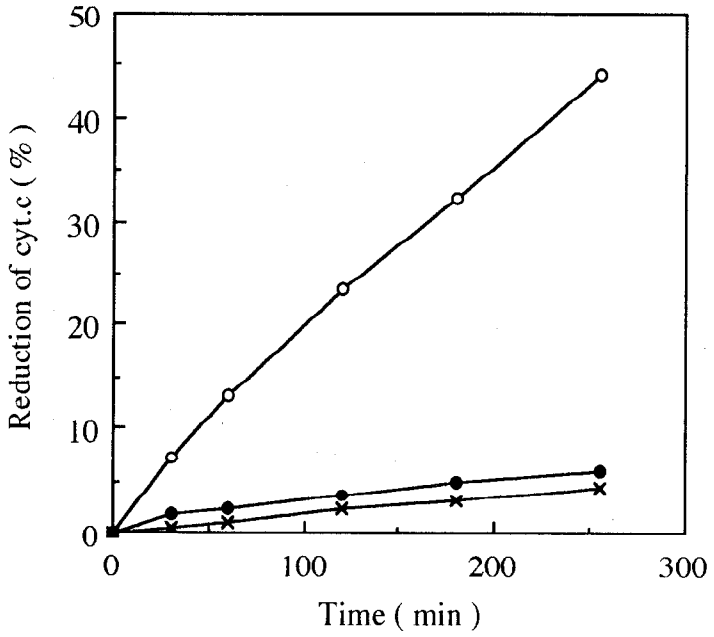

Figure 6. The effects of the 5Cz18 or 5Cz18Z membrane on the photoreduction of cyt.c in the presence of EDTA with photoirradiation: ●; 5Cz18Z/cyt.c/EDTA, ○; 5Cz18/cyt.c/EDTA, ×; cyt.c/EDTA.

Table 1. Quantum yields for photoreduction of cyt.c in the aqueous dispersion of 5Cz18 or 5Cz18Z with two different sacrificial donors, TEOA and EDTA.

	5Cz18 (%)[a]	5Cz18Z (%)[a]	without bilayer membrane (%)[b]
TEOA	0.58	0.75	0.092
EDTA	5.1	0.36	0.33

[a] The quantum yields were calculated on the basis of the number of photon absorbed by ECz groups. [b] In the absence of bilayer membranes, the number of photon absorbed by cyt.c was used for the calculation.

References and Notes

1) Dickerson, R. E.; Timkovich, R. In *The Enzymes*, 3rd ed.; Boyer, P. D., Ed.; Academic Press: New York, 1975; Vol. XIa, pp 397-547.

2) Mathews, F. S. *Prog. Biophys. Mol. Biol.* **1985**, *45*, 1.

3) Salamon, Z.; Tollin, G. *Biophys. J.* **1996**, *71*, 2.

4) Sui, S. F.; Wu, H.; Sheng, J.; Guo, Y. *J. Biochem.* **1994**, *115*, 1053.

5) Wang, J.; Wallace, C-J. A.; Clark-Lewis, I.; Caffrey, M. *J. Mol. Biol.* **1994**, *237*, 1.

6) Tanaka, H.; Hayashi, K.; Akatsuka, T.; Toyama, J.; Noda, K.; Kida, T.; Ogoma, Y.; Fujii, T.; Kondo, Y. *J. Biochem.* **1995**, *117*, 1151.

7) Willner, I.; Lion-Dagon, M.; Merx-Tibbon, S.; Katz, E. *J. Am. Chem. Soc.* **1995**, *117*, 6581.

8) Terrettaz, S.; Cheng, J.; Miller, C. J. *J. Am. Chem. Soc.* **1996**, *118*, 7857.

9) Zaslavsky, D. L.; Smirnova, I. A.; Siletsky, S. A.; Kaulen, A. D.; Millett, F.; Konstantinov, A. A. *FEBS Lett.* **1995**, *359*, 27.

10) Parker, C. A. *Proc. R. Soc., Ser. A* **1956**, *235*, 518.

11) Hatchard, C. G.; Parker, C. A. *Proc. R. Soc., Ser. A* **1956**, *235*, 518.

12) Heimburg, T.; Marsh, D. *Biophys. J.* **1995**, *68*, 536.

13) Salamon, Z.; Tollin, G. *Biophys. J.* **1996**, *71*, 848.

Part II Photoinduced Electron Transfer in a Self-Assembled Monolayer Composed of *N*-Ethylcarbazole-Containing Helical Peptides

Chapter 5

Spectroscopic Study on Direction and Inclination of Helical Peptides in a Monolayer Formed at the Air/Water Interface and on a Gold Substrate

Introduction

Peptide molecules can be designed and synthesized to adopt specific secondary structures.[1-4] It is interesting to assemble the peptide molecules therefore to construct novel molecular systems which function on the basis of their highly ordered structure.[5] For example, Ghadiri et al. have reported peptide nanotubes as artificial ion channels where cyclic β^3-peptides form a tubular structure by intermolecular hydrogen bondings.[6] Fujita et.al have prepared peptide monolayers at the air/water interface.[7] Worley et al. have synthesized poly(γ-L-benzyl glutamate) with lipoic acid at the N-terminal, and formed the peptide self-assembled monolayer (SAM) on a gold substrate under an electrostatic field.[8] Fujita et al.[9] or Miura et al.[10] have prepared the oriented α-helical peptide SAMs vertically to a gold substrate by utilizing the self-assembling property of the helical peptides. These peptide monolayers have been investigated on the conformation and inclination (molecular orientation with respect to the surface) at the air/water interface or on a metal substrate. However, the information about the direction of the helical peptide (parallel or antiparallel arrangement) in the monolayers is not obtained adequately.

In the present chapter, the orientation and arrangement of peptide molecules in monolayers at the air/water interface and in SAMs on a gold substrate were investigated by various spectroscopic

methods. All peptides have an alternating sequence of L-alanine (Ala) and α-aminoisobutyric acid (Aib) because of their high preference for adopting an α-helical structure.[11] An ECz group was covalently linked at the peptide terminal as a fluorescence probe. The structures of the peptide derivatives and a dialkyl control compound carrying an ECz group are shown in Figure 1 together with their abbreviations.

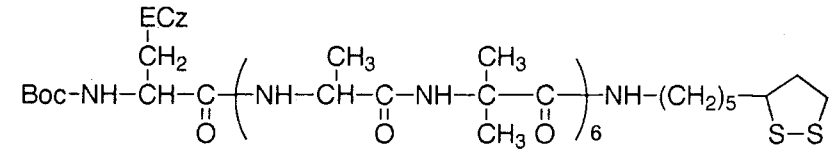

ECz-A12-SS

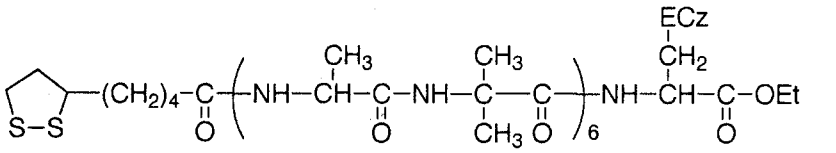

SS-A12-ECz

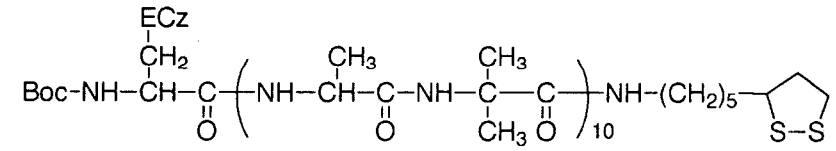

ECz-A20-SS

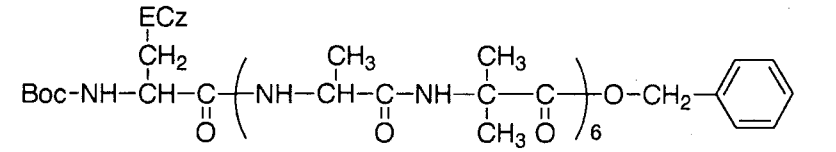

ECz-A12

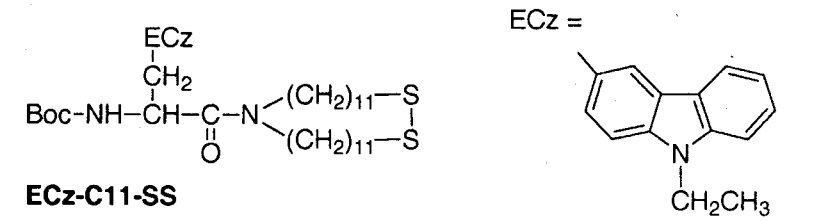

ECz-C11-SS

Figure 1. Molecular structures of peptide derivatives and a dialkyl compound carrying an ECz group.

Thiol and disulfide compounds are frequently used for covalent connection to a gold substrate via an S-Au linkage, forming highly ordered SAMs.[12] In order to obtain peptide SAMs, a disulfide group was covalently linked to the peptide terminal. The disulfide group was also used as a fluorescence quencher. ECz-A12-SS and SS-A12-ECz are tridecapeptide carrying an ECz group and a disulfide group at the terminals, however, in a reverse way about the N- or C-terminal. ECz-A20-SS is a heneicosapeptide analogous to ECz-A12-SS with respect to the positions of the functional groups. ECz-A12 is a tridecapeptide which carries an ECz group at the N-terminal but lacks disulfide group at the C-terminal. ECz-C11-SS is a disulfide compound composed of a dialkyl chain for the peptide chain.

Monolayers at the air/water interface were prepared from these compounds and the molecular orientation was investigated by π-A isotherms and circular dichroism (CD) measurements of Langmuir-Blodgett (LB) monolayers transferred on a quartz substrate. The molecular arrangement was determined by *in situ* fluorescence spectroscopy and computer simulation. The peptide SAMs on a gold substrate were investigated on the orientation and arrangement of peptide molecules by Fourier transform infrared reflection-absorption spectroscopy (FTIR-RAS) and fluorescence spectroscopy.

Experimental Section

Materials. ECz-A12-SS, SS-A12-ECz, ECz-A20-SS, ECz-A12 and ECz-C11-SS were synthesized according to Scheme 1. All peptides were synthesized by the conventional liquid-phase method. Boc-(Ala-Aib)$_2$-OH (BA4OH), Boc-(Ala-Aib)$_4$-OH (BA8OH) and Boc-(Ala-Aib)$_2$-OBzl (benzyl ester of BA4OH, BA4OBzl) were synthesized by the method in the literature.[13] All intermediates and final products were identified by ^{1}H NMR (400 MHz), and their purity was

checked by TLC. The final products were confirmed by mass spectroscopy. Solvent systems for TLC were (A) chloroform/methanol/acetic acid (90/10/3 v/v/v), (B) chloroform/methanol/acetic acid (95/5/3 v/v/v), (C) chloroform/methanol/ammonia water (13/5/1 v/v/v), (D) chloroform/methanol (9/2 v/v).

***N'*-(*tert*-Butyloxycarbonyl)-L-3-(3-*N*-ethylcarbazolyl)alanine [Boc-ECzAla].** ECzAla (173 mg) was reacted with di-*tert* -butylcarbonate (240 mg) with $NaHCO_3$ (100 mg) in water (10 ml) / dioxane (20 ml) at 0 °C for 2 h and thereafter at 25 °C for 4 h. The solvent was evaporated, and *n*-hexane was added to precipitate the reaction product (110 mg, 46.9 % yield). TLC: R_f(A)=0.65, R_f(C)=0.57. ^{1}H NMR (270 MHz, $CDCl_3$): δ (ppm) 1.37 (9H, s , $(CH_3)_3C$), 1.46 (3H, t, NCH_2CH_3), 3.26 (2H, d, $NHCHCH_2$), 4.27 (2H, q, NCH_2CH_3), 4.94 (1H, q, $NHCHCH_2$), 7.20-8.14 (7H, carbazolyl-*H*).

L-3-(3-*N*-Ethylcarbazolyl)alanine ethyl ester [ECzAla-OEt]. ECzAla (90 mg) was dissolved in ethanol (100 ml) and the solution was stirred at 0 °C for 2 h in the presence of hydrogen chloride. The reaction product was obtained by evaporation (66 mg, 67.8 % yield). TLC: R_f (A)=0.38, R_f(C)=0.93. ^{1}H NMR (270 MHz, $CDCl_3$): δ (ppm) 1.07 (3H, t, $COOCH_2CH_3$), 1.38 (3H, t, NCH_2CH_3), 3.55 (2H, d, NH_2CHCH_2), 4.06 (2H, q, $COOCH_2CH_3$), 4.26 (2H, q, NCH_2CH_3), 4.38 (1H, q, NH_2CHCH_2), 7.20-8.14 (7H, carbazolyl-*H*).

1,2-Dithia-3-(1-amino-*n*-pentyl)cyclopentane [A]. DL-α-Lipoamide (1000 mg) was dissolved in tetrahydrofuran (100 ml). The solution was added to dispersion of $LiAlH_4$ (826 mg) in tetrahydrofuran (50 ml), and the reaction solution was refluxed at 70 °C for 12 h.

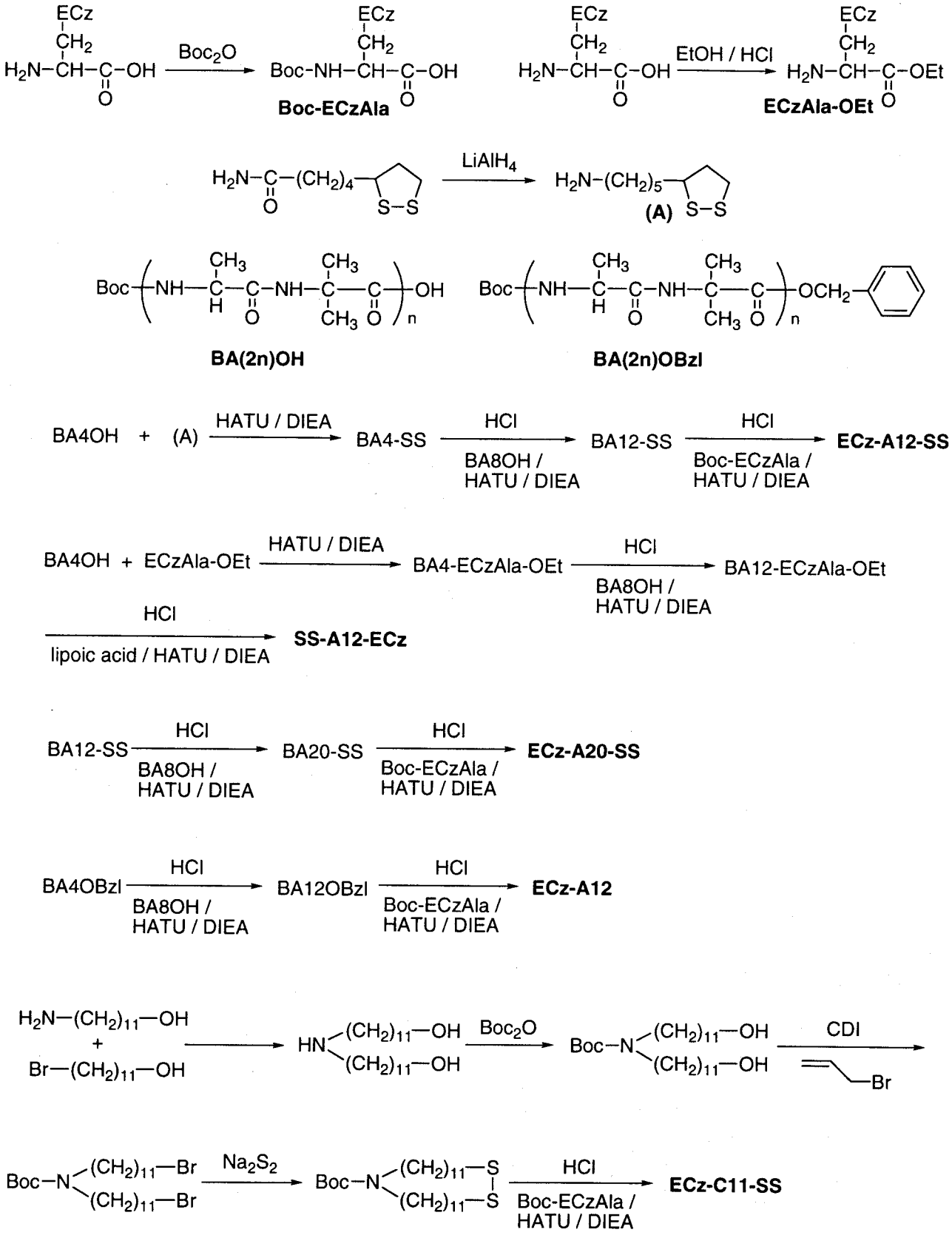

Scheme 1. Synthetic schemes of ECz-A12-SS, SS-A12-ECz, ECz-A20-SS, ECz-A12, and ECz-C11-SS.

Distilled water (8 ml) was added and the solution was stirred at 0 °C for 30 min. After evaporation of solvent, methanol was added and the insoluble solid was removed. The supernatant was evaporated and distilled water (100 ml) was added. The pH of the solution was adjusted to 6.5 with 1 N hydrochloric acid, and the solution was stirred at room temperature for 24 h. The reaction product was extracted with *n*-butanol and washed with 1 N aqueous NaOH solution and 1 N hydrochloric acid. The reaction product was obtained by solvent evaporation (396 mg, 42.5 % yield). TLC: R_f(A)=0.18, R_f(C)=0.50. ^{1}H NMR (270 MHz, $CDCl_3$): δ (ppm) 1.48 (4H, m, NH_3+$CH_2CH_2CH_2CH_2CH_2$), 1.64 (4H, m, NH_3+$CH_2CH_2CH_2CH_2CH_2$), 1.89, 2.47 (2H, m, $CHCH_2CH_2SS$), 2.88 (2H, t, NH_3+$CH_2CH_2CH_2CH_2CH_2$), 3.15 (2H, m, $CHCH_2CH_2SS$), 3.58 (1H, m, $CHCH_2CH_2SS$). MS (GC): m/z 191 (calcd for $C_8H_{17}NS_2$ [M+] m/z 191.08).

BA4-SS. BA4OH (240 mg) was dissolved in chloroform (6 ml), and was reacted with 1,2-dithia-3-(1-amino-*n*-pentyl)cyclopentane (254 mg) in the presence of HATU (318 mg) with DIEA (436 µl) at 0 °C for 10 min and thereafter at 25 °C for 24 h. The solvent was removed and the remaining solid was purified by a Sephadex LH-20 column using methanol as eluant (171 mg, 51.0 % yield). TLC: R_f(A)=0.60, R_f(C)=0.75. ^{1}H NMR (270 MHz, $CDCl_3$): δ (ppm) 1.35-1.60 (31H, brm, $NHCH(CH_3)CONHC(CH_3)_2$, $NHCH_2CH_2CH_2CH_2CH_2$, $(CH_3)_3C$), 1.63 (4H, m, $NHCH_2CH_2CH_2CH_2CH_2$), 1.85, 2.41 (2H, m, $CHCH_2CH_2SS$), 3.13 (2H, m, $CHCH_2CH_2SS$), 3.17 (2H, brs, $NHCH_2CH_2CH_2CH_2CH_2$), 3.53 (1H, m, $CHCH_2CH_2SS$), 3.87, 4.06 (2H, m, $NHCH(CH_3)CONHC(CH_3)_2$), 5.53 (1H, s, $NHCH_2CH_2CH_2CH_2CH_2$), 6.73, 6.99, 7.51 (4H, s, $NHCH(CH_3)CONHC(CH_3)_2$). MS (FAB, matrix; nitrobezylalcohol): m/z 604 (calcd for $C_{27}H_{50}N_5O_6S_2$ [(M+H)+] m/z 604.31).

BA12-SS. The Boc group of BA4-SS (42 mg) was removed by treatment with 4 N HCl in dioxane, and the product dissolved in chloroform (2 ml) was reacted with BA8OH (52 mg) in the presence of HATU (40 mg) with DIEA (27 μl) at 0 °C for 10 min and thereafter at 25 °C for 24 h. After removal of the solvent, the remaining solid was dissolved in chloroform and washed with 4 wt% $NaHCO_3$ aqueous solution and 4 wt% $NaHSO_4$ aqueous solution. The solvent was removed and the remaining solid was purified by a Sephadex LH-20 column using methanol as eluant (25 mg, 29.2 % yield). TLC: R_f(A)=0.63, R_f(C)=0.77. ^{1}H NMR (270 MHz, $CDCl_3$): δ (ppm) 1.35-1.60 (71H, brm, NHCH(CH_3)CONHC(CH_3)$_2$, $NHCH_2CH_2CH_2CH_2CH_2$, (CH_3)$_3$C), 1.85, 2.41 (2H, m, $CHCH_2CH_2SS$), 3.13 (2H, m, $CHCH_2CH_2SS$), 3.17 (2H, brs, $NHCH_2CH_2CH_2CH_2CH_2$), 3.53 (1H, m, $CHCH_2CH_2SS$), 3.95, 4.24 (6H, m, NHCH(CH_3)CONHC(CH_3)$_2$), 5.68 (1H, s, $NHCH_2CH_2CH_2CH_2CH_2$), 7.30-7.72 (12H, s, NHCH(CH_3)CONHC(CH_3)$_2$). MS (FAB, matrix; nitrobezylalcohol): m/z 1251 (calcd for $C_{55}H_{97}N_{13}O_{14}S_2Na_1$ [(M+Na)+] m/z 1250.67).

ECz-A12-SS. The Boc group of BA12-SS (25 mg) was removed by treatment with 4 N HCl in dioxane, and the product dissolved in chloroform (1 ml) was reacted with Boc-ECzAla (10 mg) in the presence of HATU (15 mg) with DIEA (10 μl) at 0 °C for 10 min and thereafter at 25 °C for 24 h. After removal of the solvent, the remaining solid was dissolved in chloroform and washed with 4 wt% $NaHCO_3$ aqueous solution and 4 wt% $NaHSO_4$ aqueous solution. The solvent was removed and the remaining solid was purified by a Sephadex LH-20 column using methanol as eluant (17 mg, 55.2 % yield). TLC: R_f(A)=0.60, R_f(C)=0.81. ^{1}H NMR (270 MHz, $CDCl_3$): δ (ppm) 1.35-1.60 (74H, brm, NHCH(CH_3)CONHC(CH_3)$_2$, $NHCH_2CH_2CH_2CH_2CH_2$, (CH_3)$_3$C, NCH_2CH_3), 1.85, 2.41 (2H, m, $CHCH_2CH_2SS$), 3.15-3.20 (6H, brm, $CHCH_2CH_2SS$, $NHCH_2CH_2CH_2CH_2CH_2$, $NHCHCH_2$), 3.53 (1H, m, $CHCH_2CH_2SS$), 3.95, 4.24 (6H, m,

NHC*H*(CH_3)CONHC(CH_3)$_2$), 4.29 (2H, q, NC*H*$_2$CH$_3$), 4.41 (1H, q, NHC*H*CH$_2$), 5.81 (1H, s, N*H*CH$_2$CH$_2$CH$_2$CH$_2$CH$_2$), 7.30-8.12 (20H, brm, N*H*CH(CH_3)CON*H*C(CH_3)$_2$, N*H*CHCH$_2$, carbazolyl-*H*). MS (FAB, matrix; nitrobezylalcohol): m/z 1515 (calcd for $C_{72}H_{113}N_{15}O_{15}S_2Na_1$ [(M+Na)+] m/z 1514.80).

BA4-ECzAla-OEt. BA4OH (67 mg) was dissolved in chloroform (2 ml) and reacted with ECzAla-OEt (54 mg) in the presence of HATU (89 mg) with DIEA (61 μl) at 0 °C for 10 min and thereafter at 25 °C for 12 h. The solvent was removed and the remaining solid was purified by a Sephadex LH-20 column using methanol as eluant (73 mg, 65.2 % yield). TLC: R_f(A)=0.65, R_f(C)=0.78. ^{1}H NMR (270 MHz, $CDCl_3$): δ (ppm) 1.07 (3H, t, COOCH$_2$C*H*$_3$), 1.25-1.44 (21H, brm, NHCH(C*H*$_3$)CONHC(C*H*$_3$)$_2$, NCH$_2$C*H*$_3$), 1.49 (9H, s, (C*H*$_3$)$_3$C), 3.25 (2H, d, NHCHC*H*$_2$), 3.83, 4.13 (2H, m, NHC*H*(CH_3)CONHC(CH_3)$_2$), 4.06 (2H, q, COOC*H*$_2$CH$_3$), 4.29 (2H, q, NC*H*$_2$CH$_3$), 4.74 (1H, q, NHC*H*CH$_2$), 5.62 (1H, d, N*H*CHCH$_2$), 7.18-8.04 (11H, carbazolyl-*H*, N*H*CH(CH_3)CON*H*C(CH_3)$_2$).

BA12-ECzAla-OEt. The Boc group of BA4-ECzAla-OEt (14 mg) was removed by treatment with 4 N HCl in dioxane, and the product dissolved in chloroform (2 ml) was reacted with BA8OH (17 mg) in the presence of HATU (13 mg) with DIEA (9 μl) at 0 °C for 10 min and thereafter at 25 °C for 24 h. After removal of the solvent, the remaining solid was dissolved in chloroform and washed with 4 wt% $NaHCO_3$ aqueous solution and 4 wt% $NaHSO_4$ aqueous solution. The solvent was removed and the remaining solid was purified by a Sephadex LH-20 column using methanol as eluant (17 mg, 65.1 % yield). TLC: R_f(A)=0.25, R_f(C)=0.61. ^{1}H NMR (270 MHz, $CDCl_3$): δ (ppm) 1.11 (3H, t, COOCH$_2$C*H*$_3$), 1.38-1.55 (66H, brm, NHCH(C

H_3)CONHC(CH_3)$_2$, NCH$_2$CH_3, (CH_3)$_3$C), 3.24 (2H, d, NHCHCH_2), 3.82, 3.95 (6H, m, NHCH(CH$_3$)CONHC(CH$_3$)$_2$), 4.06 (2H, q, COOCH_2CH$_3$), 4.32 (2H, q, NCH_2CH$_3$), 4.80 (1H, q, NHCHCH$_2$), 5.92 (1H, d, NHCHCH$_2$), 7.10-8.10 (19H, carbazolyl-H, NHCH(CH$_3$)CONHC(CH$_3$)$_2$). MS (FAB, matrix; nitrobezylalcohol): m/z 1370 (calcd for $C_{66}H_{102}N_{14}O_{16}Na_1$ [(M+Na)+] m/z 1369.76).

SS-A12-ECz. The Boc group of BA12-ECzAla-OEt (17 mg) was removed by treatment with 4 N HCl in dioxane, and the product dissolved in chloroform (1 ml) was reacted with DL-α-lipoic acid (5 mg) in the presence of HATU (14 mg) with DIEA (10 μl) at 0 °C for 10 min and thereafter at 25 °C for 24 h. After removal of the solvent, the remaining solid was dissolved in chloroform and washed with 4 wt% $NaHCO_3$ aqueous solution and 4 wt% $NaHSO_4$ aqueous solution. The solvent was removed and the remaining solid was purified by a Sephadex LH-20 column using methanol as eluant (6 mg, 33.3 % yield). TLC: R_f(A)=0.43, R_f(C)=0.89. ^{1}H NMR (270 MHz, $CDCl_3$): δ (ppm) 1.10 (3H, t, COOCH$_2$CH_3), 1.35-1.62 (63H, brm, NHCH(CH_3) CONHC(CH_3)$_2$, NCH$_2$CH_3, CH$_2$(CH_2)$_3$CHCH$_2$CH$_2$SS), 1.80, 2.40 (2H, m, CH$_2$(CH$_2$)$_3$ CHCH_2CH$_2$SS), 2.38 (2H, brs, CH_2(CH$_2$)$_3$CHCH$_2$CH$_2$SS), 3.12 (2H, m, CH$_2$(CH$_2$)$_3$ CHCH$_2$CH_2SS), 3.32 (2H, d, NHCHCH_2), 3.48 (1H, m, CH$_2$(CH$_2$)$_3$CHCH$_2$CH$_2$SS), 3.94, 4.10 (6H, m, NHCH(CH$_3$)CONHC(CH$_3$)$_2$), 4.06 (2H, q, COOCH_2CH$_3$), 4.32 (2H, q, NCH_2CH$_3$), 4.70 (1H, q, NHCHCH$_2$), 7.12-8.15 (20H, carbazolyl-H, NHCH(CH$_3$)CONHC(CH$_3$)$_2$, NHCHCH$_2$). MS (FAB, matrix; nitrobezylalcohol): m/z 1458 (calcd for $C_{69}H_{106}N_{14}O_{15}S_2Na_1$ [(M+Na)+] m/z 1457.74).

BA20-SS. The Boc group of BA12-SS (67 mg) was removed by treatment with 4 N HCl in dioxane, and the product dissolved in chloroform (3 ml) was reacted with BA8OH (60 mg) in the presence of HATU (46 mg) with DIEA (32 μl) at 0 °C for 10 min and thereafter at 25 °C for 24 h. After removal of the solvent, the remaining solid was dissolved in chloroform and washed with 4 wt% $NaHCO_3$ aqueous solution and 4 wt% $NaHSO_4$ aqueous solution. The solvent was removed and the remaining solid was purified by a Sephadex LH-20 column using methanol as eluant (101 mg, 53.9 % yield). TLC: R_f(A)=0.43, R_f(C)=0.85. ^{1}H NMR (270 MHz, $CDCl_3$): δ (ppm) 1.31-1.70 (107H, brm, NHCH(C*H*$_3$)CONHC(C*H*$_3$)$_2$, NHCH$_2$C*H*$_2$C*H*$_2$C*H*$_2$C*H*$_2$, (C*H*$_3$)$_3$C), 1.87, 2.41 (2H, m, CHC*H*$_2$CH$_2$SS), 3.07-3.14 (4H, brm, CHCH$_2$C*H*$_2$SS, NHC*H*$_2$CH$_2$CH$_2$CH$_2$CH$_2$), 3.52 (1H, m, C*H*CH$_2$CH$_2$SS), 3.93, 4.27 (10H, m, NHC*H*(CH$_3$)CONHC(CH$_3$)$_2$), 6.86 (1H, s, N*H*CH$_2$CH$_2$CH$_2$CH$_2$CH$_2$), 7.46-8.03 (20H, brm, N*H*CH(CH$_3$)CON*H*C(CH$_3$)$_2$).

ECz-A20-SS. The Boc group of BA20-SS (54 mg) was removed by treatment with 4 N HCl in dioxane, and the product dissolved in chloroform (4 ml) was reacted with Boc-ECzAla (17 mg) in the presence of HATU (25 mg) with DIEA (17 μl) at 0 °C for 10 min and thereafter at 25 °C for 24 h. After removal of the solvent, the remaining solid was dissolved in chloroform and washed with 4 wt% $NaHCO_3$ aqueous solution and 4 wt% $NaHSO_4$ aqueous solution. The solvent was removed and the remaining solid was purified by a Sephadex LH-20 column using methanol as eluant (45 mg, 72.6 % yield). TLC: R_f(A)=0.45, R_f(C)=0.90. ^{1}H NMR (270 MHz, $CDCl_3$): δ (ppm) 1.35-1.58 (110H, brm, NHCH(C*H*$_3$)CONHC(C*H*$_3$)$_2$, NHCH$_2$C*H*$_2$C*H*$_2$C*H*$_2$C*H*$_2$, (C*H*$_3$)$_3$C, NCH$_2$C*H*$_3$), 1.73, 2.35 (2H, m, CHC*H*$_2$CH$_2$SS), 2.97 (2H, m, CHCH$_2$C*H*$_2$SS), 3.15-3.30 (4H, brm, NHC*H*$_2$CH$_2$CH$_2$CH$_2$CH$_2$, NHCHC*H*$_2$), 3.52 (1H, m, C*H*CH$_2$CH$_2$SS), 3.93, 4.30 (10H, m, NHC*H*(CH$_3$)CONHC(CH$_3$)$_2$), 4.20 (2H, q, NC*H*$_2$CH$_3$), 4.28 (1H, q, NHC*H*CH$_2$), 5.92 (1H, s,

N*H*$CH_2CH_2CH_2CH_2CH_2$), 7.30-8.12 (28H, brm, N*H*$CH(CH_3)CONHC(CH_3)_2$, N*H*$CHCH_2$, carbazolyl-*H*). MS (FAB, matrix; nitrobezylalcohol): m/z 2139 (calcd for $C_{100}H_{161}N_{23}O_{23}S_2Na_1$ [(M+Na)+] m/z 2139.16).

BA12OBzl. The Boc group of BA4OBzl (233 mg) was removed by treatment with 4 N HCl in dioxane, and the product dissolved in chloroform (5 ml) was reacted with BA8OH (334 mg) in the presence of HATU (256 mg) with DIEA (176 μl) at 0 °C for 10 min and thereafter at 25 °C for 24 h. After removal of the solvent, the remaining solid was dissolved in chloroform and washed with 4 wt% $NaHCO_3$ aqueous solution and 4 wt% $NaHSO_4$ aqueous solution. The solvent was removed and the remaining solid was purified by a Sephadex LH-20 column using methanol as eluant (133 mg, 25.9 % yield). TLC: R_f(B)=0.18, R_f(C)=0.88. ^{1}H NMR (270 MHz, $CDCl_3$): δ (ppm) 1.38-1.58 (63H, brm, NHCH(CH_3)CONHC(CH_3)$_2$, (CH_3)$_3$C, NCH_2CH_3), 3.96, 4.25 (6H, m, NHC*H*(CH_3)CONHC(CH_3)$_2$), 5.11 (2H, m, OCH_2), 5.53 (1H, s, N*H*$CHCH_2$), 7.23-7.67 (17H, brm, N*H*$CH(CH_3)CONHC(CH_3)_2$, phenyl-*H*).

ECz-A12. The Boc group of BA12OBzl (20 mg) was removed by treatment with 4 N HCl in dioxane, and the product dissolved in chloroform (2 ml) was reacted with Boc-ECzAla (6.7 mg) in the presence of HATU (10 mg) with DIEA (6.8 μl) at 0 °C for 10 min and thereafter at 25 °C for 24 h. After removal of the solvent, the remaining solid was dissolved in chloroform and washed with 4 wt% $NaHCO_3$ aqueous solution and 4 wt% $NaHSO_4$ aqueous solution. The solvent was removed and the remaining solid was purified by a Sephadex LH-20 column using methanol as eluant (14 mg, 58.8 % yield). TLC: R_f(B)=0.65, R_f(C)=0.88. ^{1}H NMR (270 MHz, $CDCl_3$): δ (ppm) 1.39-1.65 (66H, brm, NHCH(CH_3)CONHC(CH_3)$_2$, (CH_3)$_3$C, NCH_2CH_3), 3.13-3.42 (2H, d, NHCHCH_2),

3.96, 4.25 (6H, m, NHC*H*(CH_3)CONHC(CH_3)$_2$), 4.37 (3H, brm, NC$H_2$$CH_3$, NHC*H*$CH_2$), 5.12 (2H, m, OC$H_2$), 5.53 (1H, s, N*H*C$HCH_2$), 7.22-8.08 (24H, brm, N*H*CH(CH_3)CON*H*C(CH_3)$_2$, phenyl-*H*, carbazolyl-*H*). MS (FAB, matrix; nitrobezylalcohol): m/z 1432 (calcd for $C_{71}H_{104}N_{14}O_{16}Na_1$ [(M+Na)+] m/z 1431.77).

***N,N*-Di(1-hydroxy-*n*-undecyl)amine.** 1-Amino-11-hydroxyundecane (480 mg) and 1-bromo-11-hydroxyundecane (643 mg) were dissolved in ethanol (20 ml) and the solution was refluxed at 80 °C for 24 h in the presence of K_2CO_3 (1060 mg). After removal of K_2CO_3 by filtration, the solvent was removed and the remaining solid was purified by a Sephadex LH-20 column using methanol as eluant (255 mg, 27.8 % yield). TLC: R_f(B)=0.29, R_f(D)=0.48. ^{1}H NMR (270 MHz, $CDCl_3$): δ (ppm) 1.25 (28H, brs, NHCH_2CH_2(CH_2)$_7$CH_2CH_2OH), 1.53 (8H, m, NHCH_2CH_2(CH_2)$_7$CH_2CH_2OH), 2.53 (4H, t, NHCH_2CH_2(CH_2)$_7$CH_2CH_2OH), 3.60 (4H, t, NHCH_2CH_2(CH_2)$_7$CH_2CH_2OH).

***N*-(*tert*-Butyloxycarbonyl)-*N,N*-di(1-hydroxy-*n*-undecyl)amine.** *N,N*-Di(1-hydroxy-*n*-undecyl)amine (234 mg) and di-*tert*-butylcarbonate (171 mg) were dissolved in chloroform (10 ml) and the solution was stirred at room temperature for 4 h. The solvent was removed and a crude product was obtained (317 mg, 106 % yield). TLC: R_f(B)=0.54, R_f(D)=0.79. ^{1}H NMR (270 MHz, $CDCl_3$): δ (ppm) 1.24 (28H, brs, NCH_2CH_2(CH_2)$_7$CH_2CH_2OH), 1.46 (9H, s, (CH_3)$_3$C), 1.53 (8H, m, NCH_2CH_2(CH_2)$_7$CH_2CH_2OH), 3.10 (4H, t, NCH_2CH_2(CH_2)$_7$ CH_2CH_2OH), 3.61 (4H, t, NCH_2CH_2(CH_2)$_7$CH_2CH_2OH).

***N*-(*tert*-Butyloxycarbonyl)-*N,N*-di(1-bromo-*n*-undecyl)amine.** *N*-(*tert*-Butyloxy-

carbonyl)-*N*,*N*-di(1-hydroxy-*n*-undecyl)amine (200 mg) was reacted with 1,1'-carbonyl-bis-1H-imidazole (CDI) (70 mg) in acetonitrile (10 ml) at room temperature for 30 min. Allylbromide (7.6 ml) was added and the solution was refluxed at 70 °C for 4 h. After removal of solvent, the reaction product was dissolved in chloroform and washed with 10 wt% aqueous citric acid solution and saturated aqueous NaCl solution. The solvent was evaporated and the reaction product was obtained (154 mg, 60.4 % yield). TLC: R_f(B)=0.91, R_f(D)=0.94. ^{1}H NMR (270 MHz, $CDCl_3$): δ (ppm) 1.24 (28H, brs, $NCH_2CH_2(CH_2)_7CH_2CH_2Br$), 1.46 (9H, s, $(CH_3)_3C$), 1.53 (8H, m, $NCH_2CH_2(CH_2)_7CH_2CH_2Br$), 3.11 (4H, t, $NCH_2CH_2(CH_2)_7CH_2CH_2Br$), 3.37 (4H, t, $NCH_2CH_2(CH_2)_7CH_2CH_2Br$).

1-(*tert*-Butyloxycarbonyl)-1-aza-13,14-dithiacyclopentacosane. *N*-(*tert*-Butyloxycarbonyl)-*N*,*N*-di(1-bromo-*n*-undecyl)amine (40 mg) was reacted with sodium hydrosulfide (77 mg) in ethanol (10 ml) at room temperature for 24 h. The solution was neutralized with acetic acid /ethanol (1/10 v/v), iodide (22 mg) was added and the solution was stirred at room temperature for 6 h. After evaporation of solvent, chloroform was added and the insoluble solid was removed. The solvent was removed and the reaction product was obtained (27 mg, 80.9 % yield). TLC: R_f (B)=0.87, R_f(D)=0.91. ^{1}H NMR (270 MHz, $CDCl_3$): δ (ppm) 1.24 (28H, brs, $NCH_2CH_2(CH_2)_7CH_2CH_2SS$), 1.46 (13H, brs, $(CH_3)_3C$, $NCH_2CH_2(CH_2)_7CH_2CH_2SS$), 1.53 (4H, m, $NCH_2CH_2(CH_2)_7CH_2CH_2SS$), 2.65 (4H, t, $NCH_2CH_2(CH_2)_7CH_2CH_2SS$), 3.10 (4H, t, $NCH_2CH_2(CH_2)_7CH_2CH_2SS$).

ECz-C11-SS. The Boc group of 1-(*tert*-butyloxycarbonyl)-1-aza-13,14-dithiacyclopentacosane (26 mg) was removed by treatment with 4 N HCl in dioxane, and the product dissolved

in chloroform (1 ml) was reacted with Boc-ECzAla (24 mg) in the presence of HATU (36 mg) with DIEA (25 μl) at 0 °C for 10 min and thereafter at 25 °C for 12 h. After concentration of the solution, methanol was added to precipitate the reaction product and the product was purified by a Sephadex LH-20 column using tetrahydrofuran as eluant (19 mg, 47.8 % yield). TLC: R_f(B)=0.78, R_f (C)=0.93. ^{1}H NMR (270 MHz, $CDCl_3$): δ (ppm) 1.25 (28H, brs, $NCH_2CH_2(CH_2)_7CH_2CH_2SS$), 1.40 (16H, brs, $NCH_2CH_2(CH_2)_7CH_2CH_2SS$, $NH_2CH_2CH_3$, $(CH_3)_3C$), 1.57 (4H, m, $NCH_2CH_2(CH_2)_7CH_2CH_2SS$), 2.66 (4H, t, $NCH_2CH_2(CH_2)_7CH_2CH_2SS$), 2.83 (4H, brs, $NCH_2CH_2(CH_2)_7CH_2CH_2SS$), 3.13 (2H, d, $NHCHCH_2$), 4.30 (2H, q, $NHCH_2CH_3$), 4.80 (1H, q, $NHCHCH_2$), 5.41 (1H, d, $NHCHCH_2$), 7.20-8.14 (7H, carbazolyl-*H*). MS (FAB, matrix; nitrobezylalcohol + thioglycerol): m/z 753 (calcd for $C_{44}H_{70}N_3O_3S_2$ [(M+H)$^+$] m/z 752.48), m/z 860 (calcd for $C_{47}H_{78}N_3O_5S_3$ [(M+ thioglycerol+ H)$^+$] m/z 860.50), m/z 966 (calcd for $C_{50}H_{86}N_3O_7S_4$ [(M+ 2thioglycerol+ H)$^+$] m/z 968.53).

Monolayer Preparation. The preparation of monolayers at the air/water interface was carried out by the procedure described in Chapter 1 except for the concentration of the preparative solution (5.0 x 10^{-4} M). LB monolayers were prepared by transferring the monolayer on the water subphase to a quartz substrate by the horizontal lifting method. The SAMs were prepared as follows. A slide glass was washed thoroughly with methanol and distilled water followed by H_2SO_4 (97 %) : H_2O_2 (30 %) = 7:3 (a piranha solution) for 3 h. A substrate coated with gold was prepared by vapor deposition of chrominium and then gold (99.99 %) onto the slide glass. The thickness of the chrominium and gold layers, monitored by a quartz oscillator, were approximately 100 and 1000 Å, respectively. The gold substrate was used for a self-assembling experiment within a few days after preparation. The gold substrate was incubated in an ethanol solution of a disulfide compound

(0.1 mM) for 24 h. After the incubation, the substrate was rinsed rigorously with ethanol and dried in stream of dry nitrogen gas.

Fluorescence Spectroscopy of Peptide Monolayers. *In situ* fluorescence spectroscopy for the monolayers at the air/water interface was performed by the apparatus described in Chapter 2. The light is sourced from a Xe lamp (500W, JASCO Co., Ltd., Japan), and a monochromatic light (half width of 10 nm) was obtained by a home-made spectrometer. Fluorescence spectra of the SAMs on the gold substrate were recorded on a fluorescence spectrometer (F4010, Hitachi Co., Ltd., Japan) in a front-face mode with a 15° angle between the gold substrate and detector.[14] All measurements were performed at room temperature.

CD Measurement. A CD spectrum of the peptide LB monolayer was measured at room temperature on a CD spectrometer (J-600, JASCO Co., Ltd., Japan) by lining up eight quartz plates on which the peptide monolayer was deposited.

Quartz Crystal Microbalance (QCM) Measurement. QCM is known to be a very sensitive mass measuring device.[15,16] The QCM used is a commercially available 9 MHz, AT-cut quartz (diameter 9 mm), purchased from USI Co., Ltd. (Japan). The quartz-crystal plates with Au deposited on both sides were used. The 9 MHz QCM was connected to a oscillator (Q-200S, USI Co., Ltd., Japan). The frequency changes were followed by a universal counter (model 53131A, Hewlett-Packard Co., Ltd., CA). The following equation (eq. (1)) has been established for an AT-cut shear mode QCM.[17]

$$\Delta F = \frac{-2F_0^2}{A\sqrt{\rho_q \mu_q}} \Delta m \qquad (1)$$

ΔF, F_0, Δm, A, ρ_q, and μ_q represent the measured frequency shift (Hz), the fundamental frequency of the QCM (9 x 10^6 Hz), the mass change (g), the electrode area (0.16 cm^2), the density of the quartz (2.65 g cm^{-3}), and the shear modulus of the quartz (2.95 x 10^{11} dyn cm^{-2}), respectively. The both sides of the Au electrode of the QCM were washed with a piranha solution in order to remove organic adsorbate impurities from the surfaces. The QCM was rinsed with Milli-Q water and methanol, and dried in a vacuum. The QCM was immersed into an ethanol solution of a disulfide compound (0.1 mM) for 3-5 h. After washing with ethanol, the QCM was dried in the air, and the mass change was calculated from the frequency shift using eq. (1).

Fourier Transform Infrared Reflection-Absorption Spectroscopy (FTIR-RAS). The FTIR spectra were recorded on a Fourier transform infrared spectrometer (Magna 850, Nicolet Japan Co., Ltd., Japan) at room temperature. For RAS measurements, a reflection attachment (model RMA-1DG/VRA, Harrick Co., Ltd., NY) was used, and a *p*-polarized beam was obtained through an Au/AuBr wire-grid polarizer (Hitachi Co., Ltd., Japan). The incident angle was set at 85° from the surface normal. The number of interferogram accumulations was 500. Molecular orientation of the peptide monolayer on the gold substrate was determined on the basis of the amide I / amide II absorbance ratio in the FTIR-RAS spectrum according to eq. (2) under the assumption of a uniform crystal of the peptide-thin layer.[18-21]

$$\frac{I_1}{I_2} = 1.5 \times \frac{(3\cos^2\gamma - 1)(3\cos^2\theta_1 - 1) + 2}{(3\cos^2\gamma - 1)(3\cos^2\theta_2 - 1) + 2} \qquad (2)$$

I_i, γ, and θ_i (i=1 or 2 corresponding to amide I or amide II) represent the observed absorbance, the tilt angle of the helix axis from the surface normal, and the angle between the transition moment and the helix axis, respectively. The values of the θ_1 and θ_2 are taken to be 39° and 75°, respectively.[22]

Results and Discussion

Orientation of Helical Peptides in Monolayers at the Air/Water Interface. The π-A isotherms of the ECz-A12-SS, SS-A12-ECz, ECz-A20-SS, ECz-A12, and ECz-C11-SS monolayers are shown in Figure 2.

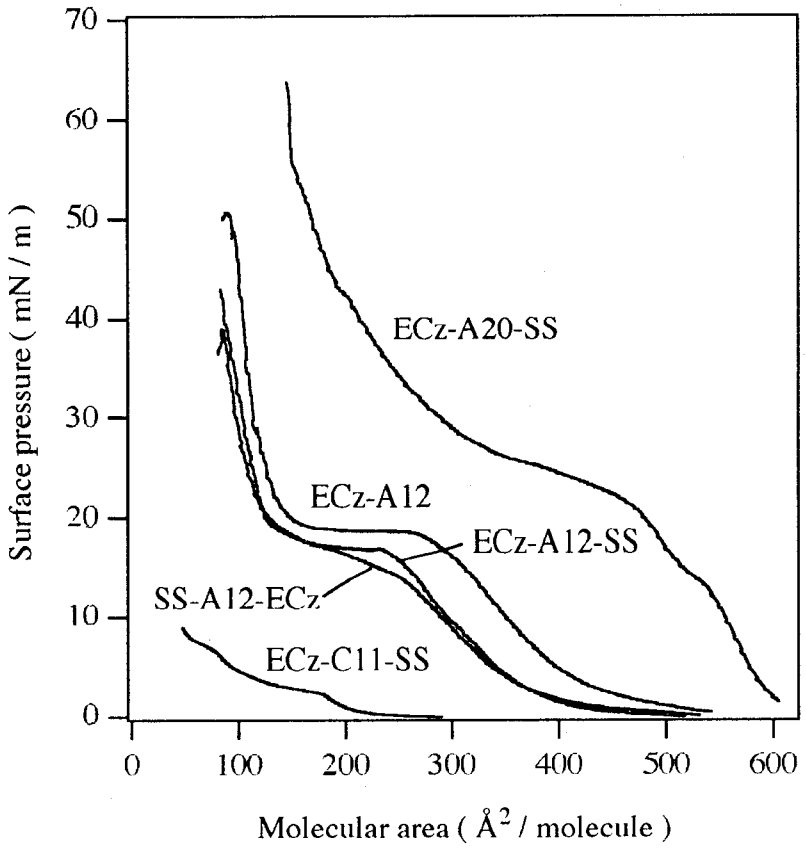

Figure 2. π-A Isotherms of ECz-A12-SS, SS-A12-ECz, ECz-A20-SS, ECz-A12, and ECz-C11-SS on the water subphase.

The isotherms of the ECz-A12-SS and SS-A12-ECz monolayers seem to be nearly the same, which present a plateau in the region of molecular area 250-120 Å^2/molecule. A molecular area of a peptide lying parallel to the water surface was calculated to be about 270 Å^2/molecule by using the length of the tridecapeptide (28 Å) for a fully helical conformation and the diameter of the helix (9.6 Å).[11] This

area corresponds to the starting point of the plateau region. It is thus considered that the peptides are lying flat on the water subphase and change the physical state upon further compression in the plateau region. The isotherm of the ECz-A12 monolayer also has analogous profile but its plateau region shifts to a larger molecular area, indicating a larger molecular size on the water subphase. The isotherm of the ECz-A20-SS molecule shifts to a larger molecular area because of the larger cross-section area of the heneicosapeptide. However, the isotherm did not show a distinct plateau region, suggesting that the peptide layer does not form a regular structure under high surface pressures. The ECz-C11-SS monolayer shows low surface pressure even in a compressed phase, indicating that the monolayer is not stable.

The change of the physical state of the tridecapeptide monolayers upon compression was investigated by CD measurements of the LB monolayers of ECz-A12 (Figure 3).

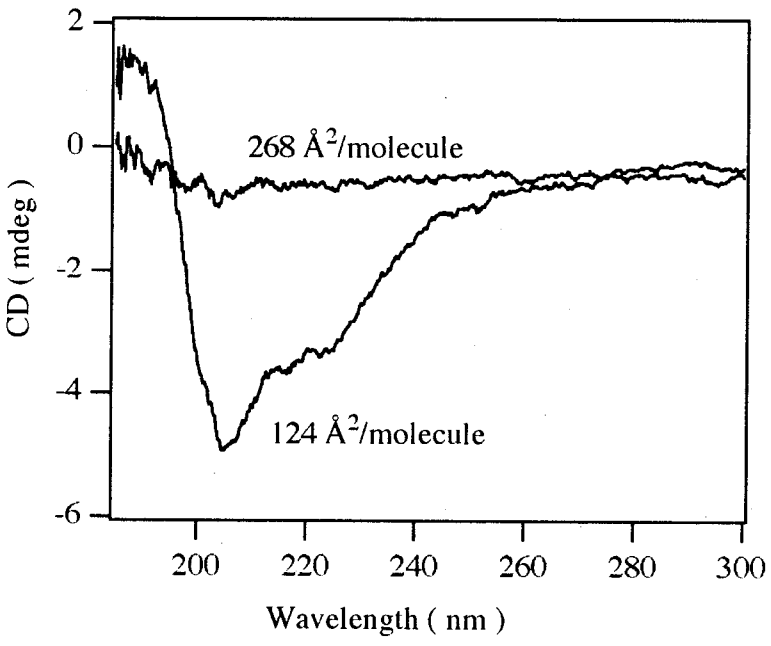

Figure 3. CD spectra of Langmuir-Brodgett monolayers of ECz-A12 which were transferred at the molecular areas of 268 Å^2/molecule and 124 Å^2/molecule on a quartz substrate.

The monolayer on the water subphase was transferred at two different molecular areas, 268 and 124 Å^2/molecule, which correspond respectively to the first and last molecular area in the plateau region

upon compression. It is obvious that the transfer of the monolayer was unsuccessful at 268 Å^2 /molecule. On the other hand, the CD spectrum of the monolayer transferred at 124 Å^2/molecule showed a double-minimum pattern, which is characteristic of an α-helical structure.[23,24] The magnitude at 208 nm is stronger than that at 222 nm, suggesting that the helices are lying parallel to the quartz substrate and probably at the air/water interface.[25] It is thus considered that the helical peptide should mount over the packed monolayer with retaining the lying orientation upon compression.[26]

***In Situ* Fluorescence Spectroscopy of Monolayers at the Air/Water Interface.** *In situ* fluorescence spectra of the ECz-A12 monolayer at various molecular areas are shown in Figure 4.

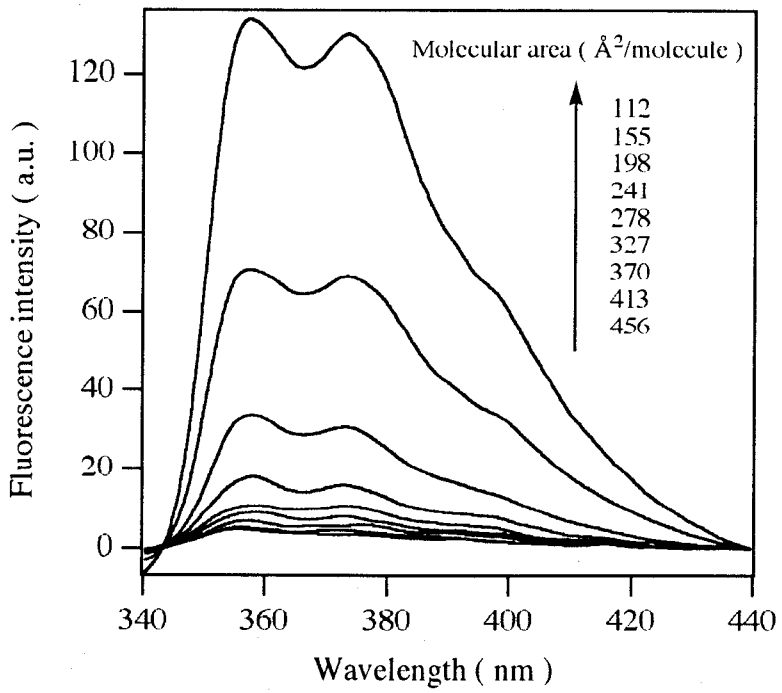

Figure 4. *In situ* fluorescence spectra of the ECz-A12 monolayer on the water subphase at various molecular areas.

Monomer emission of an ECz group (357 nm, 373 nm) was observed even at a compressed phase, indicating no excimer formation. Similar results were also obtained in the cases of the ECz-A12-SS, SS-A12-ECz, and ECz-A20-SS monolayers. The dependence of fluorescence intensity on the molecular area is shown in Figure 5. The fluorescence intensity of the ECz-A12 monolayer increases remarkably after molecular areas less than 270 Å2/molecule. This increase can not be explained by increase of the molecular number per unit area upon compression, but is explainable by the formation of bilayer at molecular areas less than 270 Å2/molecule. The fluorescence quantum yield of the ECz group at the first layer on the water subphase would be low because of an aqueous environment.

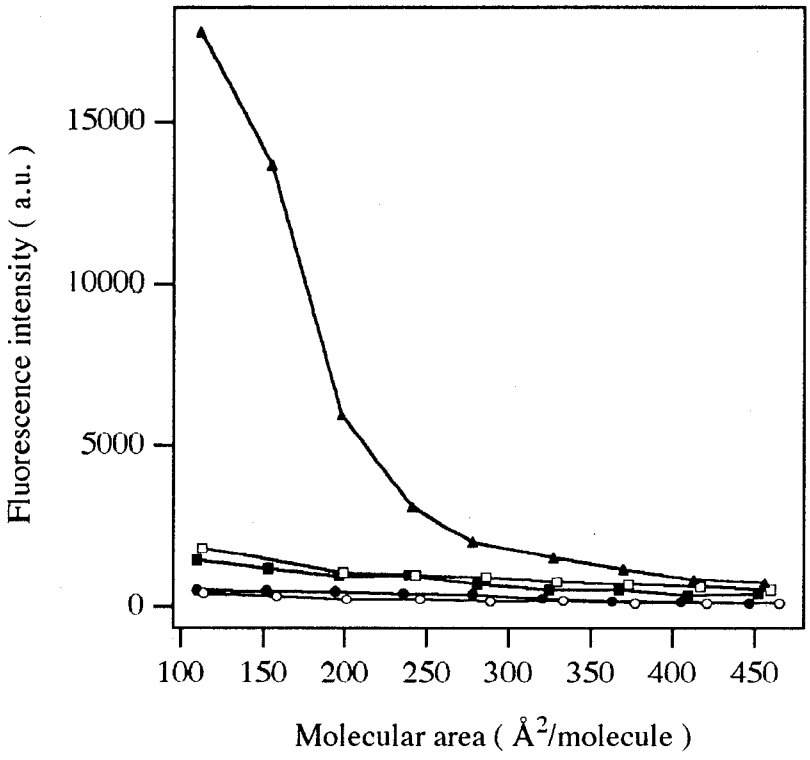

Figure 5. The relation of fluorescence intensity (integration value from 350 to 400 nm) of the helical peptide monolayers with molecular surface areas: ECz-A12-SS (●), SS-A12-ECz (○), ECz-A12 monolayer (▲), ECz-A12/ECz-A12-SS (■), ECz-A12/SS-A12-ECz bicomponent monolayer (1/1 mol/mol, □), respectively.

However, the ECz groups at the second layer on the water subphase should fluoresce intensively in a nonaqueous environment. In the other monolayers, the emission was much weaker than that in the ECz-A12 monolayer, indicating that the quenching of the ECz group by the disulfide group occurs in both monolayer and bilayer. The radius of the active sphere for the quenching of the ECz group by the disulfide group was calculated to be about 10 Å from the Stern-Volmer plot for the quenching of ethylcarbazole by DL-α-lipoic acid in toluene.[27] A disulfide group is thus considered to effectively quench the neighboring ECz groups. The fluorescence intensities of the ECz-A12-SS and SS-A12-ECz monolayers are substantially the same, suggesting that the arrangement of the helical peptides is not affected by the dipole direction.

In order to determine the arrangement of the peptide molecules at the air/water interface, the fluorescence quenching of the ECz group by the disulfide group was simulated by calculation. Schematic illustration of the computer simulation is presented in Figure 6.

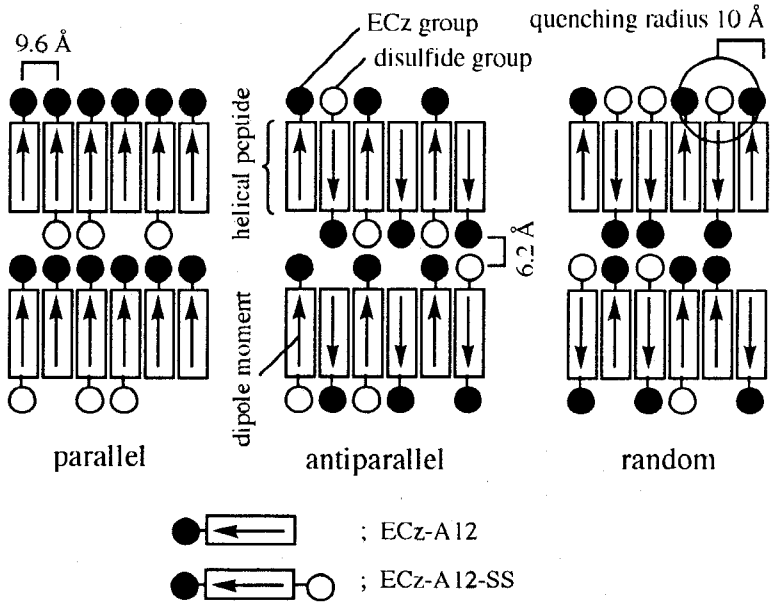

Figure 6. Schematic illustration of computer simulation for the fluorescence quenching of the ECz group by the disulfide group in the bicomponent monolayers (ECz-A12 and ECz-A12-SS) on the water subphase. The number of radiative ECz groups were calculated at three different arrangements.

Three distinct arrangements of peptide molecules, that is, parallel, antiparallel, and random arrangements were assumed. The helical peptides (10,500 molecules) were located on a two-dimensional lattice (250 x 42) according to the respective arrangement, and the number of radiative ECz groups was counted under an assumption that ECz groups within the quenching sphere of the disulfide group (radius 10 Å) are nonradiative. The lateral distance between functional groups (ECz-ECz or ECz-disulfide) was assumed to be 9.6 Å, and the distance between functional groups of neighboring layers was assumed to be 6.2 Å where the two ECz groups are in the closest contact. The result of the computer simulation at 270 Å^2/molecule is summarized in Table 1. The simulated values for the random arrangement agree well with the experimental values.

Table 1. Computer simulation results and experimental values for fluorescence quenching of the ECz group by the disulfide group in the monolayers of peptide derivatives. The fluorescence intensities were corrected by assuming the intensity of the ECz-A12 monolayer to be 100.

	experimental values	simulated values		
	at 270 Å^2/molecule	parallel	antiparallel	random
ECz-A12	100	100	100	100
ECz-A12-SS	17.1	0	0	12.2
SS-A12-ECz	8.3	0	0	12.1
ECz-A12+ECz-A12-SS	33.1	49.8	11.8	41.2
ECz-A12+SS-A12-ECz	41.1	37.9	55.9	41.6

Table 2. Computer simulation results for fluorescence quenching of the ECz group by the disulfide group in the bilayers of peptide derivatives by taking the quenching radius of the disulfide group to be 10 or 12 Å. The fluorescence intensities were corrected by assuming the intensity of the ECz-A12 monolayer to be 100.

	experimental values	simulated values	
	at 135 Å^2/molecule	quenching radius10Å	quenching radius12Å
ECz-A12	100	100	100
ECz-A12-SS	3.3	6.6	0.8
SS-A12-ECz	2.5	6.6	0.9
ECz-A12+ECz-A12-SS	8.5	31.7	14.5
ECz-A12+SS-A12-ECz	10.4	32.0	14.9

It is therefore considered that dipole-dipole interaction is not prevailing in the helical peptide monolayer probably due to hydration of helical peptides, resulting in a random arrangement.

At smaller molecular areas, the fluorescence from the disulfide containing peptide monolayers was quenched significantly in comparison with that of the ECz-A12 monolayer (Figure 5). This could be explained by energy migration among ECz groups which occurs efficiently because the fluorescence quantum yield of the ECz group in the second layer on the water subphase is high. The energy migration among ECz groups increases the encounter chance with the quencher in the peptide bilayer. The author assumes that the ECz group locating at the diagonal position of the neighboring layer is quenched by the disulfide group due to the effect of energy migration, which is reflected in the computer simulation by taking the quenching radius of 12 Å. The computer simulation for the quenching by the disulfide group in the bilayer of the helical peptides in a random arrangement was carried out taking the quenching radius to be 10 or 12 Å, and the results are summarized in Table 2. The simulated values for 12 Å quenching radius agree with the experimental values better than the values by assuming 10 Å quenching radius, indicating that energy migration among ECz groups promotes the quenching by the disulfide group. The difference between the simulated and experimental values is, however, relatively large. This may be attributed to simplicity of the model where homogeneous arrangement is assumed in the monolayers and the quenching radius is three-dimensionally isotropic.

Orientation and Arrangement of Helical Peptides in Self-Assembled Monolayers. The surface coverage of ECz-A12-SS, SS-A12-ECz, ECz-A20-SS, and ECz-C11-SS on the gold substrate were determined by QCM measurements to be 0.114, 0.145, 0.176, and 0.345 nmol cm^{-2}, respectively. The corresponding molecular areas are 146, 115, 94.4, and 48.1 $Å^2$/molecule, respectively. The molecular area of ECz-C11-SS is much smaller than those of the helical peptides because of the smaller cross section of the dialkyl group, and is nearly twice the molecular area of a single-chain *n*-alkanethiol.[28] The SAM composed of a longer peptide ECz-A20-SS was covered more densely than the SAMs of the tridecapeptides. A longer helix peptide seems to strengthen the aggregation of peptide molecules by van der Waals force in the SAM, resulting in the formation of a highly ordered monolayer. The molecular orientation of the peptide SAMs were investigated by FTIR-RAS measurements. The FTIR-RAS spectrum of the ECz-A12-SS SAM is shown in Figure 7.

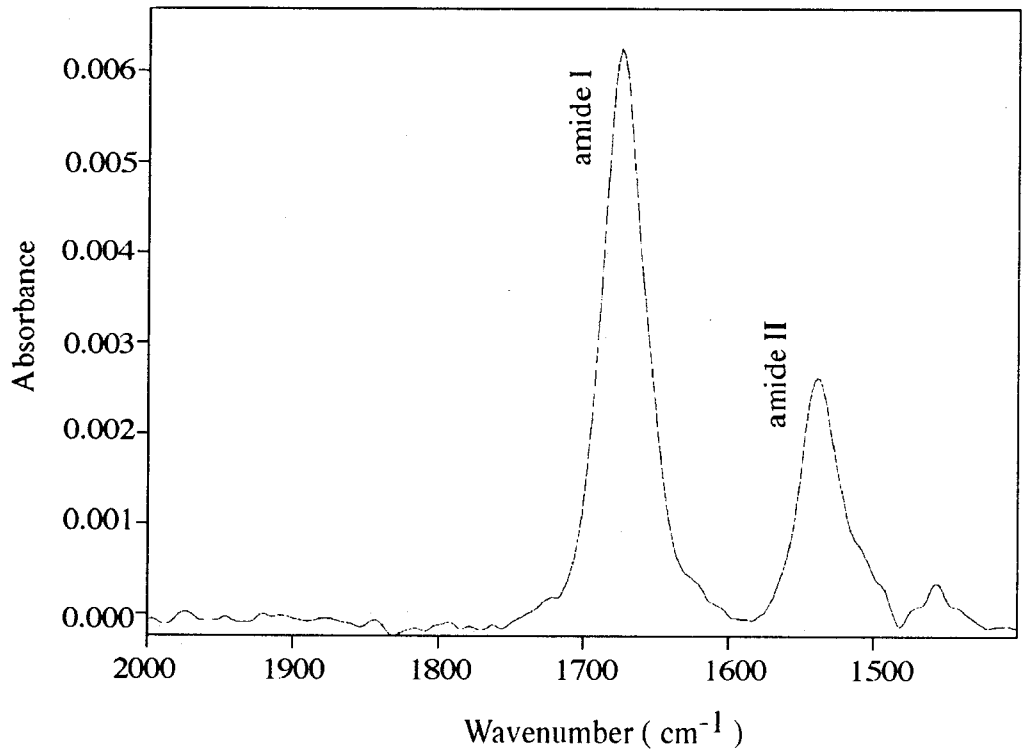

Figure 7. FTIR-RAS spectrum of the ECz-A12-SS SAM.

The absorptions observed at 1675 and 1538 cm^{-1} were assigned to amide I and amide II bands of an α-helical conformation,[29] respectively, indicating that an α-helical structure was formed on the gold substrate. The amide I / amide II absorbance ratios of the ECz-A12-SS, SS-A12-ECz, and ECz-A20-SS SAMs were 2.34, 2.71, and 3.34, respectively. The tilt angles of the helices from the surface normal were calculated to be 44°, 41°, and 36°, respectively. The molecular areas were calculated using these tilt angles to be 121, 114, and 105 $Å^2$/molecule for ECz-A12-SS, SS-A12-ECz, and ECz-A20-SS, respectively, assuming hexagonal packing of the helices and uniform orientation in the SAMs. The molecular areas of SS-A12-ECz and ECz-A20-SS determined by the FTIR-RAS coincide well with those obtained by the QCM measurements, indicating the formation of well-packed monolayers. On the other hand, the molecular area of ECz-A12-SS from the FTIR-RAS was slightly smaller than that from the QCM measurement (146 $Å^2$/molecule). Therefore, the ECz-A12-SS SAM should contain some defects or incompletely-packed regions. The disorder of the ECz-A12-SS SAM is considered to be due to the connection of the C-terminal of the helical peptide to the gold substrate through an S-Au linkage. Since the S-Au linkage has an ionic property (S^--Au^+), the negative charge of S^- should cause unfavorable interaction with the negative dipole end at the C-terminal of the helix.[30,31]

The fluorescence spectra of the SAMs are shown in Figure 8. Monomer emission was dominant in the ECz-A20-SS SAM. However, second excimer emission (375-380 nm) was also observed in the ECz-A12-SS, SS-A12-ECz, and ECz-C11-SS SAMs.[32,33] The excimer formation suggests a disorder structure in the SAMs. Because short peptides do not adopt fully helical conformation and the alkyl chains are flexible, these spacers may allow the excimer arrangement of ECz groups. The fluorescence from the ECz-A12-SS, SS-A12-ECz, and ECz-C11-SS SAMs was quenched more than that from the ECz-A20-SS SAM. The lengths along molecular axis of ECz-A12-SS, SS-A12-ECz, and ECz-A20-SS are 29, 28, and 41 Å, respectively, which are the sum of the

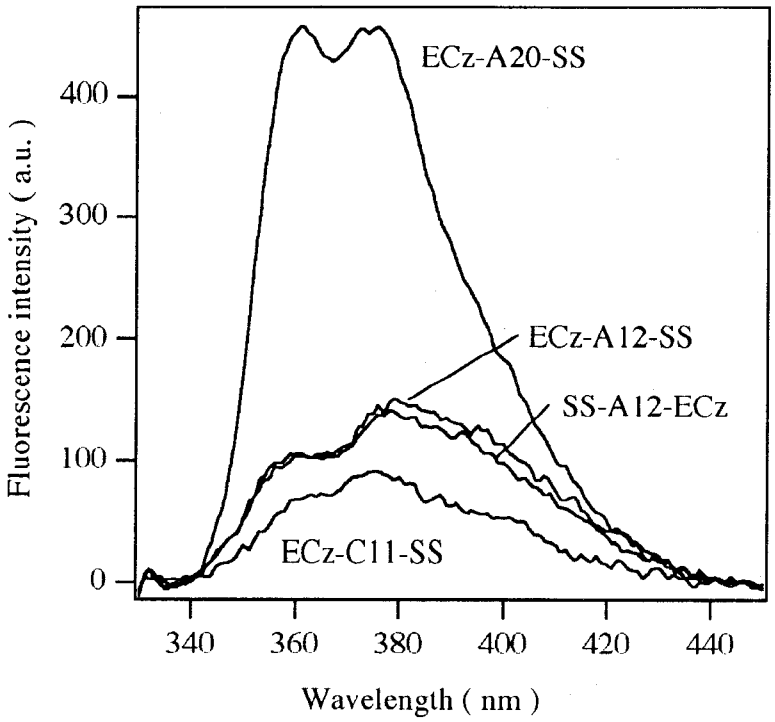

Figure 8. Fluorescence spectra of the ECz-A12-SS, SS-A12-ECz, ECz-A20-SS, and ECz-C11-SS SAMs.

lipoic part (9.5 Å for ECz-A12-SS and ECz-A20-SS, 8.2 Å for SS-A12-ECz, upon all-trans configuration) and the helical part (19.5 Å for the tridecapeptides, 31.5 Å for the heneicosapeptide). That of ECz-C11-SS is 20 Å for all-trans configuration. The tilt angles of molecular axis from the surface normal are 44°, 41°, and 36° for ECz-A12-SS, SS-A12-ECz, and ECz-A20-SS from the FTIR-RAS, and 30° for ECz-C11-SS from the literature,[28] respectively. The distances from the gold substrate to the ECz group in the SAMs were calculated to be 21, 21, 33, and 17 Å for the ECz-A12-SS, SS-A12-ECz, ECz-A20-SS, and ECz-C11-SS SAMs, respectively. The degree of quenching is therefore correlated with the distance from the gold substrate to the ECz group. The quenching mechanism should be due to energy transfer from the photoexcited ECz group to gold considering the long distance between them. All these results indicate that the helical peptides take upright orientation to the gold substrate in a parallel arrangement in the SAMs.

References and Notes

1) Burgess, A.W.; Leach, S. J. *Biopolymers* **1973**, *9*, 235.

2) Davis, J. H.; Clare, D. M.; Hodges, R. S.; Bloom, M. *Biochemistry* **1983**, *22*, 5298.

3) Richardson, J. S.; Richardson, D. C. *Trends in Biochem. Sci.* **1989**, *14*, 304.

4) Karle, I. L.; Balaram, P. *Biochemistry* **1990**, *29*, 6747.

5) Branden, C.; Tooze, J. *Introduction to Protein Structure*; Garland Publishing: New York and London, 1991.

6) Clark, T. D.; Buehler, L. K.; Ghadiri, M. R. *J. Am. Chem. Soc.* **1998**, *120*, 651.

7) Fujita, K.; Kimura, S.; Imanishi, Y.; Rump, E.; Ringsdorf, H. *Langmuir* **1994**, *10*, 2731.

8) Worley, C. G.; Linton, R. W.; Samulski, E. T. *Langmuir* **1995**, *11*, 3805.

9) Fujita, K.; Bunjes, N.; Nakajima, K.; Hara, M.; Sasabe, H.; Knoll, W. *Langmuir* **1998**, *14*, 6167.

10) Miura, Y.; Kimura, S.; Imanishi, Y.; Umemura, J. *Langmuir* **1998**, *14*, 6935.

11) Otoda, K.; Kitagawa, Y.; Kimura, S.; Imanishi, Y. *Biopolymers* **1993**, *33*, 1337.

12) Ulman, A. *An Introduction to Ultrathin Organic Films*; Academic Press: San Diego, 1991.

13) Otoda, K.; Kimura, S.; Imanishi, Y. *Biochim. Biophys. Acta* **1993**, *1145*, 33.

14) Fox, M. A.; Whitesell, J. K.; McKerrow, A. J. *Langmuir* **1998**, *14*, 816.

15) Muramatsu, H.; Dicks, J. M.; Tamiya, E.; Karube, I. *Anal. Chem.* **1987**, *59*, 2760.

16) Okahata, Y.; Matsunobu, Y.; Ijiro, K.; Mukae, M.; Murakami, A.; Makino, K. *J. Am. Chem. Soc.* **1992**, *114*, 8299.

17) Sauerbrey, G. *Z. Phys.* **1959**, *155*, 206.

18) Greenler, R. G. *J. Chem. Phys.* **1966**, *44*, 310.

19) Gremlich, H. U.; Fringeli, U. P.; Schwyzer, R. *Biochemistry* **1983**, *22*, 4257.

20) Debe, M. K. *J. Appl. Phys.* **1984**, *55*, 3354.

21) Okamura, E.; Umemura, J.; Takenaka, T. *Can. J. Chem.* **1991**, *69*, 1691.

22) Tsuboi, M. *J. Polym. Sci.* **1965**, *59*, 139.

23) Holzwarth, G.; Doty, P. *J. Am. Chem. Soc.* **1965**, *87*, 218.

24) Greenfield, N.; Fasman, G. D. *Biochemistry* **1969**, *8*, 4108.

25) Ludtke, S. J.; He, K.; Wu, Y.; Huang, H. W. *Biochim. Biophys. Acta* **1994**, *1190*, 181.

26) Takeda, F.; Matsumoto, M.; Takenaka, T.; Fujiyoshi, Y.; Uyeda, N. *J. Colloid Interface Sci.* **1983**, *91*, 268.

27) Birks, J. B. *Photophysics of Aromatic Molecules*; Wiley-Interscience: New York, 1970.

28) Strong, L.; Whitesides, G. M. *Langmuir* **1988**, *4*, 546.

29) Kennedy, D. F.; Chrisma, M.; Chapman, T. D. *Biochemistry* **1991**, *30*, 6541.

30) Nuzzo, R.G.; Fusco, F. A.; Allara, D. L. *J. Am. Chem. Soc.* **1987**, *109*, 2358.

31) Biebuyck, H. A.; Whitesides, G. M. *Langmuir* **1993**, *9*, 1766.

32) Masuhara, H.; Tamai, N.; Mataga, N.; Schryver, F. C. D.; Vandendriessche, J. *J. Am. Chem. Soc.* **1983**, *105*, 7256.

33) Tsuchida, A.; Nagata, A.; Yamamoto, M.; Fukui, H.; Sawamoto, M.; Higashimura, T. *Macromolecules* **1995**, *28*, 1285.

Chapter 6

Photocurrent Generation under a Large Dipole Moment Generated by Self-Assembled Monolayers of *N*-Ethylcarbazole-Containing Helical Peptides

Introduction

In the natural photosynthesis, long-range electron transfer between a donor and an acceptor chromophore in protein assemblies occurs efficiently.[1-3] It has been shown that the electrostatic field generated by the dipole moment of α-helical segments of proteins accelerates electron transfer effectively.[4,5] A peptide backbone, which is composed of π and n (nonbonding) orbitals, is also suggested to construct electron-transfer pathways,[6-8] and a donor chromophore might be electronically coupled with an acceptor chromophore through hydrogen bonds involved in an α-helical structure.[9] Therefore, α-helical peptide is expected to be an excellent medium for electron transfer. In the present chapter, SAMs composed of α-helical peptides on a gold substrate were prepared and photocurrent generation therein was investigated.

It is well established that thiol and disulfide compounds are covalently connected to a gold substrate via an S-Au linkage, forming highly ordered SAMs.[10] Taking the advantage of this structural regularity, photocurrent generation using SAMs has been studied extensively.[11-16] However, photocurrent generation by peptide SAMs has not been reported so far. In this chapter, the disulfide compounds including helical peptides, which were described in Chapter 5, were used for the SAM preparation (Figure 1). ECz-A12-SS is a tridecapeptide carrying an ECz group at the N-

terminal and a disulfide group at the C-terminal. The ECz group acts as a photosensitizer in this system, and is useful to avoid excimer formation even in a condensed phase. The excimer formation significantly decreases the redox capability of the excited ECz group.

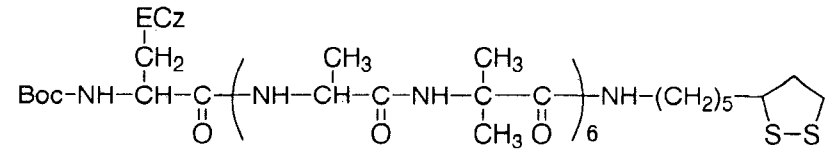

ECz-A12-SS

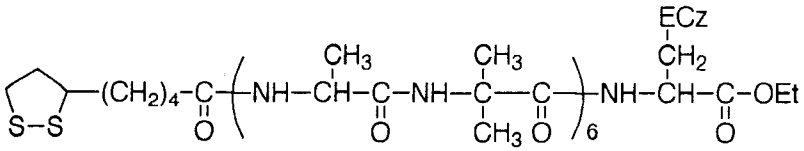

SS-A12-ECz

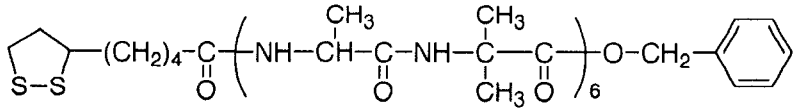

SS-A12

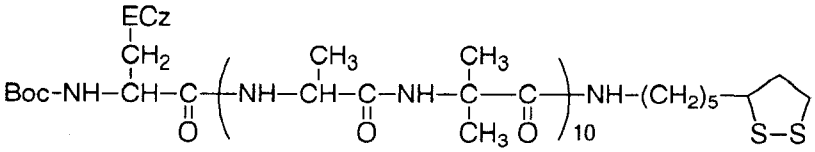

ECz-A20-SS

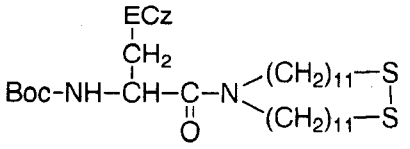

ECz-C11-SS

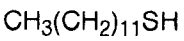

C12SH

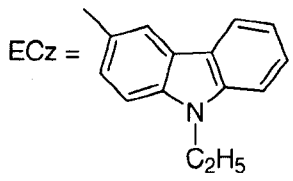

Figure 1. Molecular structures of disulfide compounds (ECz-A12-SS, SS-A12-ECz, ECz-A20-SS, and ECz-C11-SS) and reference compounds (SS-A12 and C12SH).

SS-A12-ECz is also a tridecapeptide but carries the two functional groups at the terminals in the opposite way to the case of ECz-A12-SS. ECz-A20-SS is a heneicosapeptide analogous to ECz-A12-SS in terms of the positions of the functional groups. ECz-C11-SS is a disulfide compound carrying a dialkyl chain instead of a peptide chain. SS-A12 and 1-dodecanethiol (C12SH), which do not carry ECz group, were used as control compounds.

The surface structures of the SAMs were investigated by cyclic voltammetry and impedance spectroscopy. The photocurrent generation by the SAMs was investigated, and the influence of the dipole moment, length and structure of the linker between the gold substrate and the ECz group on the rate of electron transfer were discussed.

Experimental Section

Materials. Methyl viologen trihydrate (MV^{2+}), triethanolamine (TEOA) and ethylenediaminetetraacetic acid tetrasodium salt (EDTA) were purchased from Nacalai Tesque Co., Ltd. (Japan), and used without further purification. 1-Dodecanethiol was purchased from Tokyo Kasei Co., Ltd. (Japan). The synthetic procedures of disulfide compounds were described in Chapter 5. SS-A12 was synthesized by the procedure in the literature.[17] Experimental procedure for SAM preparation was described in Chapter 5.

CD Measurement. CD spectra of the peptides were measured in a methanol solution at 20 °C on a CD spectrometer (J-600, JASCO Co., Ltd., Japan) using an optical cell of 1 cm path length.

Cyclic Voltammetry. Cyclic voltammograms were obtained using a voltammetric analyzer (model 604, BAS Co., Ltd., Japan) at room temperature. A standard three-electrode configuration

was used with the gold substrate as the working electrode, Ag/AgCl as the reference electrode, and a platinum wire as the auxiliary electrode in a glass vessel. All of the electric potentials reported in this chapter were measured with respect to the reference electrode. The area of the working electrode exposed to a electrolyte solution was 0.90 cm^2. The redox reagent used for blocking experiments was 1 mM $K_3[Fe(CN)_6]$ in 1 M KCl analyte solution. The sweep rate was set at 50 mV s^{-1} for all measurements.

Impedance Spectroscopy. Impedance measurements were carried out in the frequency range of 100 kHz to 0.01 Hz with an amplitude of 50 mV and fixed static potential of -0.5 V with the three-electrode setup described above under nitrogen atmosphere at room temperature. The supporting electrolyte used was Na_2SO_4 (0.01 M). The results were presented as Bode plots and Nyquist plots, and analyzed by comparing the experimental data with a model equivalent circuit consisting of a resistor in series with a parallel capacitor/resistor combination that generally corresponds to the monolayer.

Photocurrent Generation Experiment. Photocurrent measurements were carried out using the three-electrode setup described above at room temperature. The supporting electrolyte used was Na_2SO_4 (0.1 M). The SAM-modified substrate were photoirradiated with a Xe lamp (500W, JASCO Co., Ltd., Japan) equipped with a monochrometer. The photocurrents generated from the SAM were detected by the voltammetric analyzer described above. The concentrations of an electron acceptor (MV^{2+}) and electron donors (TEOA, EDTA) were set at 50 mM. The intensity of the irradiation light was evaluated by a potassium ferrioxalate actinometry.[18,19] The quantum efficiency of the photocurrent generation (the number of electron which flowed upon photoirradiation / the number of photon absorbed by ECz groups) was determined at light intensity of 4.73 x 10^{-11} einstein

s^{-1} for 299 nm excitation and 1.25 x 10^{-10} einstein s^{-1} for 351 nm excitation, respectively. The number of photons absorbed by ECz groups was calculated from the absorbance of the SAMs, which were derived from the surface coverage assuming that the molar absorptivities of the SAMs are the same as those of the disulfide compounds in a chloroform solution.

Results and Discussion

Conformation of Peptides in Solution. The CD spectra of the peptides carrying an ECz group and a disulfide group in a methanol solution are shown in Figure 2.

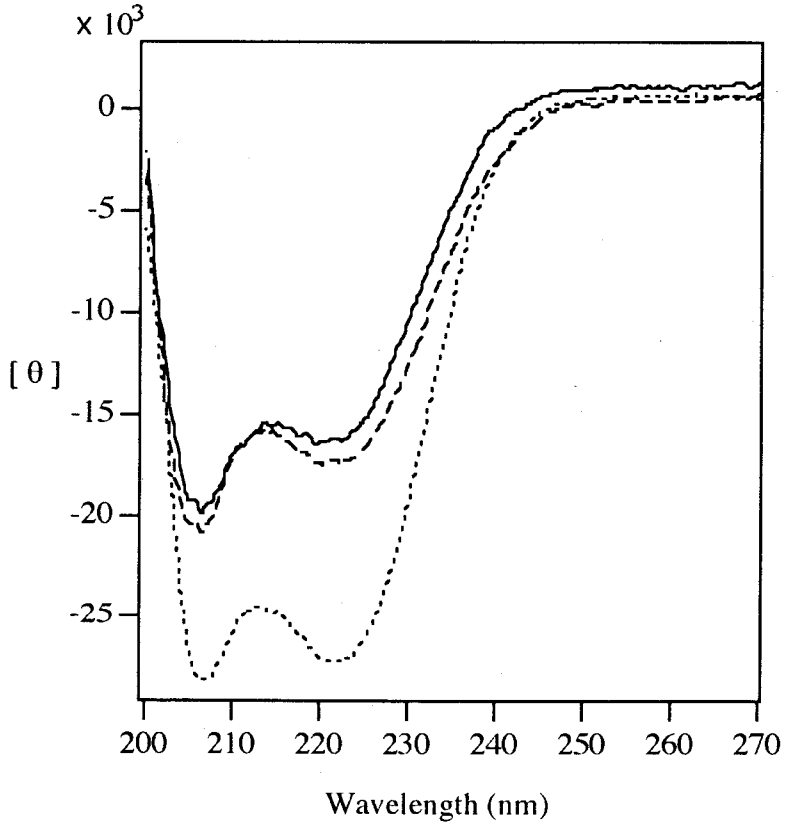

Figure 2. CD spectra of ECz-A12-SS (solid line), SS-A12-ECz (dashed line), and ECz-A20-SS (dotted line) in methanol at a concentration of 6.4 x 10^{-6} M at 20 °C.

All peptides show a double-minimum profile, which is characteristic of an α-helical structure.[20,21] The helix contents of ECz-A12-SS, SS-A12-ECz, and ECz-A20-SS were determined to be 45.4 %, 49.2 %, and 81.8 %[22], respectively, showing that the longer peptide chain stabilizes an α-helical conformation.

Surface Structures of Self-Assembled Monolayers. As described in Chapter 5, the molecular areas of ECz-A12-SS, SS-A12-ECz, ECz-A20-SS, and ECz-C11-SS on the gold substrate are 146, 115, 94.4, and 48.1 Å^2/molecule, respectively, indicating that the SAM of a tridecapeptide connected to the gold substrate at the C-terminal of the peptide was covered to a less extent than that of a tridecapeptide connected at the N-terminal.

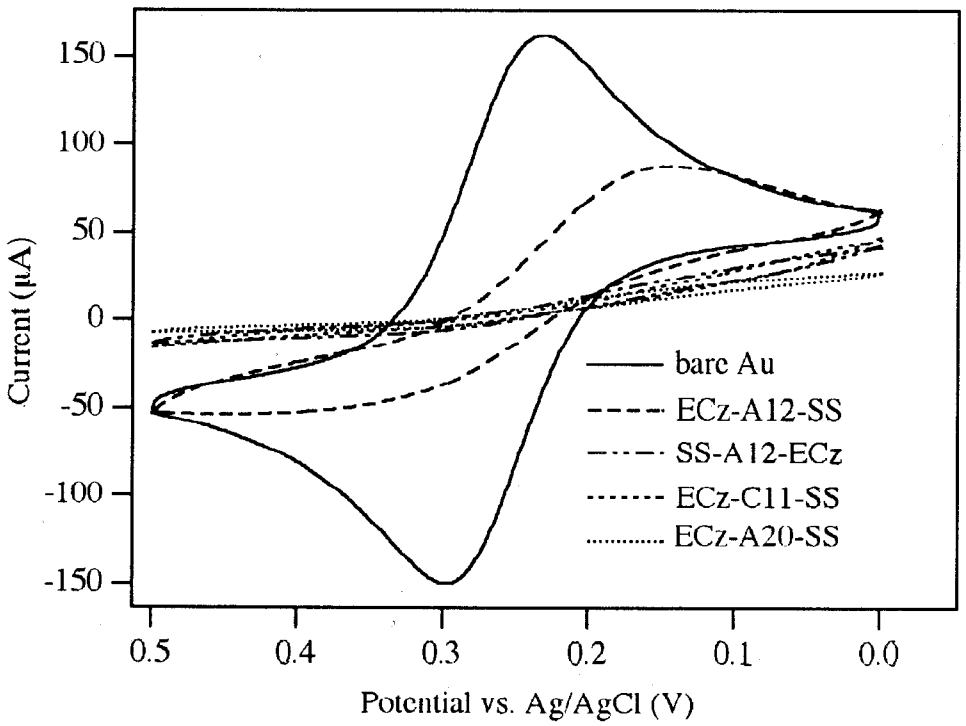

Figure 3. Cyclic voltammograms of a bare substrate and the SAM-modified substrates in a 1 mM aqueous $K_3[Fe(CN)_6]$ solution at room temperature. The sweep rate was set at 50 mV s^{-1}.

The state of the surface of the SAM was studied by cyclic voltammetry. The cyclic voltammograms of a bare substrate and the SAM-modified substrate were measured in an aqueous $K_3[Fe(CN)_6]$ solution and are shown in Figure 3. With the exception of the ECz-A12-SS SAM, other SAMs did not show redox activity, indicating that these SAMs possess a well-packed monolayer structure and an insulating property. The redox peaks of ferricyanide observed in the case of the ECz-A12-SS SAM are smaller than those of a bare substrate, showing that this monolayer possesses some defects or incompletely-packed regions where the electrolyte can diffuse in. This result agrees well with the QCM observation.

Impedance spectroscopy was investigated to examine the surface structures of the SAMs by monitoring the capacitance of the monolayers in the double-layer matrix in an Na_2SO_4 solution.[23-26] The measurements were carried out at a potential of -0.5 V, where no redox reaction occurs. The capacitance values for the ECz-A12-SS, SS-A12-ECz and ECz-C11-SS SAMs were calculated to be 5.01, 2.98 and 2.24 μF/cm², respectively. Considering the monolayer as a plate condenser, the capacitance is defined by eq. (1)

$$C_m = \frac{\varepsilon_0 \varepsilon_m}{d} \qquad (1)$$

where C_m, ε_0, ε_m, and d represent the capacitance of the monolayer, the dielectric permittivity of free space and the relative dielectric constant of the monolayer, and the thickness of the monolayer, respectively. The thickness of the SAMs was calculated to be about 21 Å for the tridecapeptide SAMs and 17 Å for the ECz-C11-SS SAM as described in Chapter 5. The ε_m values were calculated by eq. (1) to be 12, 7.4, 4.3 for the ECz-A12-SS, SS-A12-ECz, and ECz-C11-SS SAMs, respectively. The dielectric constant of the ECz-A12-SS is considerably high, indicating penetration of electrolytes or water molecules into the SAM through the defects.

Cathodic Photocurrent Generation by Self-Assembled Monolayers. Photocurrent generation by the SAMs was investigated in an aqueous MV^{2+} solution. The mechanism of the cathodic photocurrent generation by the SAMs is presented schematically in Figure 4.

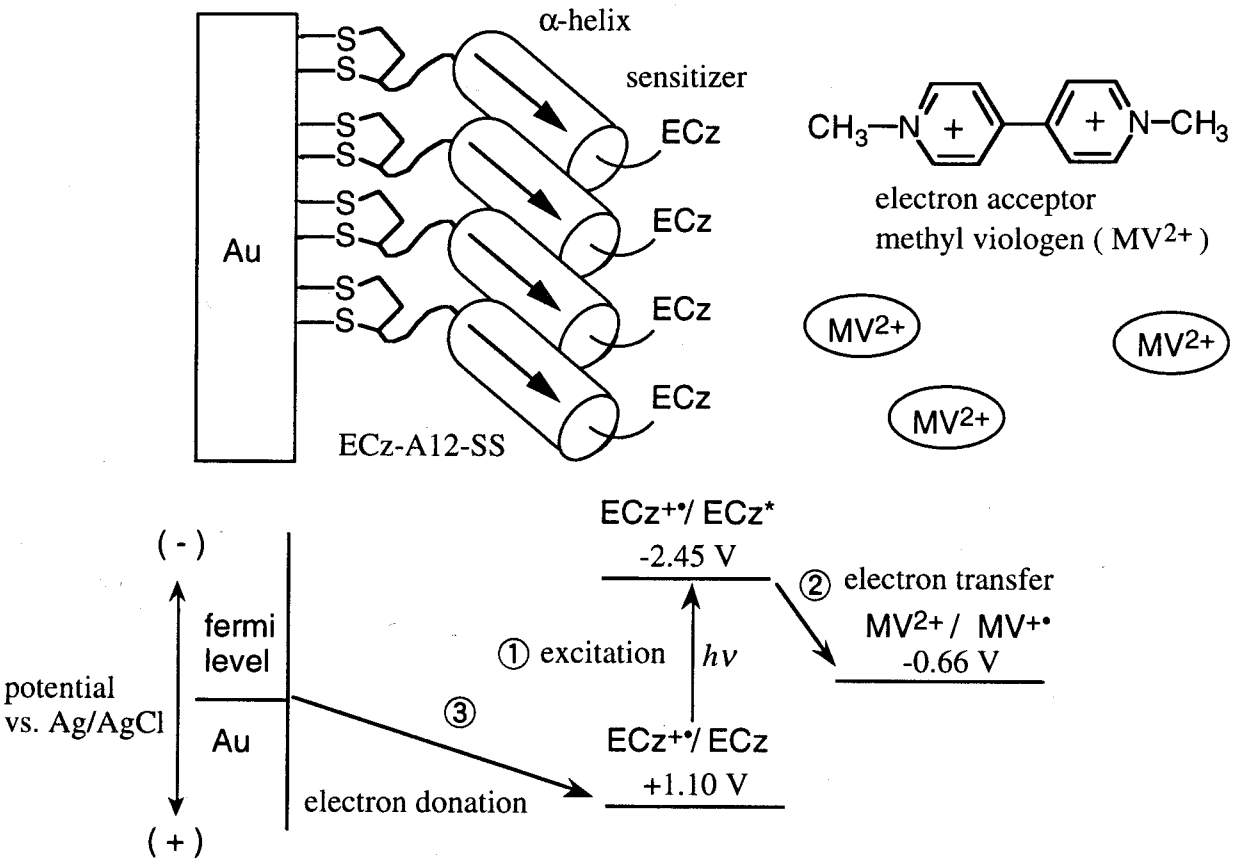

Figure 4. Schematic illustration of cathodic photocurrent generation by the α-helical peptide SAM in the presence of MV^{2+}.

Upon photoexcitation of the ECz group, electron transfer occurs from the excited ECz group to the electron acceptor MV^{2+}, followed by electron donation from gold to the oxidized ECz group (the radical cation of the ECz group). The reduced viologen diffuses to the auxiliary electrode and transfers an electron, resulting in the generation of a photocurrent. The photocurrent generation by photoirradiating the SAMs with a monochromic light of 351 nm (10 nm bandwidth) are shown in Figure 5 with repeating on-off switchings of the photoirradiation.

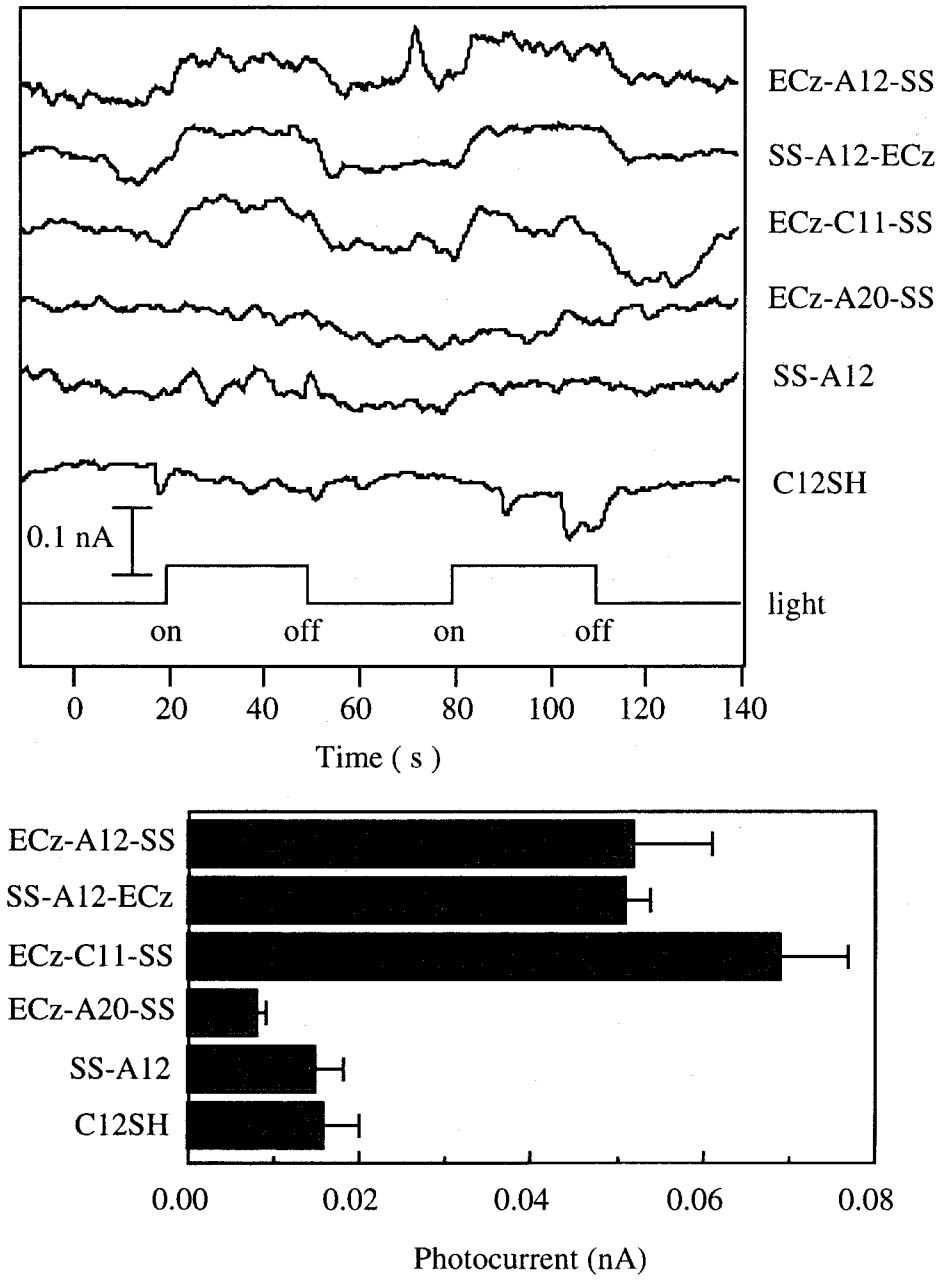

Figure 5. Time course of the photocurrents by the SAMs in an aqueous MV^{2+} solution at 0 V upon photoirradiation at 351 nm (1.25×10^{-10} einstein s^{-1}) at room temperature (top). Photocurrents by the SAMs (bottom).

The largest photocurrent was observed in the ECz-C11-SS SAM. The photocurrent of the ECz-A12-SS SAM was nearly equal to that of the SS-A12-ECz SAM. However, since the density of the ECz group is not the same in these SAMs, the quantum efficiencies of the cathodic photocurrent

generation were calculated and summarized in Table 1.

Table 1. Quantum efficiencies of the cathodic photocurrent generation in an aqueous MV^{2+} solution and the anodic photocurrent generation in an aqueous TEOA or EDTA solution.

	MV^{2+} (%)	TEOA (%)	EDTA (%)
ECz-A12-SS	0.43	0.19	0.17
SS-A12-ECz	0.33	0.45	0.42
ECz-C11-SS	0.19	0.10	0.04
ECz-A20-SS	0.04	0.07	0.03

The tridecapeptide SAMs show higher quantum efficiencies than the alkane ECz-C11-SS SAM. In addition, the efficiency of the ECz-A12-SS SAM where the dipole of α-helix directs toward the aqueous phase so as to accelerate the electron donation from gold to the ECz group was higher than that of the SS-A12-ECz SAM having the dipole moment reverse-directed to that in the ECz-A12-SS SAM. The difference in the efficiencies is, however, too small to be explained by the dipole effect of the peptide. The ECz-A12-SS SAM contains structural defects to allow the electrolytes and water to penetrate in, which may weaken the dipole effect in the monolayer.

A photocurrent was hardly observed in the ECz-A20-SS SAM (Figure 5). The distance between the gold substrate and the ECz group in the SAM is calculated to be about 41 Å as described in Chapter 5. The length of ECz-A20-SS chain is too long for efficient electron transfer to occur. The SS-A12 and C12SH SAMs which lack ECz group did not generate a significant photocurrent, showing that the photoexcitation of the ECz group initiates the photocurrent generation. In addition, the action spectrum of the photocurrent by the ECz-C11-SS SAM agrees well with the absorption spectrum of ECz-C11-SS in a chloroform solution, indicating that the ECz group is the photosensitizing species (Figure 6).

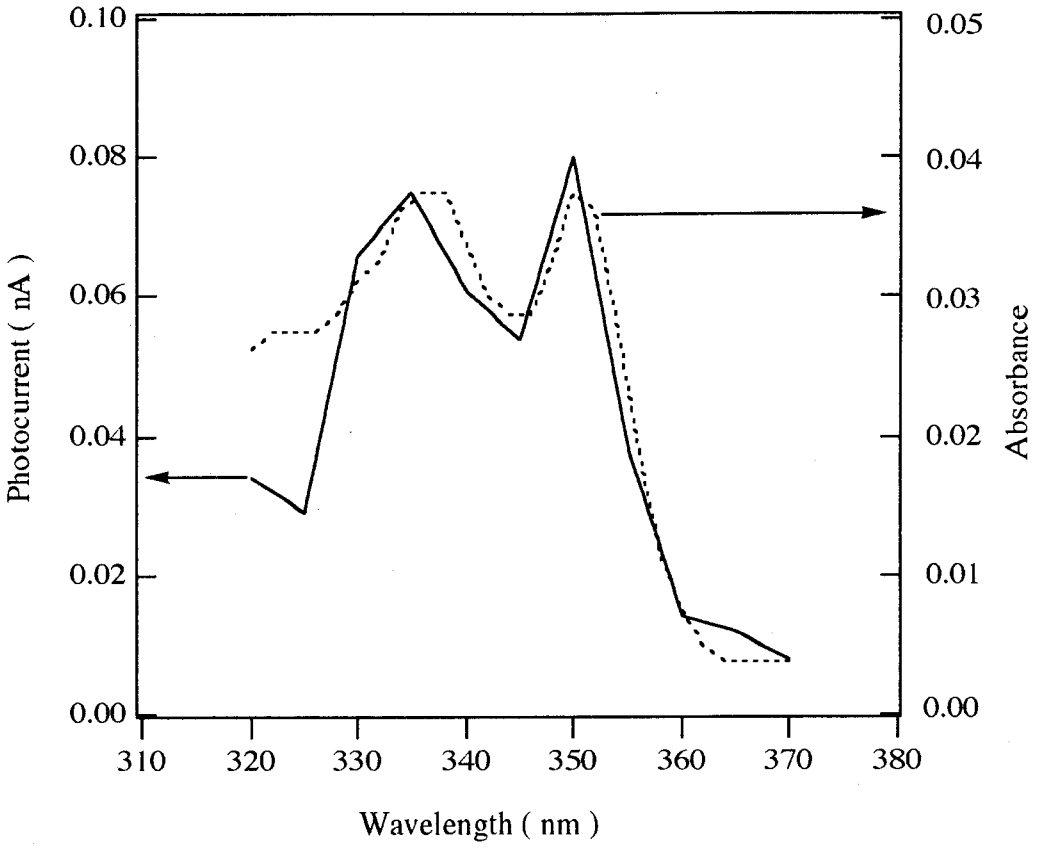

Figure 6. Photocurrent action spectrum of the ECz-C11-SS SAM (solid line) and the absorption spectrum of ECz-C11-SS in chloroform (dotted line).

Anodic Photocurrent Generation by Self-Assembled Monolayers. Anodic photocurrent generation by the SAMs was investigated in the presence of an electron donor, TEOA or EDTA. The photocurrents generated upon photoirradiation with a monochromic light of 299 nm (10 nm bandwidth) in the presence of TEOA are shown in Figures 7. The observed photocurrents are summarized in Figure 8. The most abundant photocurrent was obtained in the SS-A12-ECz SAM, and the less amount of current was obtained in the ECz-A12-SS and ECz-C11-SS SAMs. The quantum efficiencies of the anodic photocurrents are also summarized in Table 1. The large quantum efficiency of the SS-A12-ECz SAM is possibly due to the helix dipole directing towards the gold substrate, significantly accelerating electron transfer from the ECz group to gold. The action spectrum of the SS-A12-ECz SAM was also measured and is shown to agree with the absorption

spectrum of SS-A12-ECz in a methanol solution (Figure 9).

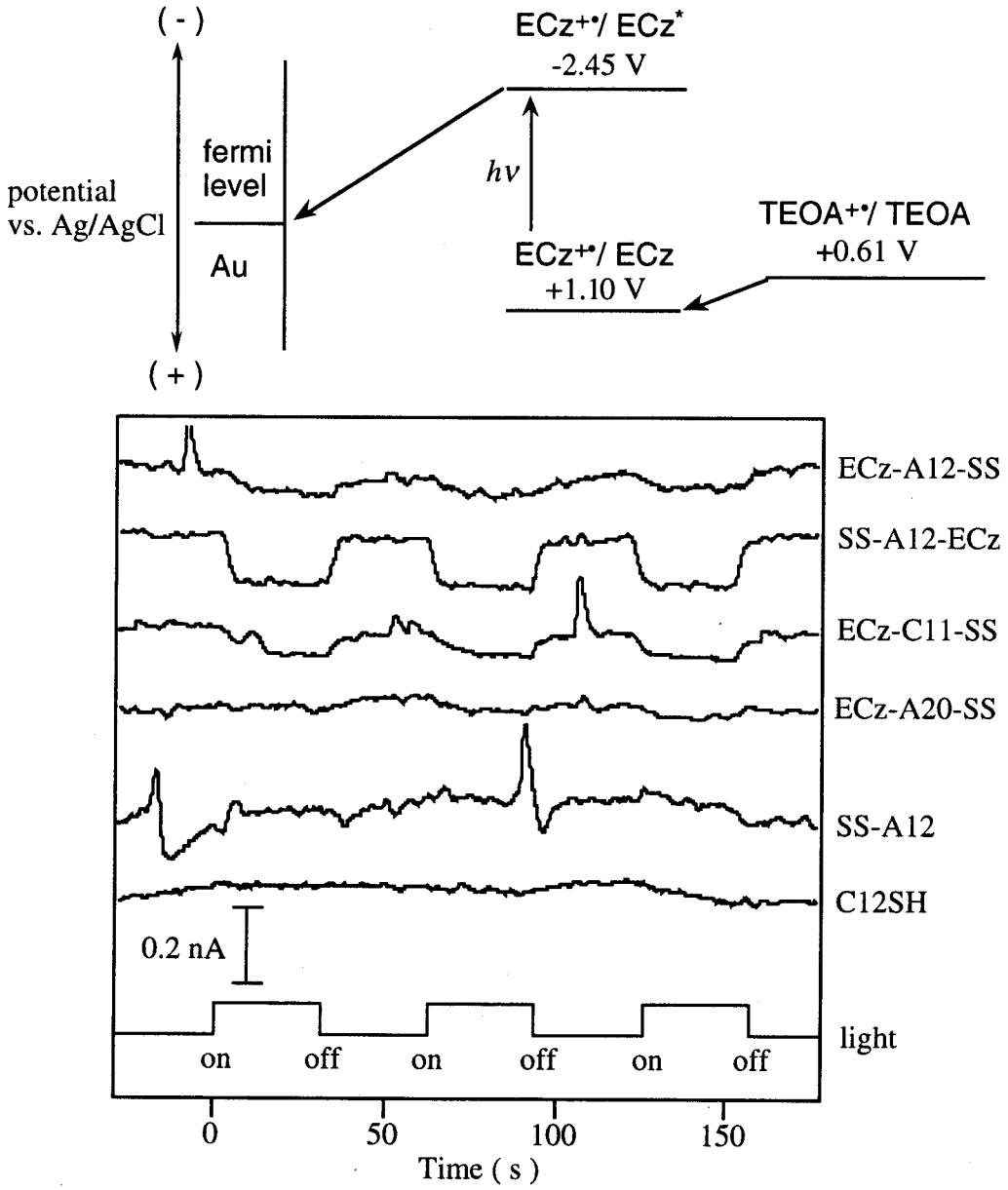

Figure 7. Energy diagram for anodic photocurrent generation in the presence of TEOA (top). Time course of the photocurrent by the SAMs in an aqueous TEOA solution at 0 V upon photoirradiation at 299 nm (4.73×10^{-11} einstein s^{-1}) at room temperature (bottom).

In the case of anodic photocurrent generation using TEOA or EDTA as an electron donor, a remarkable acceleration of electron transfer by the helix dipole was observed for the SS-A12-ECz SAM. On the other hand, the effect of the helix dipole direction between the ECz-A12-SS and SS-

A12-ECz SAMs on the cathodic photocurrent using MV^{2+} as an electron acceptor was not significant. This fact would be due to that the effective dipole moment of the ECz-A12-SS SAM might be weakened by electrolytes or water molecules penetrating into the SAM mentioned above.

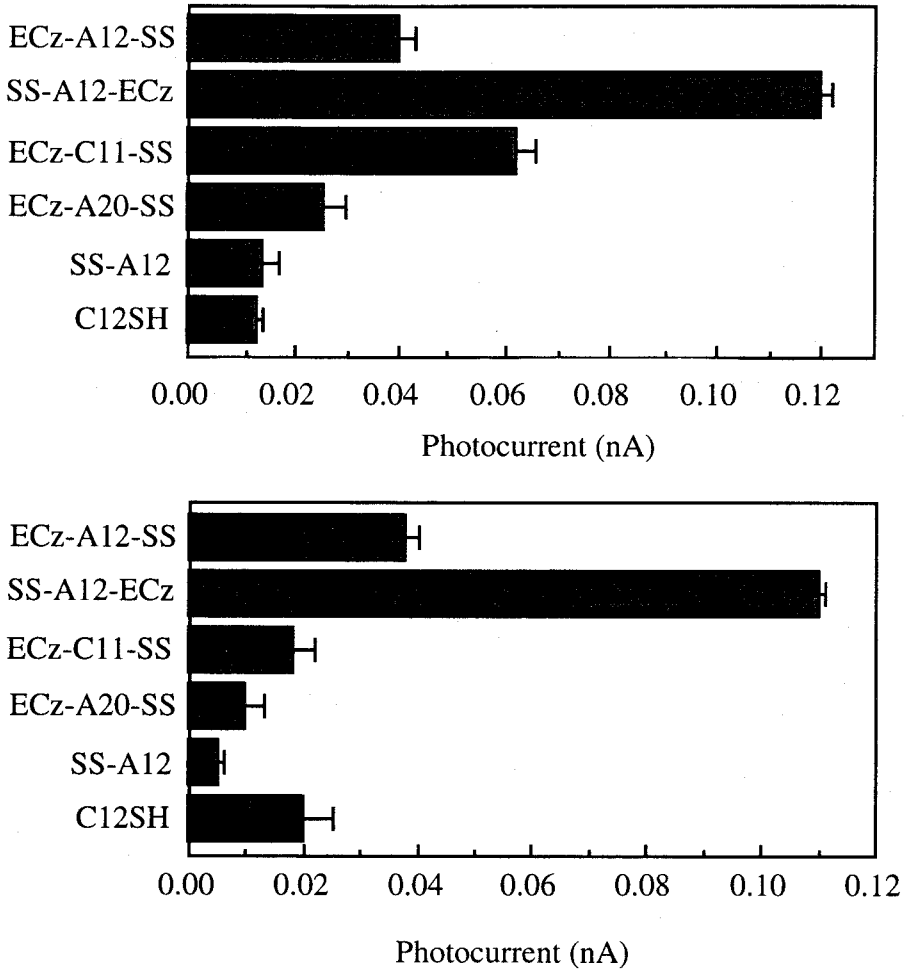

Figure 8. Anodic photocurrents by the SAMs in an aqueous TEOA (top) or EDTA solution (bottom) at 0 V upon photoirradiation at 299 nm at room temperature.

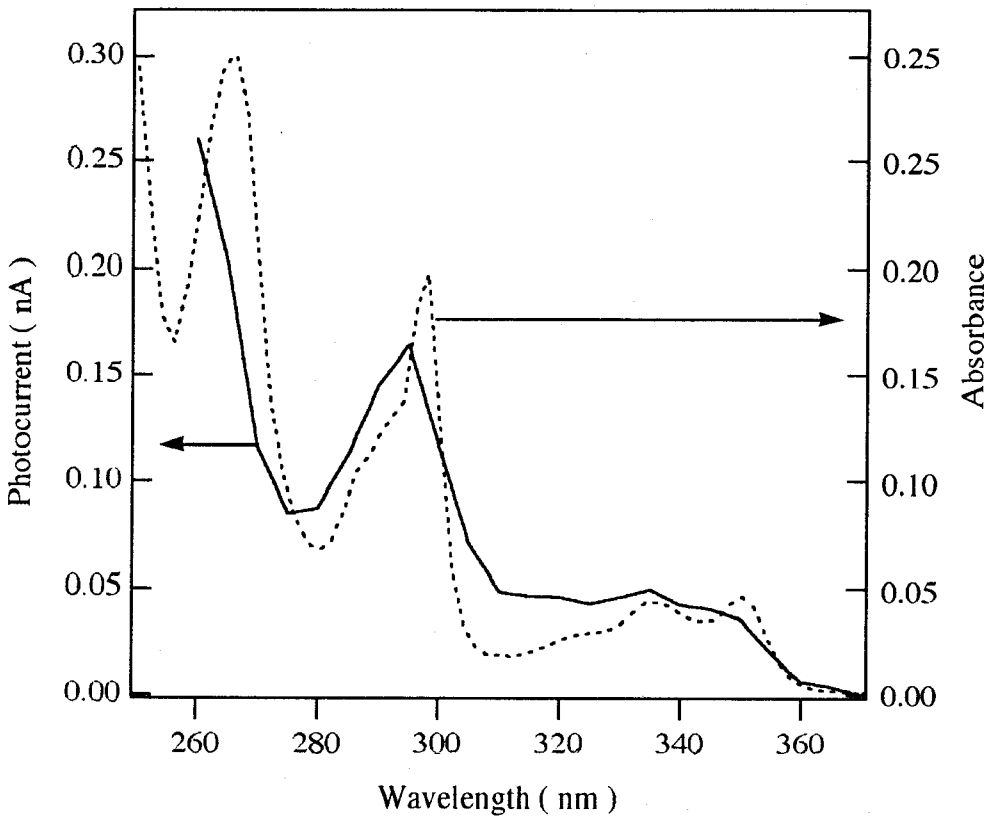

Figure 9. Photocurrent action spectrum of the SS-A12-ECz SAM in an aqueous TEOA solution (solid line) and the absorption spectrum of SS-A12-ECz in methanol (dotted line).

Electronic Coupling through Helical Peptides. To investigate the mediation of electron transfer by peptide molecules, the dependence on the electric potential of the quantum efficiency for the anodic photocurrent generation using EDTA was investigated (Figure 10). In all the SAMs, a decrease in the anodic photocurrent was observed with an increase of the negative bias to the working electrode, and the photocurrent disappeared at a certain potential (zero-current potential). The negative bias reduces the energy gap between the oxidation potential of excited ECz group and the Fermi level of gold, resulting in the decrease of anodic photocurrent. The anodic photocurrent was changed to a cathodic photocurrent by applying the negative bias higher than the zero-current potential. A specific electron acceptor, such as H^+ in an aqueous solution, may accept an electron from the photoexcited ECz group to generate the cathodic photocurrent. Therefore, the observed

photocurrent should be the sum of anodic and cathodic photocurrents. At the zero-current potential, the opposing photocurrents cancel each other, leading apparently to a no current state.

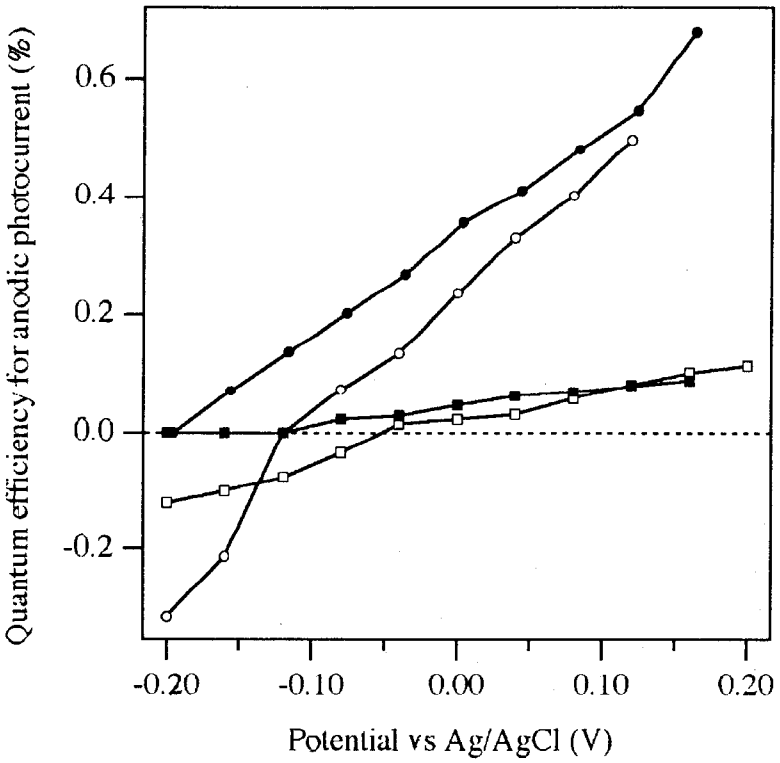

Figure 10. Effect of electric potential on the anodic photocurrent generation using EDTA in the ECz-A12-SS (○), SS-A12-ECz (●), ECz-A20-SS (■), and ECz-C11-SS (□) SAMs.

An anodic photocurrent generation, using EDTA as an electron donor, is composed of two electron transfer steps ; from EDTA to the photoexcited ECz group and from the radical anion of the ECz group to gold. The latter should be the rate-limiting step because of the long distance between the donor and acceptor. Thus the quantum efficiency of the photocurrent generation should be influenced directly by the rate constant for the latter electron transfer. The rate constant of electron transfer (k_{ET}) from a donor to an acceptor at a fixed distance is described by eq. (2) on the basis of the semiclassical theory.[27] The present data are discussed in terms of eq. (2), because it is essentially the same as the equation for the electron transfer on a metal surface.[28-30]

$$k_{ET} = \sqrt{\frac{4\pi^3}{h^2 \lambda k_B T}} H_{DA}^2 \exp\left[-\frac{(\Delta G_0 + \lambda)^2}{4\lambda k_B T}\right] \qquad (2)$$

$$H_{DA}^2 = (H_{DA}^0)^2 \exp(-\beta r)$$

h, λ, k_B, T, H_{DA}^2, $(H_{DA}^0)^2$, ΔG_0, β, and r represent Planck's constant, the reorganization energy, the Boltzmann's constant, the absolute temperature, the electronic coupling strength between the donor and acceptor, the coupling strength at the closest contact, the driving force for the reaction, the tunneling parameter for the medium, and the edge-to-edge distance between the donor and acceptor, respectively. On the basis of the simple model where the peptide dipole influences only the electric potential around the ECz groups, the driving force in the electron transfer in each SAM is the same at the relative potential to the zero-current potential. According to eq. (2), k_{ET} is proportional to H_{DA}^2 under the same driving force (ΔG_0). Therefore, the difference in the quantum efficiencies of the photocurrent generation can be explained in terms of H_{DA}^2. The relationship between the quantum efficiency of the photocurrent generation and the electric potential appears to be linear (Figure 10). The slope for the tridecapeptide SAM was larger than that for the ECz-C11-SS SAM, indicating that the electronic coupling strength in the peptide SAM should be larger than that in the ECz-C11-SS SAM. This difference can be understood in terms of different tunneling parameters for electron-transfer medium (β). The donor (ECz group) - acceptor (gold) distance along the molecular axis is calculated to be 29 Å (ECz-A12-SS), 28 Å (SS-A12-ECz), 41 Å (ECz-A20-SS), and 20 Å (ECz-C11-SS) as described in Chapter 5. If the β value for ECz-C11-SS is taken to be 0.9 Å^{-1} according to the reported value for alkanes,[31] the β values for helical peptides are calculated to be 0.58 (ECz-A12-SS), 0.60 (SS-A12-ECz), and 0.46 Å^{-1} (ECz-A20-SS). Therefore, the peptide molecule is a favorable medium for electron transfer than a saturated hydrocarbon chain by about 40 % reduction of

the β value. However, the ECz-A12-SS SAM contains electrolytes and water molecules in the monolayer as shown by the cyclic voltammetry and impedance spectroscopy. Therefore, the β value for the ECz-A12-SS remains uncertain, although the value is in accord with that for SS-A12-ECz.

The Effect of Dipole Moment on Photocurrent Generation. In order to clarify the possibility whether the peptide dipole accelerates electron transfer in the SAMs, the dependence on the electric potential of the quantum efficiency for the anodic photocurrent generation using TEOA as an electron donor was investigated (Figure 11).

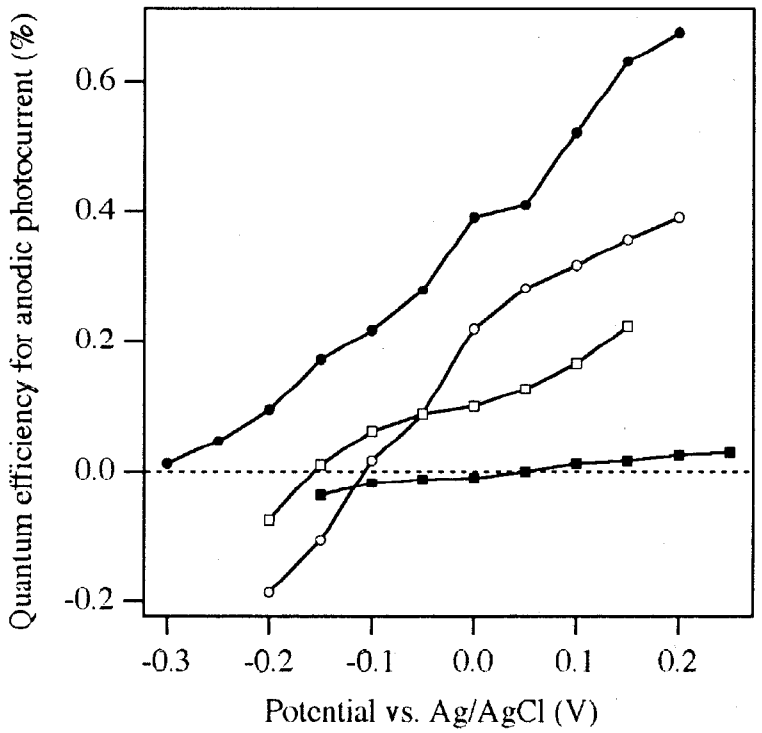

Figure 11. Effect of electric potential on the anodic photocurrent generation using TEOA in the ECz-A12-SS (○), SS-A12-ECz (●), ECz-A20-SS (■), and ECz-C11-SS (□) SAMs.

In the case of all the SAMs, a decrease in the anodic photocurrent was observed with an increase of the negative bias to the working electrode as observed in the case of using EDTA as an electron

donor. The zero-current potentials for the ECz-A12-SS, SS-A12-ECz, ECz-A20-SS, and ECz-C11-SS SAMs are -0.11 V, -0.30 V, +0.05 V, and -0.16 V, respectively. The SS-A12-ECz SAM shows a negative potential shift from that for the ECz-C11-SS SAM (-0.14 V). On the other hand, a positive potential shift from that for the ECz-C11-SS SAM was observed for the ECz-A12-SS SAM (+0.05 V) or for the ECz-A20-SS SAM (+0.21) . These shifts are therefore explainable by the negative potential or the positive potential around the ECz group induced by the neighboring negative terminals or the positive terminals of the corresponding helical dipoles. The negative shift in the SS-A12-ECz SAM causes larger driving force at any potentials than that in the other SAMs, leading to acceleration of electron transfer from the ECz group to gold. The expected potential shift induced by the dipole moment of the helical peptide (ϕ) can be calculated by eq. (3),[32,33]

$$\phi = \frac{m n_a \cos\gamma}{\varepsilon_0 \varepsilon_m (1 + 9\alpha n_a^{3/2})} \qquad (3)$$

where m, n_a, γ, ε_0, ε_m, and α represent the helix dipole moment, the surface coverage of the monolayer, the tilt angle of helix axis from the surface normal, the dielectric permittivity of free space, the relative dielectric constant of the monolayer, and the polarizability of the peptide molecule, respectively. The dipole moment along helix axis and the polarizability were calculated to be 42.0 D and 65.7 Å^3 for the tridecapeptide, and 71.6 D and 105.3 Å^3 for the heneicosapeptide by using MOPAC calculation. On the basis of eq. (3), the ϕ values were calculated to be 0.49, 0.95, 1.50 V for the ECz-A12-SS, SS-A12-ECz, and ECz-A20-SS SAMs, respectively. However, these potentials induced by the dipole moment are reduced by the ionic property of S$^-$-Au$^+$ linkage[34] and/or the charge transfer from gold to the peptide layer.[33] Indeed, the surface potential for the SAM of a hexadecapeptide connected to the gold substrate via the N-terminal was -0.12 V due to the dipole

moment of the peptides. Therefore, the experimental values for the present SAMs are agreeable with the surface potentials determined for the other helical peptide. In addition, the magnitude of the shift is approximately proportional to the expected values (5 : 14 : 21), indicating that the potential shift should arise from the dipole moment of the helical peptide. The β values were also calculated on the basis of the slope in Figure 11 to be 0.60, 0.62, and 0.48 for the ECz-A12-SS, SS-A12-ECz, and ECz-A20-SS SAMs, respectively. These values are in good agreement with the results obtained in the EDTA system described above.

References and Notes

1) Beratan, D. N.; Onuchic, J. N.; Hopfield, J. J. *J. Phys. Chem.* **1987**, *86*, 4488.

2) Closs, G. L.; Miller, J. R. *Science* **1988**, *240*, 440.

3) McDermott, G.; Prince, S. M.; Freer, A. A.; HawthornthwaiteLawless, A. M.; Papiz, M. Z.; Cogdell, R. J.; Isaacs, N. W. *Nature* **1995**, *374*, 517.

4) Hol, W. G. J. *Prog. Biophys. Mol. Biol.* **1985**, *45*, 149.

5) Galoppini, E.; Fox, M. A. *J. Am. Chem. Soc.* **1996**, *118*, 2299.

6) Evans, M. G.; Gergeley, J. *Biochim. Biophys. Acta* **1949**, *3*, 188.

7) Halpern, J.; Orgel, L. E. *Discuss Faraday Soc.* **1960**, *29*, 32.

8) Isied, S. S.; Ogawa, M. Y.; Wishart, J. F. *Chem. Rev.* **1992**, *92*, 381.

9) Gray, H. B.; Winkler, J. R. *J. Electroanal Chem.* **1997**, *438*, 43.

10) Ulman, A. *An Introduction to Ultrathin Organic Films*; Academic Press: San Diego, CA, 1991.

11) Yamada, S.; Kohrogi, H.; Matsuo, T. *Chem. Lett.* **1995**, 639.

12) Akiyama, T.; Imahori, H.; Ajawakom, A.; Sakata, Y. *Chem. Lett.* **1996**, 907.

13) Byrd, H.; Suponeva, E. P.; Bocarsly, A. B.; Thompson, M. E. *Nature* **1996**, *380*, 610.

14) Yamada, S.; Koide, Y.; Matsuo, T. *J. Electroanal. Chem.* **1997**, *426*, 23.

15) Uosaki, K.; Kondo, T.; Zhang, X.-Q.; Yanagida, M. *J. Am. Chem. Soc.* **1997**, *119*, 8367.

16) Imahori, H.; Norieda, H.; Ozawa, S.; Ushida, K.; Yamada, H.; Azuma, T.; Tamaki, K.; Sakata, Y. *Langmuir* **1998**, *14*, 5335.

17) Miura, Y.; Kimura, S.; Imanishi, Y.; Umemura, J. *Langmuir* **1998**, *14*, 6935.

18) Parker, C. A. *Proc. R. Soc., Ser. A* **1956**, *235*, 518.

19) Hatchard, C. G.; Parker, C. A. *Proc. R. Soc., Ser. A* **1956**, *235*, 518.

20) Holzwarth, G.; Doty, P. *J. Am. Chem. Soc.* **1965**, *87*, 218.

21) Greenfield, N.; Fasman, G. D. *Biochemistry* **1969**, *8*, 4108.

22) Chen, Y. H.; Yang, J. T.; Martinez, H. M. *Biochemistry* **1972**, *11*, 4120.

23) Plant, A. L.; Gueguetchkeri, M.; Yap, W. *Biophys. J.* **1994**, *67*, 1126.

24) Gafni, Y.; Weizman, H.; Libman, J.; Shanzer, A.; Rubinstein, I. *Chem. Eur. J.* **1996**, *2*, 759.

25) Steinem, C.; Janshoff, A.; Ulrich, W.-P.; Sieber, M.; Galla, H.-J. *Biochim. Biophys. Acta* **1996**, *1279*, 169.

26) Motesharei, K.; Ghadiri, M. R. *J. Am. Chem. Soc.* **1997**, *119*, 11306.

27) Marcus, R. A.; Sutin, N. *Biochim. Biophys. Acta* **1985**, *811*, 265.

28) Zusman, L. D. *Chem. Phys.* **1987**, *112*, 53.

29) Chidsey, C. E. D. *Science* **1991**, *251*, 919.

30) Weber, K.; Hockett, L.; Creager, S. E. *J. Phys. Chem. B* **1997**, *101*, 8286.

31) Creager, S.; Yu, C. J.; Bamdad, C.; O'Connor, S.; Maclean, T.; Lam, E.; Chong, Y.; Olsen, G. T.; Luo, J.; Gozin, M.; Kayyem, J. F. *J. Am. Chem. Soc.* **1999**, *121*, 1059.

32) Knapp, A. G. *Surface Sci.* **1973**, *34*, 289.

33) Ito, E.; Iwamoto, M. *J. Appl. Phys.* **1997**, *81*, 1790.

34) Miura, Y.; Kimura, S.; Kobayashi, S.; Iwamoto, M.; Imanishi, Y.; Umemura, J. *Chem. Phys. Lett.*, in press.

Chapter 7

Photocurrent Generation by the Self-Assembled Monolayer Composed of a Photoenergy-Harvesting *N*-Ethylcarbazole-Containing Compound and an Electron-Transporting Helical Peptide

Introduction

In the first stage of natural photosynthesis, facile energy transfer among chlorophyll pigments in the thylakoid membrane is a key factor for the efficient photoenergy harvesting.[1,2] The cascade of the energy transfer is composed of the chromophores in a highly ordered arrangement. In Part I, the author have prepared monolayers and bilayer membranes of dialkyl-type amphiphiles carrying an ECz group, and showed that the membranes harvest photoenergy efficiently due to energy migration among ECz groups in a high density and no energy-dissipating site such as excimer in the membrane. The ECz group connected to the dialkyl-type amphiphile is arranged regularly in the membrane, resulting in an artificial photoenergy-harvesting system.

Following the photoenergy transfer, the photoexcited reaction center in the photosynthesis sensitizes electron transfer from an electron donor to an acceptor, resulting in a charge separation. The separated charges are transferred to each limb of the membrane along an electron-transport system composed of protein assemblies containing chromophores.[3] The mechanism for the vectorial long-range electron transfer has been discussed, and found to arise from several important factors. The first is a highly ordered location of chromophores possessing different redox potentials.[4] The second is acceleration of electron transfer by the electrostatic field generated by the dipole moment of α-helical segments in the proteins.[5,6] The third is that the electron-transfer pathway is composed of

through-bond, though-hydrogen-bond, and a few through-space jumps.[7,8] An oriented assembly of α-helical peptides is thus expected to become an excellent mediator for an electron-transport system. The helical peptides will provide a suitable electron-transfer pathway[9,10] due to π and nonbonding n orbitals, and hydrogen bonds in the peptide backbones.[11] In addition the large dipole moment of the helices will accelerate the electron transfer.

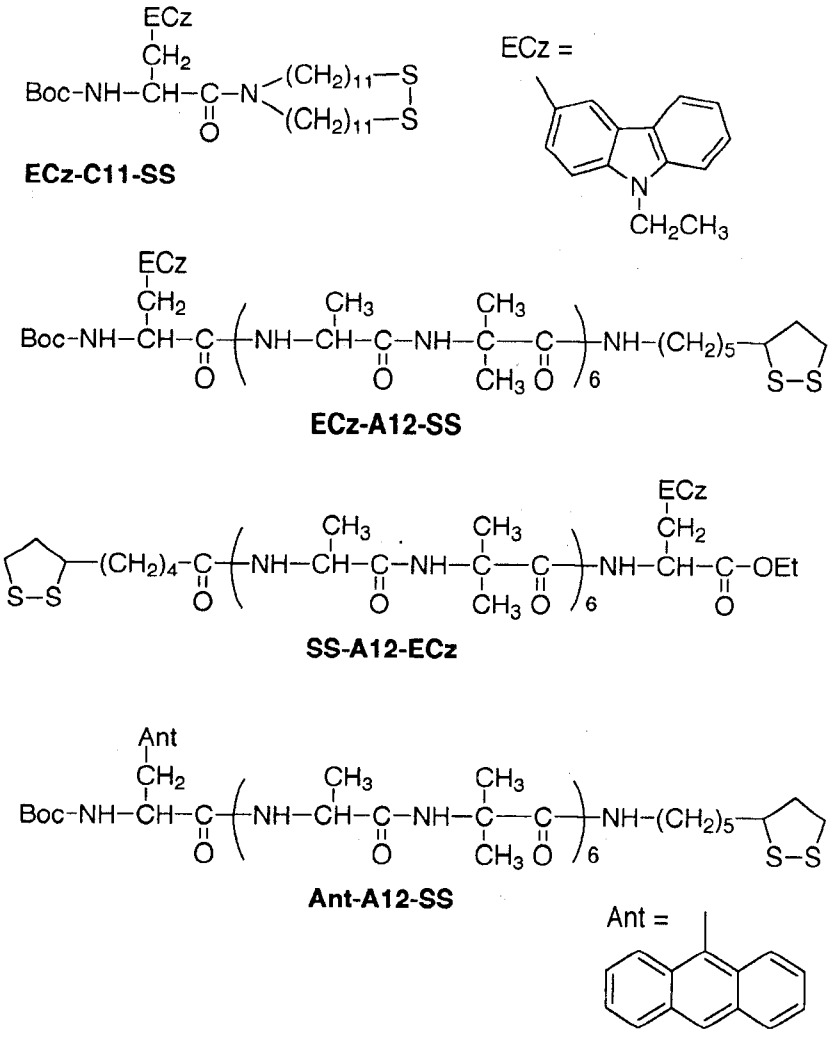

Figure 1. Molecular structures of disulfide compounds (ECz-C11-SS, ECz-A12-SS, SS-A12-ECz, and Ant-A12-SS).

In Chapter 6, the author described that photocurrent generation by the SAM composed of α-helical peptides was effectively promoted by the dipole moment of the helical peptide. In this chapter, the author attempted enhancement of photocurrent generation by combination of a photoenergy-harvesting system composed of dialkyl-type compounds carrying an ECz group and an electron-transport system composed of helical peptides carrying an anthryl (Ant) group.

The molecular structures of the disulfide compounds are shown in Figure 1 together with their abbreviations.

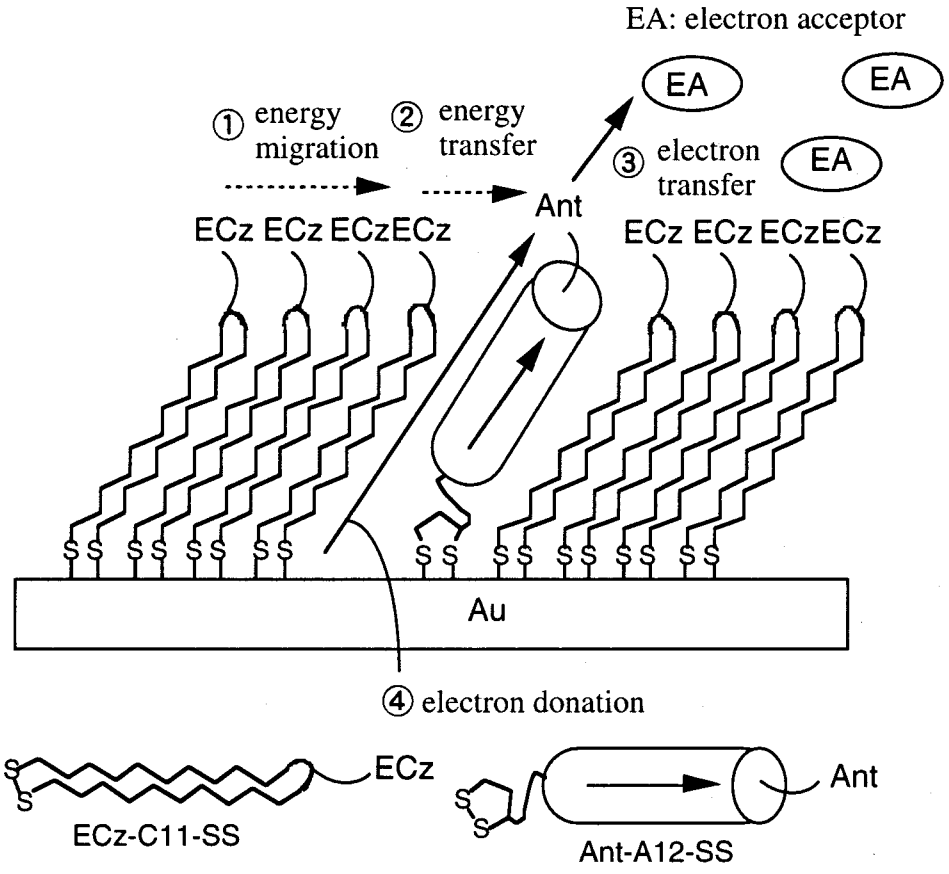

Figure 2. Schematic illustration of a photocurrent generation system integrating photoenergy-harvesting and electron-transport systems in the bicomponent self-assembled monolayer (SAM) composed of ECz-C11-SS and Ant-A12-SS.

As described in Chapter 5, ECz-C11-SS is a dialkyl-type compound carrying an ECz group and a disulfide group at the each terminal. ECz-A12-SS is a tridecapeptide carrying an ECz group at the N-terminal and a disulfide group at the C-terminal, and SS-A12-ECz is a tridecapeptide carrying two functional groups at the reverse positions in the peptide to the case of ECz-A12-SS. Ant-A12-SS is also a tridecapeptide but carries an Ant group at the N-terminal and a disulfide group at the C-terminal.

In the bicomponent SAM of ECz-C11-SS and Ant-A12-SS, excitation of an ECz group will initiate energy migration among ECz groups, and energy transfer from the excited ECz group to the neighboring Ant group occurs (Figure 2). The excited Ant group, then, reduces an electron acceptor in an aqueous phase, followed by electron donation from gold to the oxidized Ant group. The electron donation from gold is expected to be accelerated by the dipole moment directing toward the aqueous phase. Since this photocurrent generation system is composed of a photoenergy-harvesting system possessing high density of chromophores and an electron-transport system composed of helical peptides, the system is interesting in terms of an artificial photosynthetic system as well as solar-energy conversion and molecular photoelectronic devices.

Experimental Section

Materials. Nicotinamide adenine dinucleotide phosphate sodium salt (NADP) was purchased from Nacalai Tesque Co., Ltd. (Japan), and used without further purification. Synthesis of ECz-C11-SS, ECz-A12-SS and SS-A12-ECz was described in Chapter 5. Ant-A12-SS was synthesized in a similar way to the synthesis of ECz-A12-SS by coupling D-Boc-9-anthrylalanine with the dodecapeptide carrying a disulfide group at the C-terminal (26 mg, 51.3 % yield). The purity of the product was checked by TLC. The product was identified by ^{1}H NMR (400 MHz) and mass spectroscopy. The solvent systems for TLC were (A) chloroform/methanol/acetic acid (90/5/3

v/v/v), (B) chloroform/methanol/ammonia water (13/5/1 v/v/v). TLC: R_f(A)=0.37, R_f(B)=0.84. ^{1}H NMR (270 MHz, $CDCl_3$): δ (ppm) 1.25-1.58 (71H, brm, NHCH(CH_3)CONHC(CH_3)$_2$, NHCH$_2$CH_2CH$_2$CH$_2$CH$_2$, (CH_3)$_3$C), 1.84, 2.45 (2H, m, CHCH_2CH$_2$SS), 2.99-3.09 (4H, brm, CHCH$_2$CH_2SS, NHCH_2CH$_2$CH$_2$CH$_2$CH$_2$), 3.52 (1H, m, CHCH$_2$CH$_2$SS), 3.92, 4.29 (6H, m, NHCH(CH$_3$)CONHC(CH$_3$)$_2$), 3.99 (2H, m, NHCHCH_2), 4.24 (1H, q, NHCHCH$_2$), 5.92 (1H, s, NHCH$_2$CH$_2$CH$_2$CH$_2$CH$_2$), 7.25-7.75 (18H, brm, NHCH(CH$_3$)CONHC(CH$_3$)$_2$, NHCHCH$_2$, anthryl-H), 8.00, 8.18, 8.41 (4H, anthryl-H). MS (FAB, matrix; nitrobezylalcohol): m/z 1498 (calcd for $C_{72}H_{110}N_{14}O_{15}S_2Na_1$ [(M+Na)+] m/z 1497.77).

The experimental procedures for monolayer preparation, QCM measurements, cyclic voltammetry, and photocurrent measurements were described in Chapter 5 and 6.

Results and Discussion

Surface Coverage of Self-Assembled Monolayers. The surface coverage of the ECz-C11-SS, SS-A12-ECz, and Ant-A12-SS SAMs were investigated by QCM measurements, and were calculated to be 0.345, 0.145, and 0.090 nmol cm^{-2}, respectively. The corresponding molecular areas were 48.1, 115, and 184 Å^2/molecule, respectively. The molecular area of ECz-C11-SS on the gold substrate is much smaller than those of the helical peptides and is nearly twice the molecular area of a single-chain *n*-alkanethiol. The high density of the ECz group in the ECz-C11-SS SAM is appropriate for an efficient photoenergy-harvesting system. As described in Chapter 5, the molecular area of SS-A12-ECz on the gold substrate is identical to the molecular area calculated under the assumption of the hexagonal packing of the peptides in the orientation determined by the FTIR-RAS. These results indicates that both of the ECz-C11-SS and SS-A12-ECz SAMs possess a well-packed monolayer structure. On the other hand, the Ant-A12-SS SAM where the peptides are connected to

the gold substrate at the C-terminal was less covered than the SS-A12-ECz SAM where the peptides are connected at the N-terminal. This fact is considered to be due to unfavorable electrostatic repulsion between the dipole moment of the helical peptide directing toward the aqueous phase and the dipole moment of an S-Au linkage (S⁻-Au⁺) opposing the helix dipole moment as well as the case of the ECz-A12-SS SAM described in Chapter 5. The Ant-A12-SS SAM is thus considered to possess some defects or incompletely-packed regions.

The state of the surface of the SAM was investigated by cyclic voltammetry. The cyclic voltammograms of the bare gold substrate and the unicomponent and bicomponent SAMs of ECz-C11-SS and Ant-A12-SS in an aqueous $K_3[Fe(CN)_6]$ solution are shown in Figure 3. With the exception of the Ant-A12-SS SAM, the voltammograms of the ECz-C11-SS SAM and all the bicomponent SAMs (ECz-C11-SS and 4.3, 7.3, and 12.2 mol% of Ant-A12-SS) showed no redox activity, indicating that these SAMs possess a well-packed structure to exhibit an insulating property.

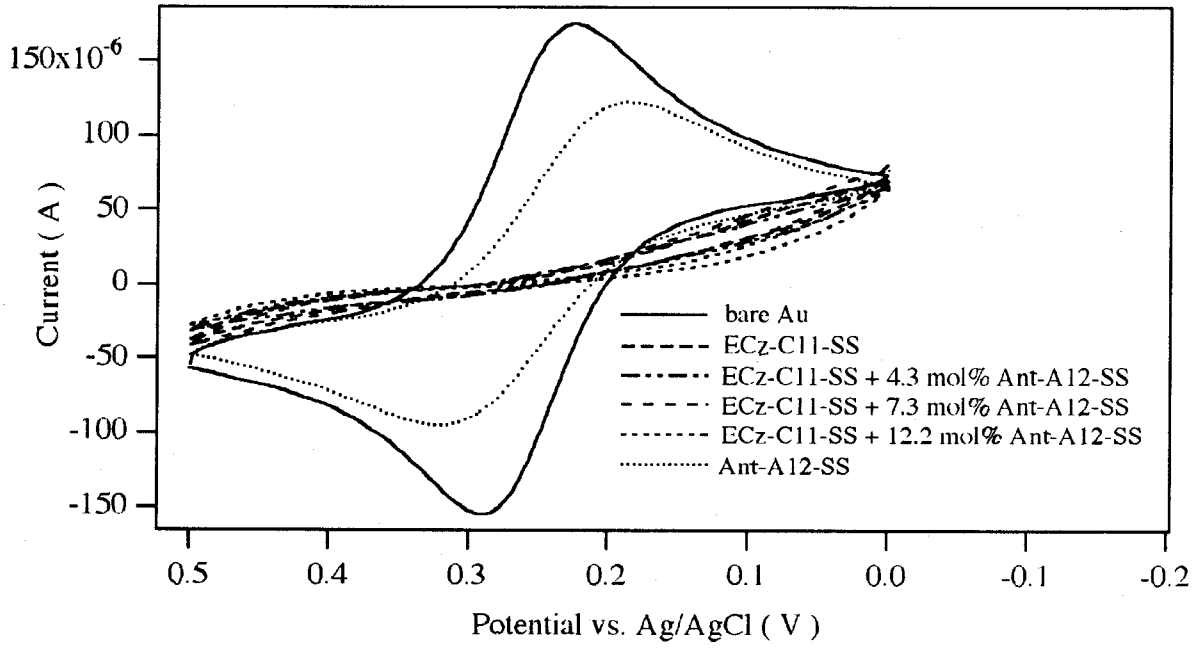

Figure 3. Cyclic voltammograms of a bare gold substrate and the unicomponent and bicomponent SAMs composed of ECz-C11-SS and Ant-A12-SS in a 1 mM aqueous $K_3[Fe(CN)_6]$ solution at room temperature. The sweep rate was set at 50 mV s^{-1}.

On the other hand, redox peaks of the ferricyanide ion observed in the case of the Ant-A12-SS SAM indicated that this monolayer possesses many defects or incompletely-packed regions where the electrolyte can diffuse in. This result agrees with the QCM observation.

The cyclic voltammograms of the unicomponent and bicomponent SAMs of SS-A12-ECz and Ant-A12-SS are shown in Figure 4. The voltammograms of the SS-A12-ECz SAM and the bicomponent SAM containing 3.5 mol% Ant-A12-SS showed no redox activity. However, the bicomponent SAMs containing 7.5 mol% and 13.4 mol% Ant-A12-SS showed redox peaks, suggesting that Ant-A12-SS produced some defects in the monolayer at the concentrations above 7.5 mol%.

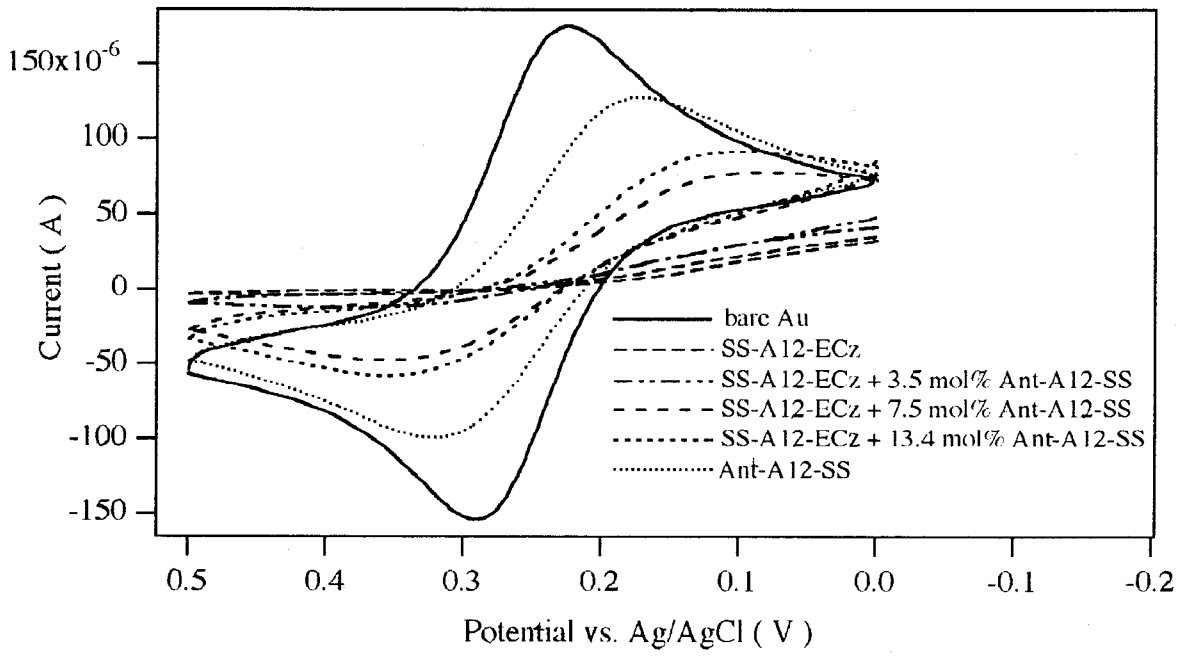

Figure 4. Cyclic voltammograms of a bare gold substrate and the unicomponent and bicomponent SAMs composed of SS-A12-ECz and Ant-A12-SS in a 1 mM aqueous $K_3[Fe(CN)_6]$ solution at room temperature.

Photocurrent Generation by Unicomponent Self-Assembled Monolayers. Photocurrent generation by the unicomponent SAMs was investigated in an aqueous NADP solution. The mechanism of the cathodic photocurrent generation by the SAM is presented schematically in Figure 5. Upon photoexcitation of the ECz or Ant group, electron transfer from the excited chromophore to the electron acceptor NADP occurs, followed by electron donation from gold to the oxidized chromophore (the radical cation of the ECz or Ant group). The reduced NADP diffuses to the auxiliary electrode and transfers an electron, resulting in the generation of a cathodic photocurrent. The photocurrent generation by repeating on-off switchings of the photoirradiation with a monochromic light at 351 nm (10 nm bandwidth) are shown in Figure 6.

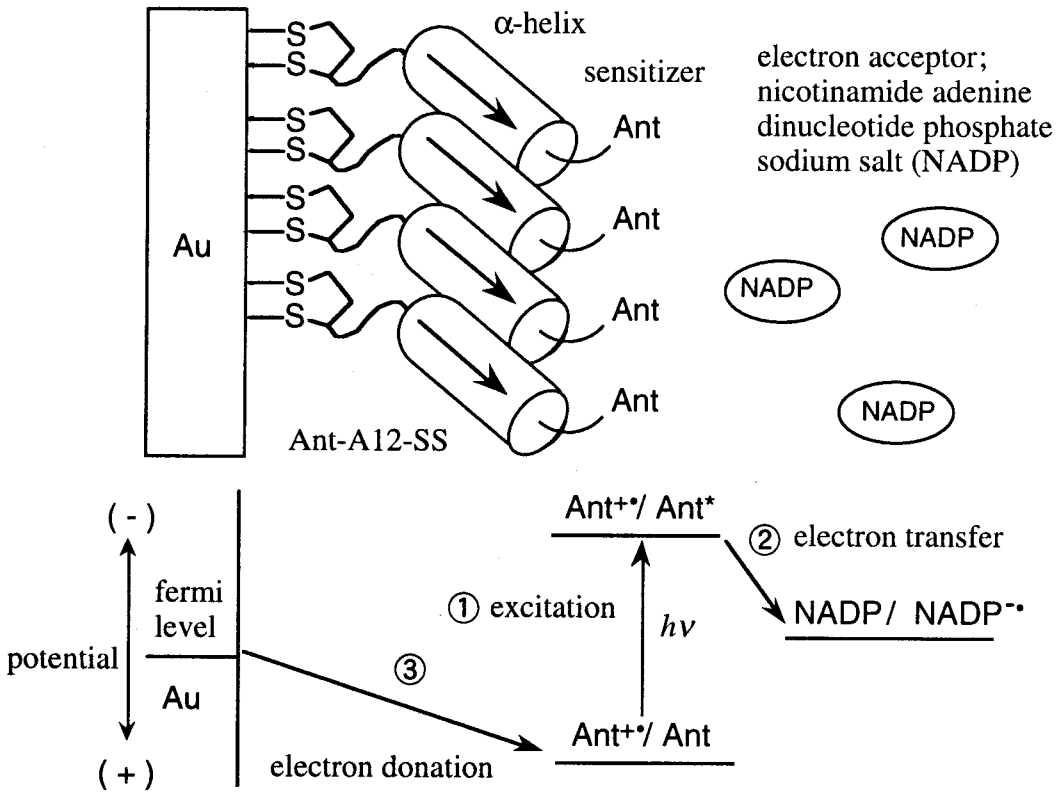

Figure 5. Schematic illustration of cathodic photocurrent generation by the SAM composed of Ant-A12-SS in the presence of nicotinamide adenine dinucleotide phosphate sodium salt (NADP).

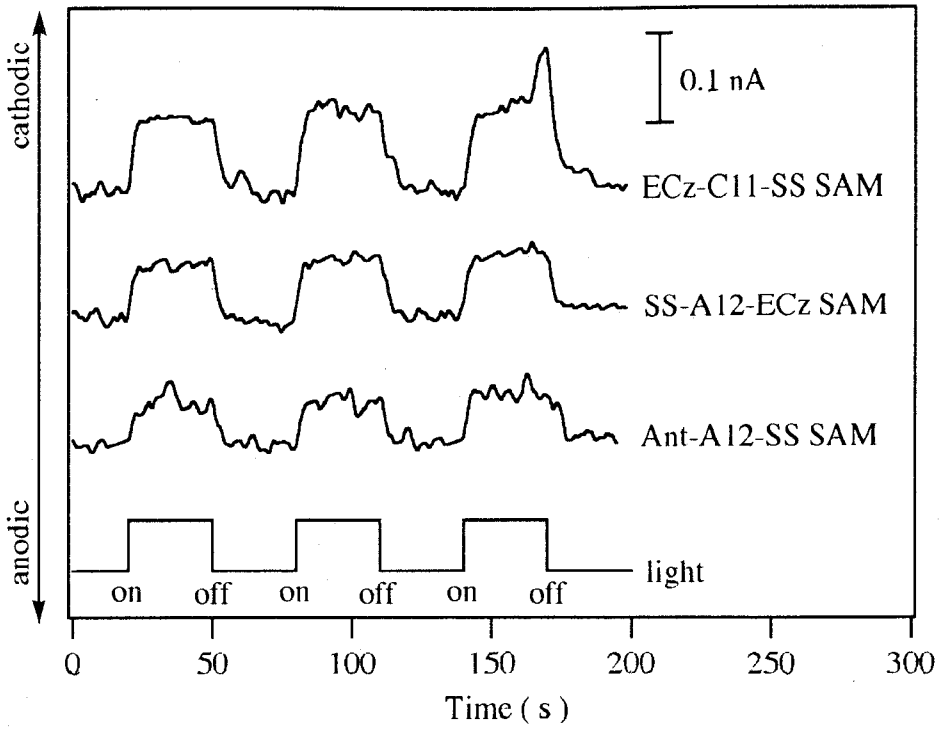

Figure 6. Time course of the photocurrents by the unicomponent SAMs in an aqueous NADP solution at 0 V upon photoirradiation at 351 nm (1.25×10^{-10} einstein s^{-1}) at room temperature.

The photocurrents were 0.091±0.002, 0.068±0.003, and 0.054±0.002 nA for the ECz-C11-SS, SS-A12-ECz, and Ant-A12-SS SAMs, respectively. The largest photocurrent was observed in the ECz-C11-SS SAM because of the high density of ECz group. Since the density of the ECz group is not the same in these SAMs, the quantum efficiencies of the photocurrent generation were calculated for comparison. The quantum efficiencies are 0.25 %, 0.44 %, and 0.38 % for the ECz-C11-SS, SS-A12-ECz, and Ant-A12-SS SAM, respectively. The efficiency of the Ant-A12-SS SAM where the dipole moment of α-helix directs toward the aqueous phase so as to accelerate the electron donation from gold to the Ant group was lower than that of the SS-A12-ECz SAM where the direction of the dipole moment is opposite. Therefore, the electron donation from gold to the oxidized chromophore was not accelerated by the dipole moment of the helical peptide in the Ant-

A12-SS SAM. This may be due to the weakening of the dipole moment by penetrating electrolytes into the monolayer through large defects and/or to the more facile energy transfer from the photoexcited Ant group to gold.

The action spectra of the ECz-C11-SS SAM and the Ant-A12-SS SAM were shown in Figure 7. The action spectrum of the ECz-C11-SS SAM agrees well with the absorption spectrum of ECz-C11-SS in a solution, indicating that the ECz group is the photosensitizing species for the electron transfer. On the other hand, the action spectrum of the Ant-A12-SS SAM deviates from the absorption spectrum in a solution around 330 nm. Although the Ant group sensitizes the electron transfer, the direct electron transfer between the photoexcited gold and the NADP molecule may occur partly, because NADP penetrates in the Ant-A12-SS SAM through large defects.

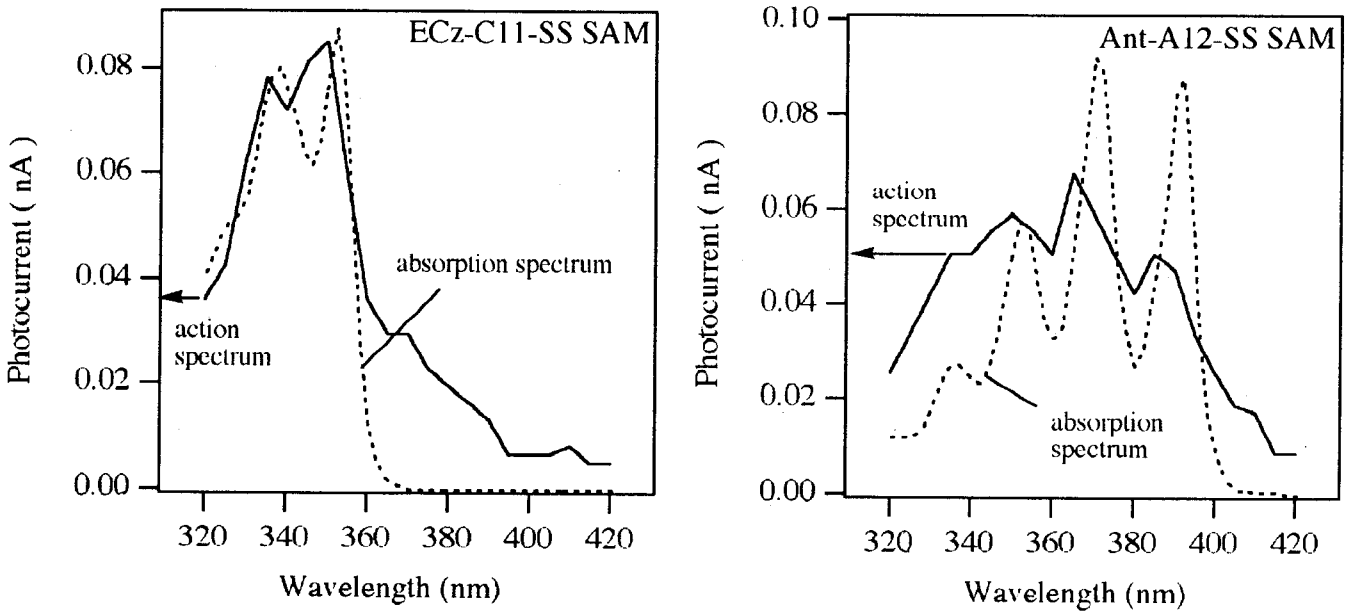

Figure 7. Photocurrent action spectra of the ECz-C11-SS SAM (left, solid line) and the Ant-A12-SS SAM (right, solid line) with the respective absorption spectra of the compounds in a chloroform solution (dotted line).

Photocurrent Generation by Bicomponent Self-Assembled Monolayers. The bicomponent SAMs integrating the photoenergy-harvesting system (ECz-C11-SS or SS-A12-ECz) and the electron-transport system (Ant-A12-SS) were investigated. The mole percentages of Ant-A12-SS in the bicomponent SAMs (ECz-C11-SS and Ant-A12-SS) were determined from the action spectra of the photocurrent generation (Figure 8) as follows. The action spectra of the bicomponent SAMs showed both contributions of the ECz group around 335-350 nm and the Ant group around 370-390 nm. Under assumption that the photocurrents are proportional to the product of the surface density of the chromophores (ECz or Ant group) and the molar absorptivities of the chromophores, the mole percentages of Ant-A12-SS against ECz-C11-SS on the gold substrate can be calculated from the magnitudes of photocurrents at the corresponding wavelengths to the ECz and Ant group of photoirradiation.[12]

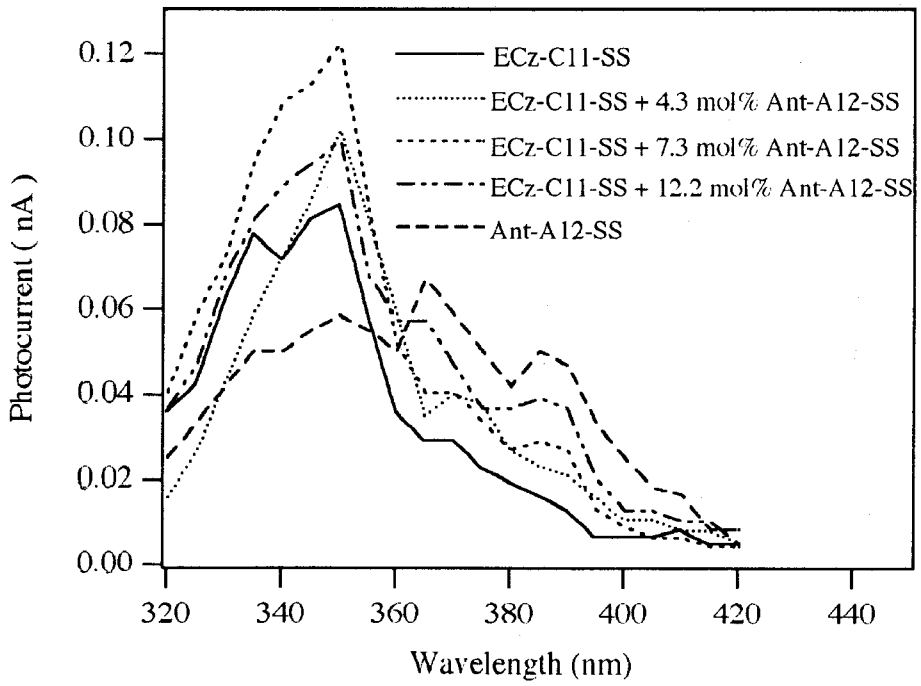

Figure 8. Photocurrent action spectra of the unicomponent and bicomponent SAMs of ECz-C11-SS and Ant-A12-SS.

The percentages of Ant-A12-SS in the bicomponent SAMs are 4.3, 7.3, and 12.2 mol%, respectively, but these values are at most because of the assumption of equal quantum efficiency between ECz-C11-SS and Ant-A12-SS, and the real percentages should be lower. The photocurrents generated by photoirradiation at 351 nm are summarized in Figure 9.

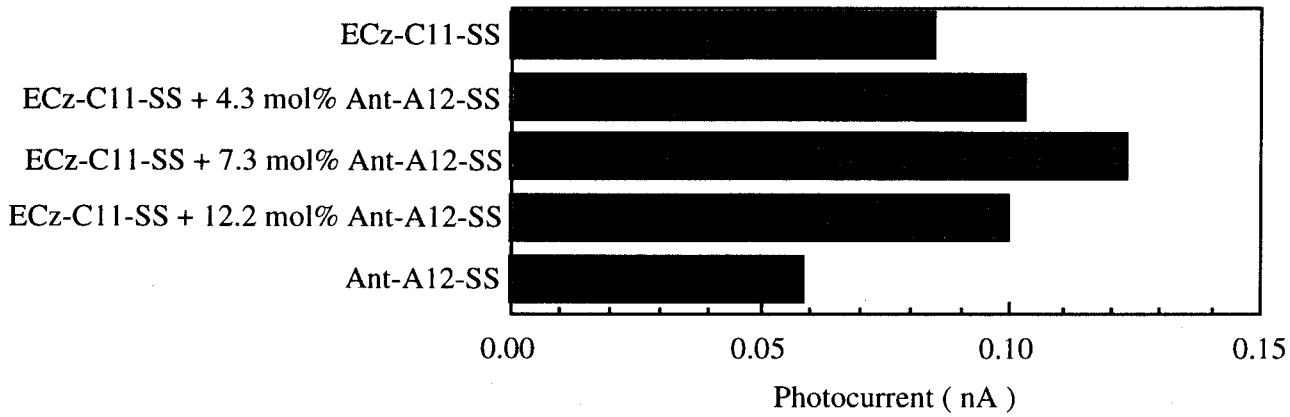

Figure 9. Photocurrents with 351 nm light by the unicomponent and bicomponent SAMs of ECz-C11-SS and Ant-A12-SS.

All the photocurrents in the bicomponent SAMs are larger than that in the unicomponent SAM of ECz-C11-SS or Ant-A12-SS. Especially, the bicomponent SAM containing 7.3 mol% Ant-A12-SS showed a 1.5 fold larger photocurrent than that of the ECz-C11-SS SAM. The enhanced photocurrents in the bicomponent SAMs should be due to the integration of the photoenergy-harvesting system and the electron-transport system. In Chapter 3, the author described that via efficient energy migration among ECz groups, about 70 % of photoenergy of the ECz group was transferred to the Ant group in the bilayer membrane composed of ECz-containing amphiphiles and Ant-containing amphiphiles (3 mol%), where the distance between the neighboring ECz groups was 9.2 Å. As the distance between the neighboring ECz groups in the present bicomponent SAM is calculated to be 7.5 Å, which is shorter than that in the bilayer membrane, the photoenergy of the ECz group would be transferred quantitatively to the Ant group.

On the other hand, the action spectra for the bicomponent SAMs composed of SS-A12-ECz and

Ant-A12-SS showed that the photocurrents of the bicomponent SAMs are smaller than that in the unicomponent SAM of SS-A12-ECz or Ant-A12-SS (Figure 10). In these bicomponent SAMs, the cooperativity of the two components was not effective because of the low density of ECz group in the SAMs and the structural defects as indicated by the cyclic voltammogram of the SAMs (Figure 4).

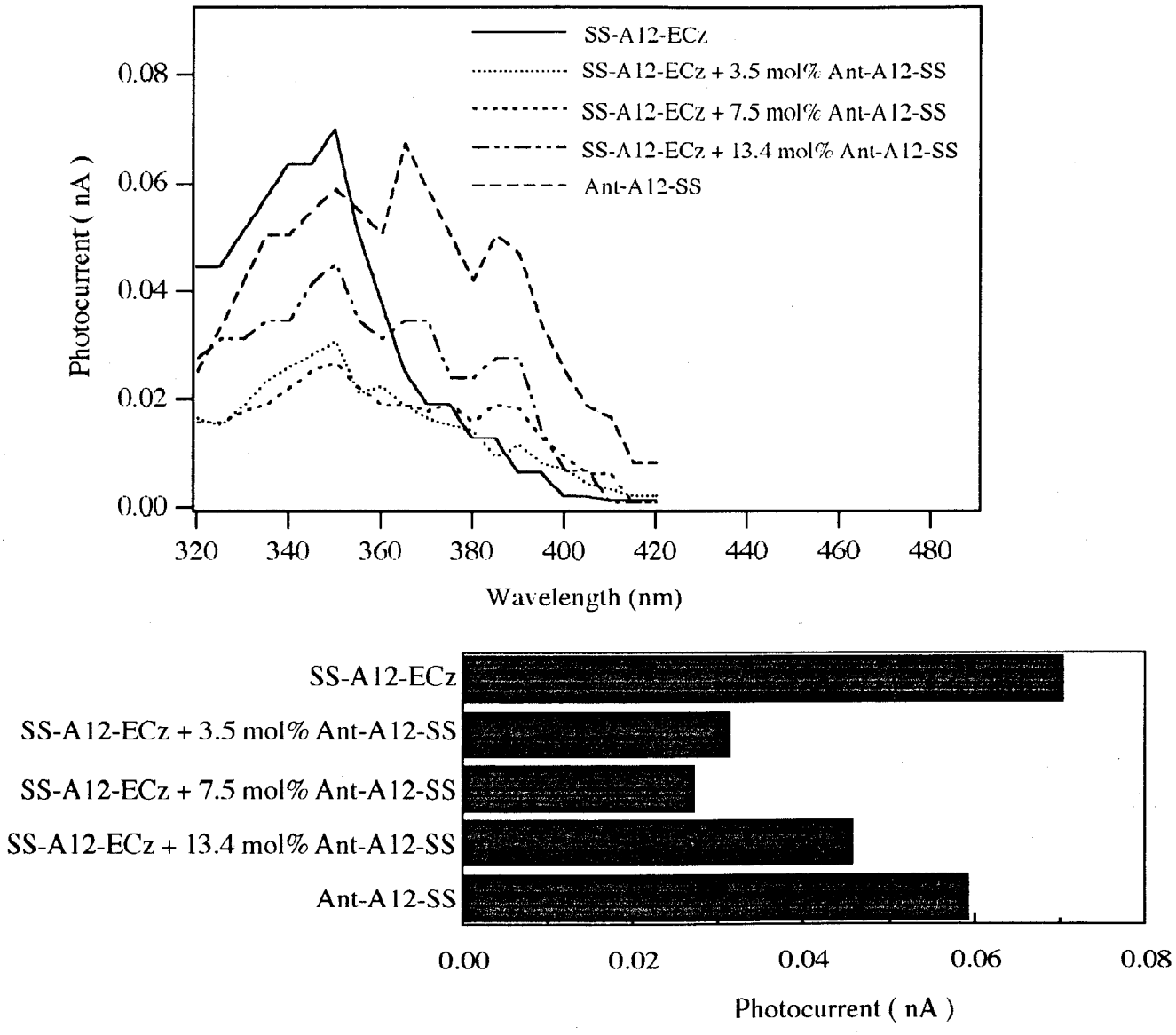

Figure 10. Photocurrent action spectra of the unicomponent and bicomponent SAMs of SS-A12-ECz and Ant-A12-SS (top), and the measured photocurrents with 351 nm light (bottom).

Two types of the bicomponent SAMs were investigated. The bicomponent SAM composed of the dialkyl-type compound carrying an ECz group (ECz-C11-SS) and Ant-A12-SS showed higher photocurrent generation than that composed of the tridecapeptide carrying an ECz group (SS-A12-ECz) and Ant-A12-SS. The dialkyl-type compound is useful for a photoenergy-harvesting system due to the high density in the monolayer. In addition, the alkyl-type compound forms a good matrix for the helical peptide being incorporated regularly to produce no structural defects with respect to the cyclic voltammetry (Figure 3). Ant-A12-SS should function as an electron-transport system by taking a vertical orientation in the bicomponent SAM.

References and Notes

1) Förster, T. *Comprehensive Biochemistry, vol 22*; Elsevier: Amsterdam, 1967.

2) Duysens, L. N. M. *Transfer of Excitation Energy in Photosynthesis, PhD Thesis*: Utrecht, 1952.

3) Austin, R., Buhks, E., Chance, D., DeVault, D., Dutton, P. L., Frauenfelder, H., Gol'denskii, V. I., Eds. *Protein Structure: Molecular and Electronic Reactivity*; Springer-Verlag: New York, 1987.

4) Deisenhofer, J.; Michel, H. *Angew. Chem., Int. Ed. Engel.* **1989**, *28*, 829.

5) Hol, W. G. J. *Prog. Biophys. Mol. Biol.* **1985**, *45*, 149.

6) Galoppini, E.; Fox, M. A. *J. Am. Chem. Soc.* **1996**, *118*, 2299.

7) Beratan, D. N.; Onuchic, J. N.; Winkler, J. R.; Gray, H. B. *Science* **1992**, *258*, 1740.

8) Betts, J. N.; Beratan, D. N.; Onuchic, J. N. *J. Am. Chem. Soc.* **1992**, *114*, 4043.

9) Larsson, S. *J. Chem. Soc., Faraday Trans. 2* **1983**, *79*, 1375.

10) Isied, S. S.; Ogawa, M. Y.; Wishart, J. F. *J. Phys. Chem.* **1993**, *97*, 11456.

11) Gray, H. B.; Winkler, J. R. *J. Electroanal Chem.* **1997**, *438*, 43.

12) The 100 mol% photocurrent of the Ant-A12-SS SAM generated by photoirradiation at 391 nm was theoretically calculated to be $I_{ECz351} \times \varepsilon_{Ant391} / \varepsilon_{ECz351}$, where I_{ECz351}, ε_{Ant391}, and ε_{ECz351} represent the photocurrent of the ECz-C11-SS SAM generated by photoirradiation at 351 nm, the molar absorptivity for the Ant group at 391 nm, and the molar absorptivity for the ECz group at 351 nm, respectively. This photocurrent is for the membrane at the Ant density same as the ECz density of the ECz-C11-SS SAM under the assumption that the quantum efficiencies for the photocurrent generation are the same between the SAMs using the Ant and ECz group as a photosensitizer. The mol percentages of Ant-A12-SS with respect to ECz-C11-SS in the bicomponent SAMs were calculated from the photocurrent difference at 391 nm between the bicomponent SAM and the ECz-C11-SS SAM divided by the 100 mol% photocurrent.

Concluding Remarks

This section briefly summarizes the results of investigation on the photoinduced electron transfer in supramolecular thin films composed of compounds carrying an *N*-ethylcarbazolyl (ECz) group.

In Part I of this thesis, the photoinduced energy transfer or electron transfer by energy migration among ECz groups in monolayers or bilayer membranes composed of amphiphiles carrying an ECz group was investigated.

In Chapter 1, photoenergy migration and hole transfer in a bilayer membrane composed of amphiphilic compounds carrying an ECz group (5Cz18) were investigated. Energy migration among ECz groups was evaluated by computer simulation of fluorescence quenching of the ECz group by a terephthaloyl group introduced in the bilayer membrane. The quenching phenomena were well simulated by taking the number of energy migration to be 360 and 113 below and above the phase-transition temperature of the bilayer membrane (Tc), respectively. Two-photon excitation of the ECz group in the membrane produced a radical cation of the ECz group. The lifetime of the radical cation was 40 μs above the Tc. It became longer below the Tc and upon dilution of the chromophores in the membrane, indicating that the rate of hole transfer is comparable to the lateral diffusion of the amphiphile in the membrane.

In Chapter 2, bicomponent monolayers composed of zwitter-ionic amphiphiles having an ECz group (5Cz18Z) and fatty acids carrying an anthryl (Ant) group were prepared, and energy migration among ECz groups and energy transfer from the ECz group to the Ant group in the monolayer were investigated by *in situ* fluorescence spectroscopy. A double logarithmic plot of the fluorescence intensity of the Ant group vs. the average distance between ECz groups in the monolayer showed a linear relationship with a slope of -6, indicating occurrence of energy migration via dipole-dipole

interaction according to the Förster's mechanism. Fluorescence quenching of the ECz group by cytochrome c (cyt.c) in the monolayer was also investigated. It was found that fluorescence from the 5Cz18Z monolayer was well quenched by cyt.c in the subphase of monolayer. However, the dependence of the quenching rate on the surface pressure was complex, and took the maximum value at a molecular area of 160 $Å^2$/molecule. Under high surface pressures, cyt.c might be partially dissociated from the monolayer.

In Chapter 3, a novel photoinduced electron transfer system was constructed by introducing an amphiphilic acceptor carrying an Ant group (energy acceptor) and a viologen group (electron acceptor) in a molecule into the 5Cz18Z bilayer membrane. By energy migration among ECz groups in the membrane, the photoenergy is transferred efficiently to the Ant group, and the excited Ant group transfers electron to the viologen group. The whole quantum yield of this process is 0.67 in the presence of 3 mol% acceptor. The photoinduced electron transfer process was simulated successfully to determine the number of the excitation migration steps to be 78. Interestingly, the transient absorption spectroscopy revealed that the photooxidized chromophore decays faster than the reduced viologen which has a longer lifetime than a millisecond, suggesting the electron donation to the oxidized chromophore from amide groups in the amphiphile molecules.

In Chapter 4, photoreduction of cyt.c in the presence of the bilayer membrane of 5Cz18 or 5Cz18Z was investigated. In the membrane, efficient energy migration among ECz groups promoted photoreduction of cyt.c in the presence of a sacrificial electron donor. It was found that the yield of cyt.c reduction is not so sensitive to the amount of cyt.c partitioned to the membrane because of efficient energy migration among ECz groups, but is affected sensitively by the amount of the sacrificial donor bound to the membrane.

In Part II of this thesis, the photoinduced electron transfer in self-assembled monolayers composed of α-helical peptides carrying an ECz group was investigated.

In Chapter 5, monolayers at the air/water interface and self-assembled monolayers (SAMs) on a gold substrate were prepared from helical peptides carrying an ECz group and a disulfide group at each end of a chain, and the peptide arrangement and orientation were investigated. It was found by π-A isotherms and circular dichroism spectroscopy that in the compressed phase of the monolayer at the air/water interface, helical peptides mounted on the packed monolayer retaining lying orientation to the water surface. As a result of computer simulation of fluorescence intensity of the ECz group in the monolayer, the helical peptides were found to be randomly arranged. On the other hand, Fourier transform infrared reflection-absorption spectroscopy and quartz crystal microbalance measurements indicated that in SAMs, helical peptides have an upright parallel orientation. In both monolayer systems, the direction of the dipoles of helical peptides did not influence seriously the structure of monolayers and the environment of the ECz group.

In Chapter 6, photocurrent generation by photoexcitation of the ECz group of the peptide SAMs in an aqueous solution was investigated. In the presence of an electron acceptor, electron was donated from gold to the ECz group upon photoexcitation. On the other hand, in the presence of an electron donor, the direction of photocurrent was reversed. The electron transfer occurred from the ECz group to gold and was remarkably accelerated by the dipole moment directing toward the gold substrate. Furthermore, the electronic coupling between the ECz group and gold through the peptide chain was found to occur more strongly than that through a saturated hydrocarbon chain. Helical peptides were shown to be a favorable medium for electron transfer.

In Chapter 7, bicomponent SAMs composed of dialkyl-type compounds carrying an ECz group and helical peptides carrying an Ant group were prepared, and the effect of photoenergy harvesting on photocurrent generation was investigated. The photocurrent generated by photoirradiation of the

bicomponent SAMs immersed in an aqueous electron acceptor solution was larger than that in unicomponent monolayer of dialkyl compound or helical peptide. This result indicates the occurrence of energy transfer from the excited ECz group to the Ant group after energy migration among ECz groups in the bicomponent monolayers. The excited anthryl group transfers electron to an acceptor in an aqueous phase. The electron donation from gold to the oxidized Ant group is accelerated by the dipole moment of helical peptide, generating a larger cathodic photocurrent. To conclude, the photoenergy harvesting by favorable migration enhances photocurrent generation.

In the present investigation, artificial systems mimicking photoenergy harvest and electron transport in the initial stage of photosynthesis and a combination of the two processes were brought to fruition by supramolecular assembly. Photophysical processes consisting of photoenergy transfer and photoinduced electron transfer were investigated in detail on the basis of spectroscopic and electrochemical approach. In each system, elemental processes took place on the molecular level, leading to photofunctionality. Each functional group participating in these processes can be regarded as molecular-sized processing units. Notably, the helical peptide carrying a chromophoric group can be referred to as a molecular diode. Orientation of these molecular-sized components to a tailored arrangement led to the manifestation of aimed photofunction. The present approach opens the way to the development of organic molecular photoelectronic devices which create fundamental technology to support the 21st century.

List of Publications

Chapter 1 "Photoenergy Migration and Hole Transfer in a Bilayer Membrane Composed of Amphiphilic Compounds Carrying an *N*-Ethylcarbazolyl Group"
Morita, T.; Kimura, S.; Imanishi, Y.
J. Phys. Chem. B. **1997**, *101*, 4536-4538.

Chapter 2 "*In situ* Fluorescence Spectroscopic Studies of Energy Migration and Energy Transfer in the Monolayer of *N*-Ethylcarbazole-Containing Amphiphile"
Morita, T.; Kimura, S.; Imanishi, Y.
Langmuir **1998**, *14*, 171-175.

Chapter 3 "Donor-Sensitizer-Acceptor Triad System for Photoenergy Migration, Photoenergy Transfer, and Electron Transfer in a Bilayer Membrane"
Morita, T.; Kimura, S.; Imanishi, Y.
J. Am. Chem. Soc. **1999**, *121*, 581-586.

Chapter 4 "Efficient Photoreduction of Cytochrome c in the Presence of a Bilayer Membrane of *N*-Ethylcarbazole-Containing Amphiphiles"
Morita, T.; Kimura, S.; Imanishi, Y.
Chem. Lett., submitted.

Chapter 5 "Spectroscopic Study on Direction and Inclination of Helical Peptides in a Monolayer Formed at the Air/Water Interface and on a Gold Substrate"
Morita, T.; Kimura, S.; Kobayashi, S.; Imanishi, Y.
Bull. Chem. Soc. Jpn., submitted.

Chapter 6 "Photocurrent Generation under a Large Dipole Moment Formed by Self-Assembled Monolayers of Helical Peptides Having an *N*-Ethylcarbazolyl Group"
Morita, T.; Kimura, S.; Kobayashi, S.; Imanishi, Y.
J. Am. Chem. Soc., submitted.

Chapter 7 "Photocurrent Generation by the Self-Assembled Monolayer Composed of a Photoenergy-Harvesting *N*-Ethylcarbazole-Containing Compound and an Electron-Transporting Helical Peptide"
Morita, T.; Kimura, S.; Kobayashi, S.; Imanishi, Y.
J. Am. Chem. Soc., submitted.

Acknowledgement

The present research was carried out from 1995 to 1999 at the Department of Material Chemistry, Graduate School of Engineering, Kyoto University.

The author would like to express his sincere gratitude to Professor Shiro Kobayashi of the Department of Material Chemistry, Graduate School of Engineering, Kyoto University, for his guidance on the thesis.

The author would like to express his sincere appreciation to Professor Yukio Imanishi of the Graduate School of Materials Science, Nara Institute of Science and Technology and formerly of the Department of Material Chemistry, Graduate School of Engineering, Kyoto University, for his continuous guidance and encouragement, and for detailed criticisms on the manuscript.

The author is deeply grateful to Professor Shunsaku Kimura of the Department of Material Chemistry, Graduate School of Engineering, Kyoto University, for his constant guidance and encouragement throughout the course of this work.

The author would like to express his thanks to Professor Shinzaburo Ito of the Department of Polymer Chemistry, Graduate School of Engineering, Kyoto University, for his instructive comments.

The author is grateful to Dr. Hiroshi Uyama of the Department of Material Chemistry, Graduate School of Engineering, Kyoto University, for his valuable suggestion on this work.

The author would like to thank his colleagues in the Imanishi Laboratory and Kobayashi Laboratory in Kyoto University for their encouragement during the course of this research.

Finally, the author wishes to express hearty thanks to his mother and sister for their encouragement and support.

December, 1999

Tomoyuki Morita